Relaxation Phenomena of Magnetic Anisotropy and Magnetization Ripple in Vacuum-Deposited Permalloy Films

by Shigeru TSUNASHIMA

Department of Electrical Engineering

Faculty of Engineering

Nagoya University

C O N T E N T S

Chapter 1

Introduction

1.1 Permalloy Films in Memory Applications[1)]

Thin films of conducting, magnetic and dielectric materials are employed in ever increasing ways in electronic applications. The largest portion of researches in magnetic films has been devoted to polycrystalline films of nickel-iron alloys, particularly the alloys near the nonmagnetostrictive composition of 81%Ni-19% Fe (sometimes called Permalloy) deposited on smooth substrates in the presence of a magnetic field parallel to the film plane. Such films show unique magnetic properties as follows: The magnetization M is confined to the film plane by the demagnetizing field; a uniaxial magnetic anisotropy is induced in the film plane with the easy axis (EA) along the field direction during the deposition so that M is stable in either sense of the EA and can reverse its sense through a coherent rotation in a few nanoseconds by the application of magnetic fields of a few Oersteds. Furthermore large high density arrays of such films can be manufactured easily by the use of batch evaporation. Permalloy films have been therefore thought to be a candidate for the memory element in high speed digital computers.

A typical film of this variety is vacuum-deposited with the normal incidence of vapor in a vacuum of better than 10^{-5} Torr. onto a polished glass substrate. The thickness of the film is about 1000Å, and the temperature of the substrate during the deposition is kept about 200°C. Such a film consists of randomly oriented grains of about 100Å in diameter. The resulting magnetic parameters are typically anisotropy field $H_k \simeq 3 \sim 4$ Oe, coercive force $H_c \simeq 1$ Oe and anisotropy dispersion (see Sec. 1.4.2) $\alpha_{90} \simeq 1°$.

A schematic illustration of four bits in a flat film memory array is shown in Fig. 1.1a[2]. Such a memory can be constructed by fabricating individual bits by suitable masking techniques during deposition or by selective etching of a continuous film.

Recently the cylindrical-film memory[3] has become increasingly popular (Fig. 1.1b). Such a memory consists of parallel array of spatially spanned Beryllium-Copper wires onto which 81%Ni-19%Fe has been electroplated, with a set of word lines placed perpendicular to the wires. A major advantage of this type memory is the closed flux path of the bits; for the absence of demagnetizing fields permits a greater film thickness (about 1 μ) and hence a lager readout signal.

1.2 Stoner-Wohlfarth Model[4]

The anisotropy energy of a uniaxial ferromagnetic film is given by

$$E_a = K_u \sin^2\phi_0 \ , \tag{1.1}$$

where K_u is the uniaxial anisotropy constant and ϕ_0 is the angle between M and the EA. If M is assumed to stay and remain perfectly uniform in the film plane, its direction can be predicted by the Stoner-Wohlfarth model for any applied field H in the plane of the film at an angle β to the EA. In this situation the total energy is given by the sum of the field energy and the anisotropy energy:

$$E = K_u \sin^2\phi_0 - H\,M\cos(\beta-\phi_0). \tag{1.2}$$

It is convenient to define the normalized quantities of

$\epsilon = E/MH$, $h = H/H_k$, $h_{\parallel} = H\cos\beta/H_k$ and $h_{\perp} = H\sin\beta/H_k$.

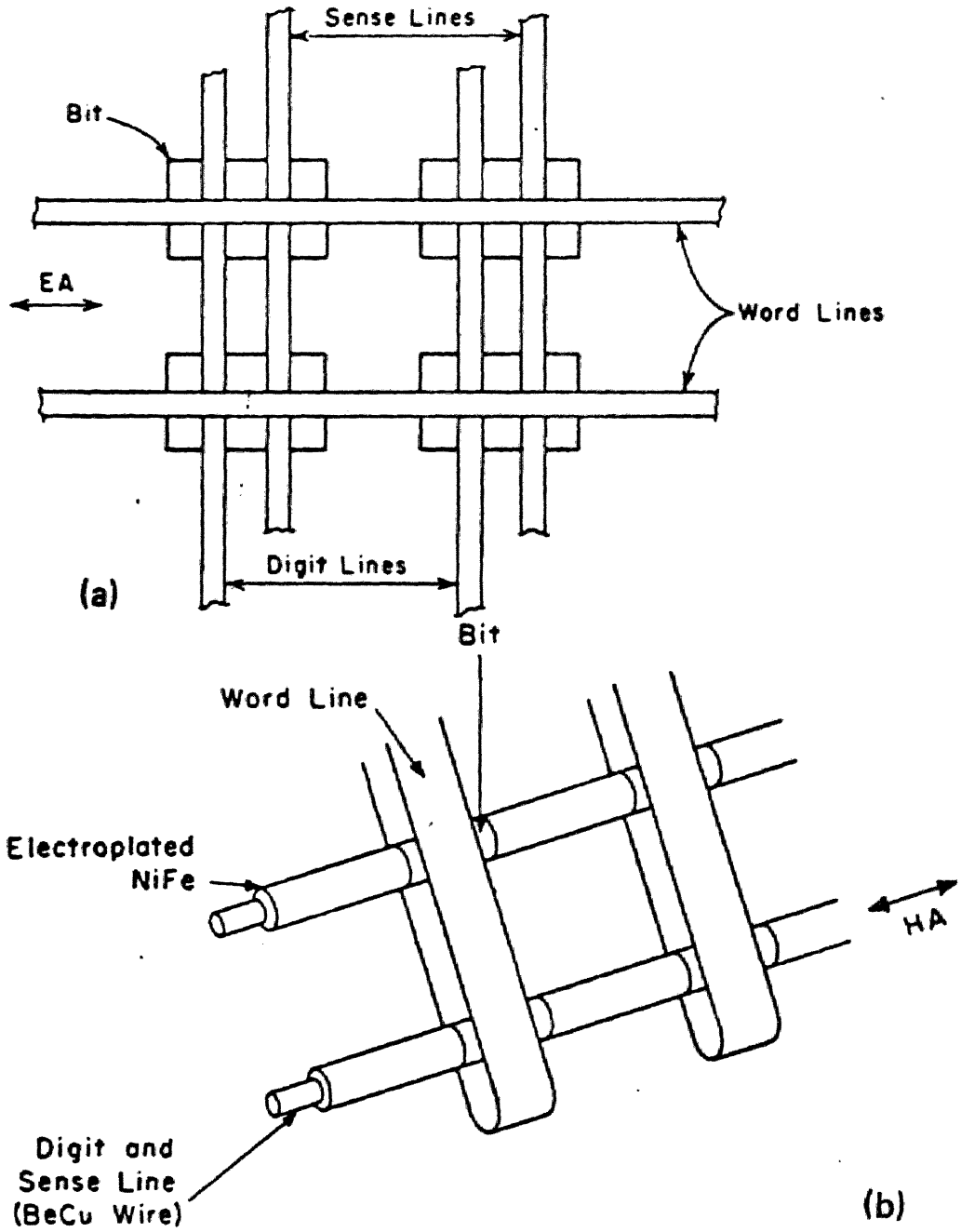

Fig. 1.1 Schematic illustration of wiring arrangement for a memory using uniaxially anisotropic ferromagnetic (a) flat films, (b) electroplated cylindrical films[1].

Here $H_k = 2Ku/M$ is known as the anisotropy field, and the subscript $\parallel$ and $\perp$ denote the longitudinal and transverse field components parallel and perpendicular to the EA, respectively. Then eq. (1.2) becomes

$$\varepsilon = \frac{1}{2} \sin^2\phi_0 - h_\parallel \cos\phi_0 - h_\perp \sin\phi_0 . \qquad (1.3)$$

Energy extrema are found by setting $\partial\varepsilon/\partial\phi_0 = 0$, which is equivalent to the fact that the net torque on M vanishes. Thus

$$\frac{\partial\varepsilon}{\partial\phi_0} = \frac{1}{2} \sin 2\phi_0 + h_\parallel \sin\phi_0 - h_\perp \cos\phi_0 = 0 \qquad (1.4)$$

The values of ϕ_0 satisfying eq. (1.4) represent stable equilibriums (minimum energy states) only when $\partial^2\varepsilon/\partial\phi_0^2 > 0$, which is written as,

$$\frac{\partial^2\varepsilon}{\partial\phi^2} = \cos 2\phi_0 + h \cos(\phi_0 - \beta) = h_1 > 0 \qquad (1.5)$$

Here h_1 is known as the "uniform effective (or single domain) field". From eq. (1.4) the quasi-static M-H curve can be calculated for arbitrary azimuth angle β of the applied field h.

1.3 Outline of M-Induced Uniaxial Anisotropy

When a saturation magnetic field is applied in the plane of a magnetic film during its deposition, a uniaxial magnetic anisotropy is induced with the EA parallel to the applied field [5]. The anisotropy energy obtained is strongly dependent on the film composition and the substrate temperature.

In the case of bulk Ni-Fe alloy, it is well known that heat treatment in a field induces a uniaxial anisotropy (the

name "M-induced anisotropy" originates in this fact) [6,7]. The interpretation accepted for this anisotropy is that the short-range directional order is produced by the atomic rearrangement during high temperature annealing ; i.e. owing to the pseudodipolar magnetic interactions, a preferred orientation of like-atom pairs is developed. When the sample is cooled, this directional order is frozen in, and results in an uniaxial anisotropy. In Ni-Fe alloys, the anisotropy due to the directional order was theoretically calculated [8-10] and the theory was supported experimentally [6].

In the case of magnetic films, a uniaxial anisotropy can be induced even in single element films of Ni, Fe and Co[4] . This fact suggests that even if pair-order anisotropy is operating in magnetic films, at least one additional anisotropy source must be involved. For this reason, several workers have considered the following strain-magnetostriction mechanism[11,12] :
At a sufficiently high temperature, the film is free from its substrate and will sustain a saturation magnetostriction under a magnetic field. When the film is cooled down after the deposition, the atoms lose their mobility so that the film is constrained, involving an uniaxial stress from the substrate.

For the purpose of investigating the origin of the anisotropy in films, the composition dependence of the uniaxial anisotropy constant K_u has been examined (Fig. 1.2)[11,13-15].
For the low deposition temparature, K_u has a minimum near the nonmagnetostrictive composition of 81%Ni, and with the increase of the deposition temperature, K_u decreases approaching to the bulk Ni-Fe data[10] . Thus the anisotropy in the case of low

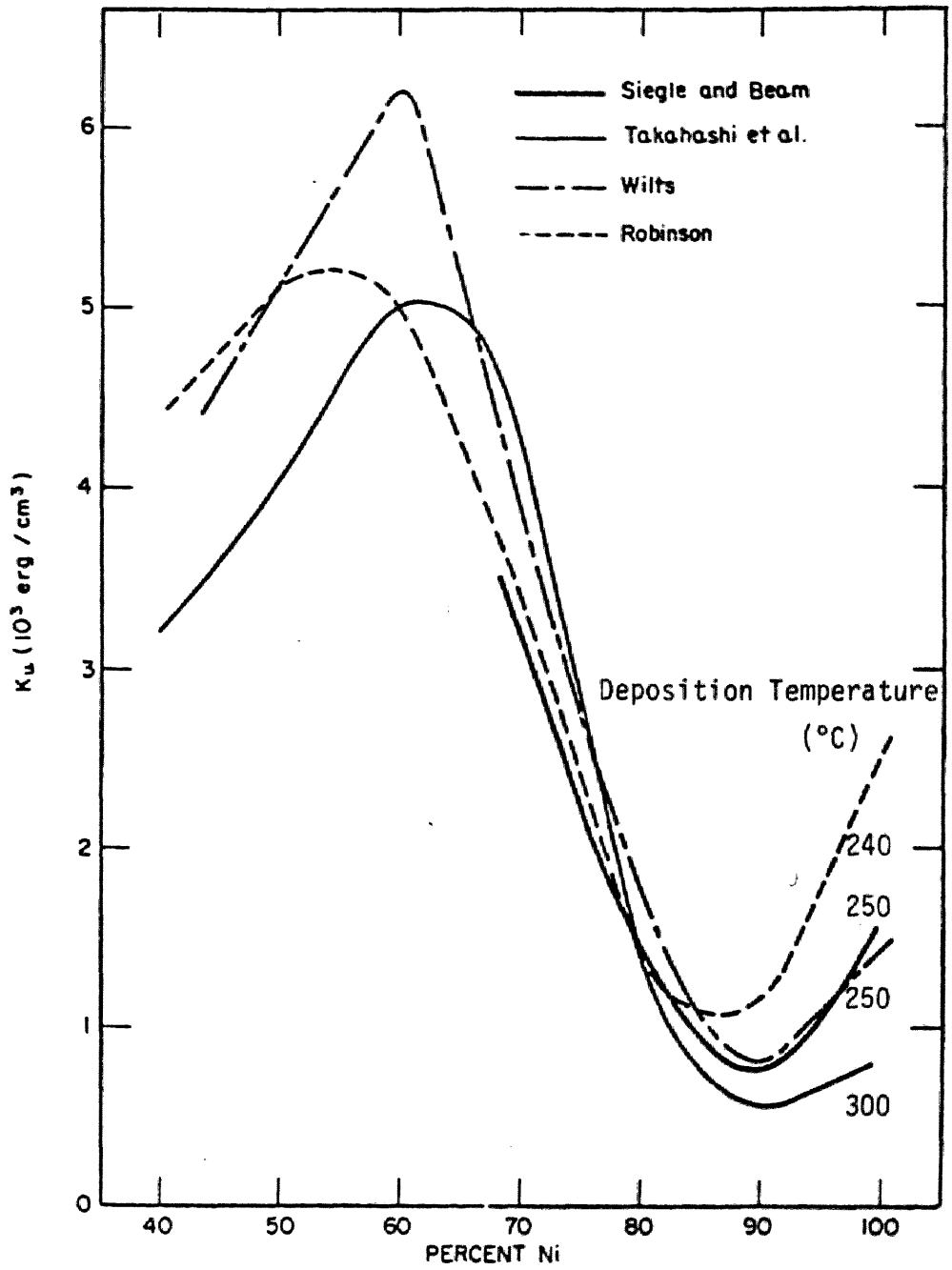

Fig. 1.2 Composition dependence of uniaxial anisotropy constant K_u in Ni-Fe films[11,13-15].

deposition temperature is thought to consist of two different mechanisms, namely, the pair-order anisotropy and the strain-magnetostriction anisotropy.

For a more precise insight into the origin of the anisotropy, magnetic annealing experiments have been carried out by many workers[16-19]. When a HA field is applied during annealing, H_k decreases monotonically, and an interchange of EA and HA takes place at relatively low annealing temperature. In these annealing experiments, the film was usually subjected to annealing in the HA field at a constant temperature T_a after the deposition. The change of H_k during the heat treatment was traced against the annealing time t . The H_k vs. time t data (Fig. 1.3) were analyzed by the superposition of independent several 1-st order reaction terms. Under the HA field, the annealing (relaxation) process of H_k is expressed by

$$H_k(t) = \sum_i H_{ki}^0 \left\{ 2 \exp(-\frac{t}{\tau_i}) - 1 \right\} , \qquad (1.6)$$

where H_{ki}^0 and τ_i are respectively the intial value of H_k and the relaxation time for the i-th anisotropy component, and τ_i is related to the activation energy E_i as,

$$\tau_i = \tau_{i\infty} \exp(\frac{E_i}{k_B T_a}) . \qquad (1.7)$$

This analysis has shown that several annealing stages with different activation energies are operative even in nonmagnetostrictive films (Table 1.1). Most of activation energies listed in the table are considerably lower than that for bulk Ni-Fe alloys of 3.0 eV[20] which corresponds to the self-diffusion of constituent atoms[21] .

Table 1-1 Summary of magnetic annealing results

i) Kneer and Zinn (81%Ni-19%Fe)[16]

process	H_K^0 (%)	$\tau_{i\infty}$(s)	E_i(eV)	
I	20	1.5	0.15	
II	8	0.03	0.4	
III	16	0.30	0.4	constraint
IV	56	2.0×10^{-8}	1.5	pair order

ii) Fujii et at. (81.5%Ni-18.5%Fe)[18]

process	H_K^0 (%)	$\tau_{i\infty}$(s)	E_i(eV)	
I	44	0.56	0.17	
II	44	1.1×10^{-4}	0.5	magnetoelatic
III	44	9×10^{-4}	0.5	magnetoelatic
IV	25	4.8×10^{-6}	1.1	
V	25	2×10^{-5}	1.1	
VI	31	1.0×10^{-10}	2.0	pair order

iii) Smith, Wiess and Harte (83%Ni-17%Fe)[17]

process	H_K^0 (%)	$\tau_{i\infty}$(s)	E_i(eV)
I	6.25	7×10^{-2}	0.18
II	5	1.5×10^{-3}	0.34
III	7.5	2.0	0.15
IV	6.25	6.0×10^{-6}	0.48
V	3.75	3.0×10^{-2}	0.26

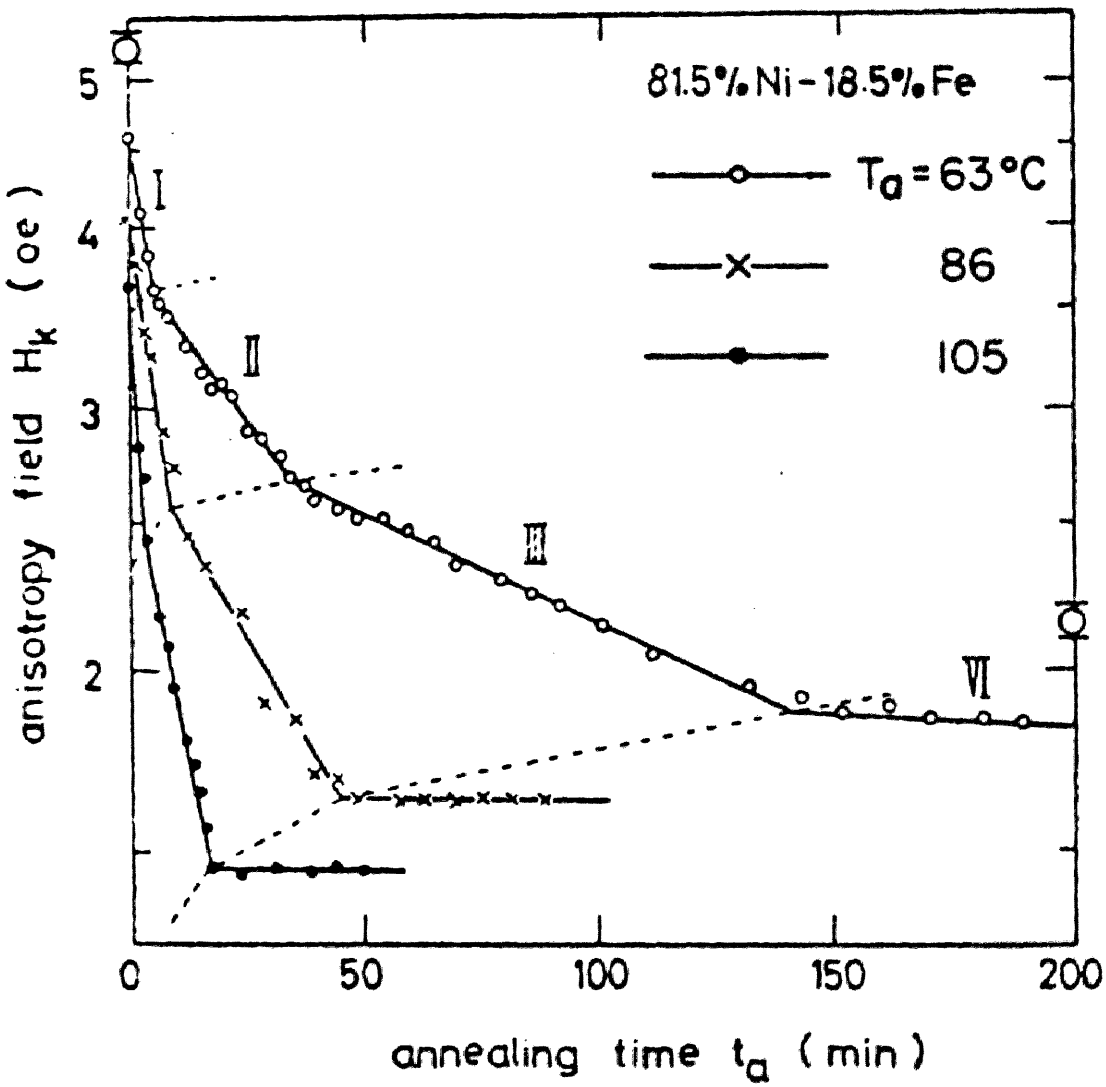

Fig. 1.3 Isothermal annealing curves of anisotropy field H_k in nonmagnetostrictive Permalloy films saturated along the HA.[18)]

At that time, the annealing stages with different activation energies were thought to correspond to the different anisotropy sources, for example, the directional order of lattice defects (interstitials, vacancies) involved in thin films with high concentration. Such anisotropies are, however, too hard to seek after, because $\tau_{i\alpha}$ is abnormally large for usual lattice defects. It was therefore thought that the anisotropy of nonmagnetostrictive films originate only in directional order of atom pairs, and that structural defects affect the reorientation process of atom pairs. From this point of view, the influence of structural defects on the anisotropy relaxation will be examined theoretically in chapter 2 and experimentally in chapters 3 and 4.

1.4 Outline of Magnetization Ripple

In an actual uniaxial film, the magnetization is not uniform in direction throughout the film, but it fluctuates quasi-periodically a few degrees around its average direction. This magnetization fluctuation is known as "magnetization ripple". The magnetization ripple is thought to originate in the local magnetic anisotropy associated with randomly oriented crystallites composing the film. The realized ripple is primarily longitudinal rather than transverse (Fig. 1.4) ; i.e., the wave front of the ripple is perpendicular rather than parallel to the average magnetization direction. This is because the longitudinal mode has lower magnetostatic energy. From the observation of Lorentz electron microscopy or magneto-optic microscopy, the ripple wave length and angle are estimated to be of the order of 1μ and 1°, respectively.

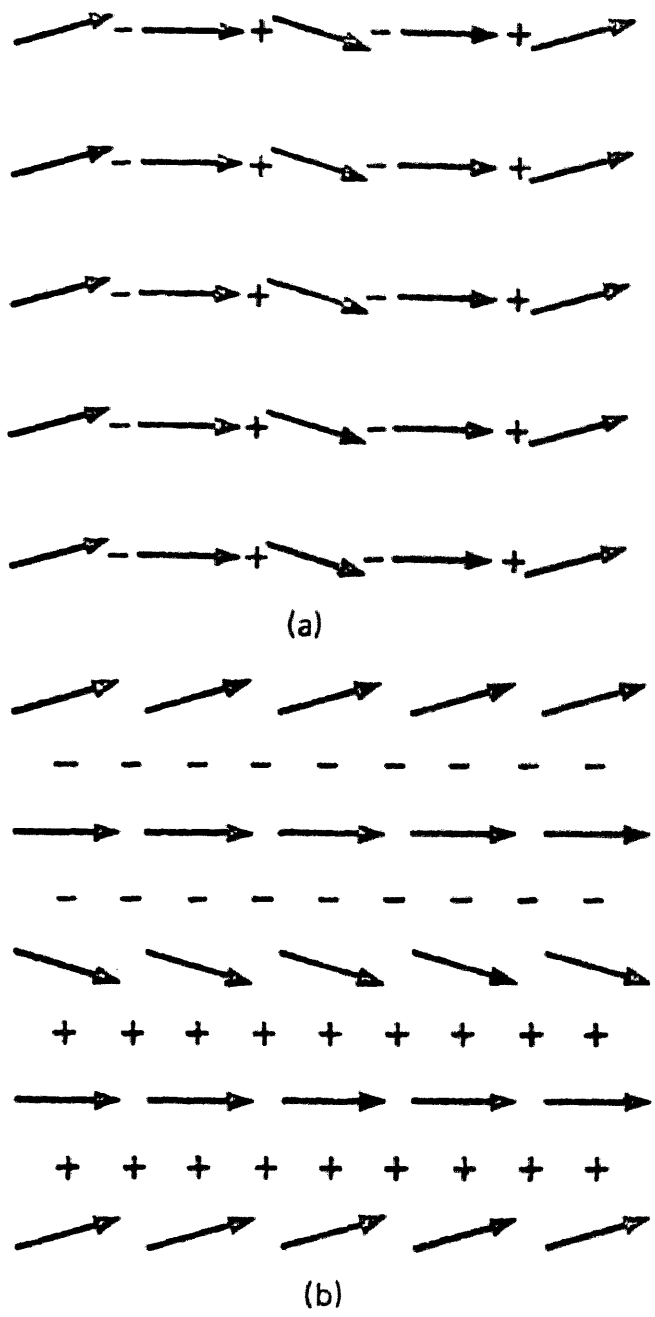

Fig. 1.4 Schematic illustration of local magnetization for (a) logitudinal and (b) transverse ripple configurations and their volume magnetic poles[22].

The first model to explain such properties dependent on ripple as HA domain splitting (Sec. 1.4.2), ripple hysteresis [23], initial susceptibility (Sec. 2.2) etc., was based on the dispersion of the anisotropy (Anisotropy-dispersion model or protodomain model [24]). This model has an advantage of computational simplicity since the Stoner-Wohlfarth model applies separately to each independent region named "protodomain": the EA of each protodomain slightly differs from the average EA, and film properties are easily obtained from the collection of such protodomains.

Since the anisotropy-dispersion model ignores the interaction among the protodomains, this model does not permit precise explanation of the ripple. The problems related to the ripple has therefore been approached by the use of a micromagnetic model. Successful micromagnetic ripple theories have been developed by Hoffmann [25-29] and Harte [22] independently.

1.4.1 Hoffmann's ripple theory

The local magnetization distribution in the film must be determined by the consideration of the free energy related to the local magnetization direction. The total free energy density E_t is given by

$$E_t = E_H + E_{Ku} + E_{ex} + E_K + E_{mag} \quad . \tag{1.8}$$

Here E_H is the field energy, E_{Ku} the uniaxial anisotropy energy, E_{ex} the exchange energy; E_k represents the local anisotropy energy which is associated with randomly oriented crystallites;

and E_{mag} is the energy originating in the stray field caused by the local magnetization fluctuation. It is E_{mag} term which causes the greatest mathematical difficulties in the micromagnetic approach. When E_t is expressed as a function of the direction of the local magnetization $\phi(r)$, then $\phi(r)$ is obtained by solving the variational problem of $\delta \int E_t(\phi(r))\, dr = 0$. According to Hoffmann's calculation, the rms value of ripple amplitude $\phi_1(r)$, which is defined by $\phi(r) = \phi_0(r) + \phi_1(r)$, is given by [26]

$$\langle \phi_1^2(r) \rangle^{\frac{1}{2}} = \frac{1}{8\pi\sqrt{2}} \frac{D^2 K^2 \sigma_1^2}{n} \cdot \frac{1}{M\sqrt{d}} (A K_u h)^{-\frac{3}{4}} . \qquad (1.9)$$

Here D is the diameter of crystallites, d the film thickness; K represents the effective crystalline anisotropy commonly called "local anisotropy", σ_1 the numerical constant depending on the symmetry of the crystalline anisotropy ($\sigma_1 = \sqrt{8/105}$ for the ordinal crystalline anisotropy), n the number of crystallites through the film thickness, and A the exchange stiffness.

1.4.2 HA domain splitting

When a magnetic field H much larger than H_k is applied parallel to the HA, the film is saturated in the field direction and the ripple is suppressed.

As the value of H is reduced, the ripple grows until HA domain splitting or fall-back begins at a "blocking field" which is slightly larger than H_k. As H decreases further, the local magnetization, which deviates to the right (left) side of the HA, rotates clockwise (counter-clockwise) toward the EA. Finally

the film is divided into an array of slender domains (Fig. 1.5). The Stoner-Wohlfarth model predicts only the uniform rotation of M and thus does not describe HA domain splitting. According to the anisotropy-dispersion model, ripple-inducing regions, having local easy axes distributed on either side of the average EA, are equally probable as shown in Fig. 1.6, so that when H is applied just parallel to the HA, equal numbers of domaines magnetized in clockwise and counterclockwise directions are produced, giving a vanishing EA remanence. However, when H is applied at an angle α to the right side of the HA, only in regions with easy axes, which deviate from the average EA direction by an angle greater than α , the magnetization rotates counter-clockwise and in all other regions clockwise, thus giving a remanence in the EA direction. As α increases, the counter-clockwise-domain density decreases and the EA remanence increases, until, when α is greater than the maxmum easy axis dispersion angle, all the domains rotate clockwise to the EA.

The domain splitting angle (angular dispersion) α_{90} , i.e. the field angle α giving 90% remanence is often quoted as a useful parameter for characterizing uniaxial films.

According to the micromagnetic ripple theory developed by Hoffmann [26], α_{90} is not a measure of the angular dispersion of the local EA, but is only an index of the magnetization ripple, namely, the quantative connection between the ripple angle and α_{90} is complicated. When H (or single domain field h_1) is reduced from the saturation, the ripple (local magnetization) reorients freely and the ripple angle increases monotonously as is given by eq. (1.8). When H reaches the blocking field,

Fig. 1.5 HA fallback revealed by Lorentz microscopy. Sample is saturated along the HA (vertical), after that HA field is reduced. [1)]

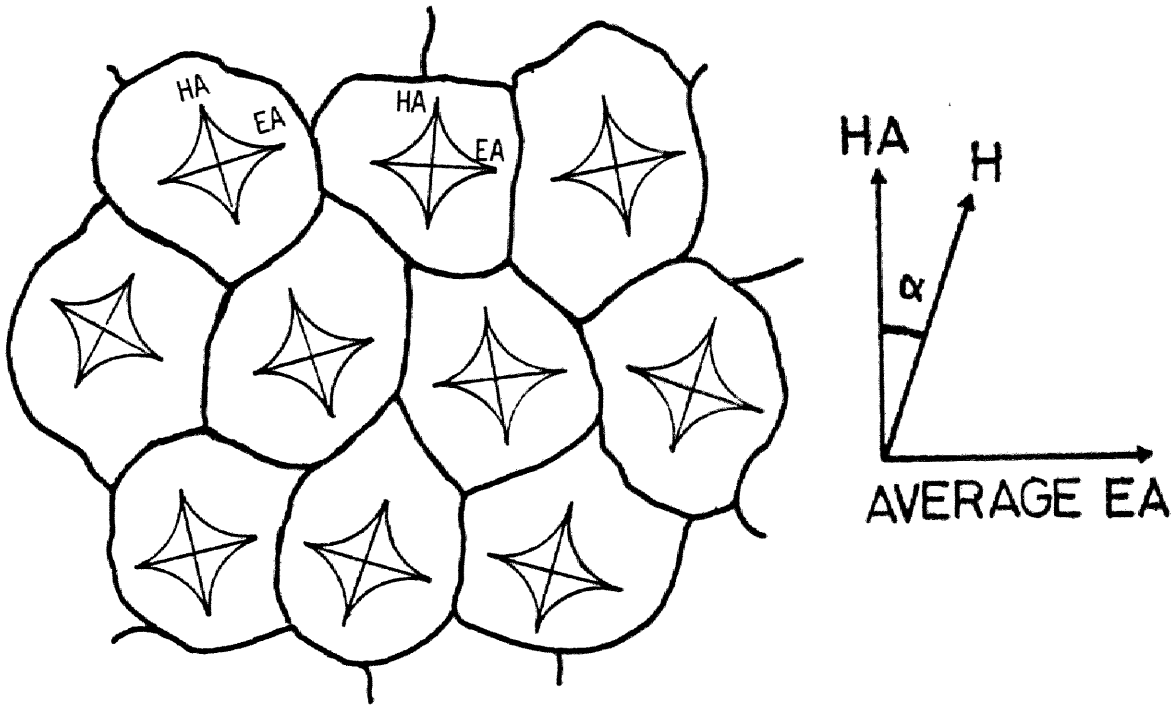

Fig. 1.6 Protodomains behaving independently with each other. The EA of each domain is distributed on the either side of arevage EA. Stoner-Wolfarth asteroid switching curve is applicable to each domain.

the ripple becomes unstable in the region where $\phi = 0$ (Fig. 1.7), and the ripple no longer reorients freely. If H is reduced below the blocking field, the magnetization in each region rotates toward the nearest EA direction. On the basis of this consideration, Hoffmann has deduced that α_{90} is proportional to K^2 (K : the local anisotropy constant). In chapter 5, this micromagnetic ripple (dispersion) theory will be experimentally examined and found to be reliable.

1.4.3 Origin of magnetization ripple

According to the Lorentz-microscopy investigation[30], the ripple vanishes in the film with the composition of vanishing magnetocrystalline anisotropy. This fact suggests that the ripple originates in the magnetocrystalline anisotropy. On the other hand, the magneto-optic observation of HA domain splitting[31] shows that α_{90} becomes minimum at the zeromagnetostrictive composition, supporting the magetostrictive origin. These conflicting results were well explained by the works of Uchiyama, Fujii et al.[32, 33], who observed small area of films in order to obtain local measurement of the fall back angle α_{90}. As shown in Fig. 1.8, both long-range ($\sim$ millimeters) and local ($\sim$ microns) contribution to α_{90} were found. The long-range contribution originates in the strain-magnetostriction, while the local portion originates in both the strain-magnetostriction and magnetocrystalline anisotropy. The latter conclusion was based on the local α_{90} vs. composition data at various deposition temperature T_d : As shown in Fig. 1.9, a minimum of

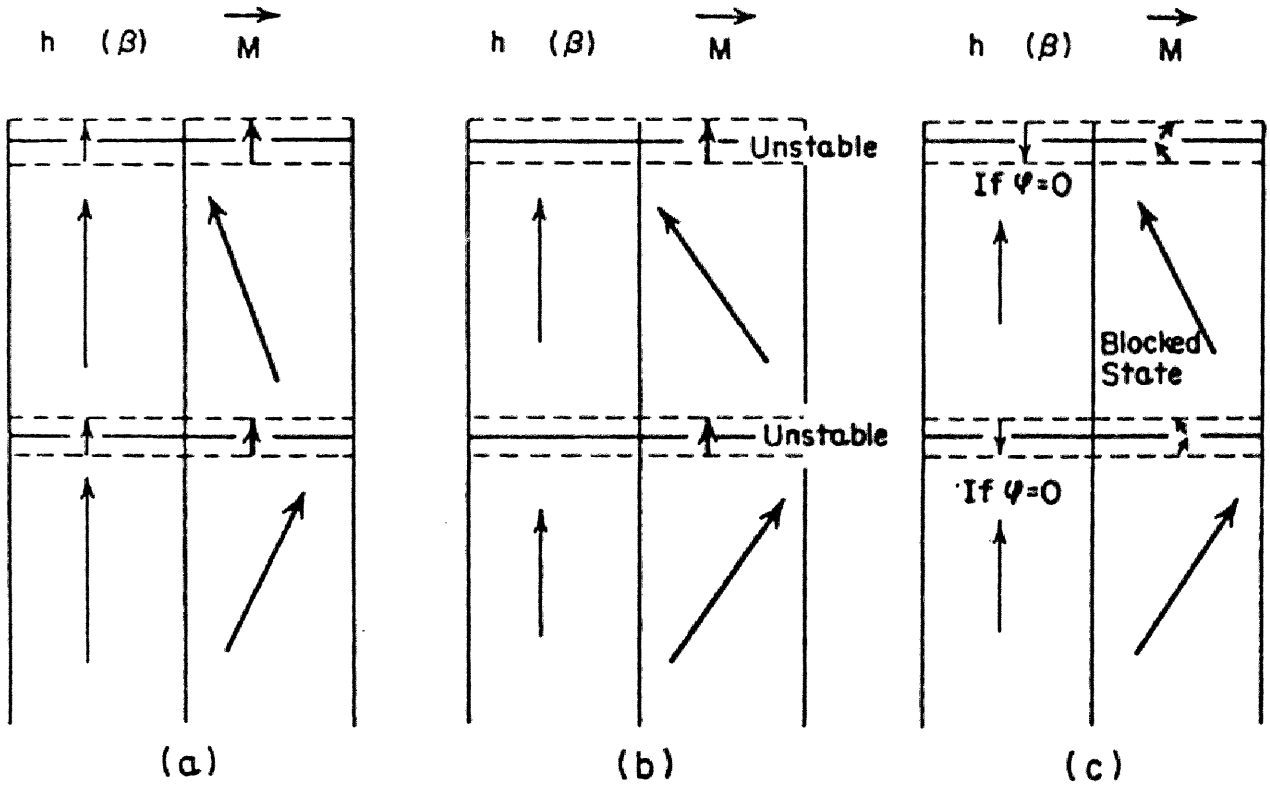

Fig. 1.7 Schematic illustration of local magnetization (right) and effective field (left) (a) before, (b) during and (c) after blocking.

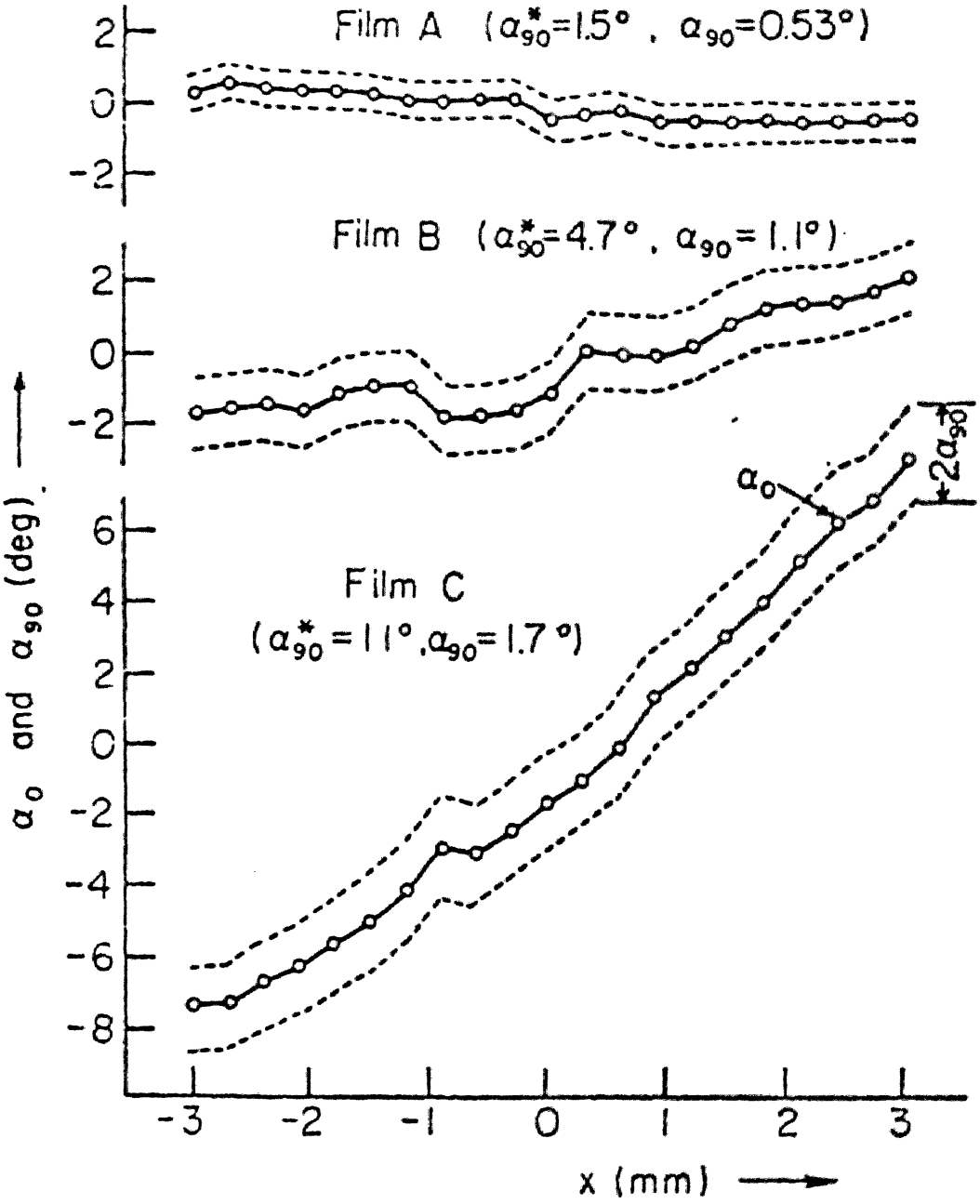

Fig. 1.8 Local HA direction α_0 and fallback angle α_{90} in small areas of Permalloy films observed along its average EA direction. Three films shown in figure are examples having largely different long-range dispersion α_{90}^*.

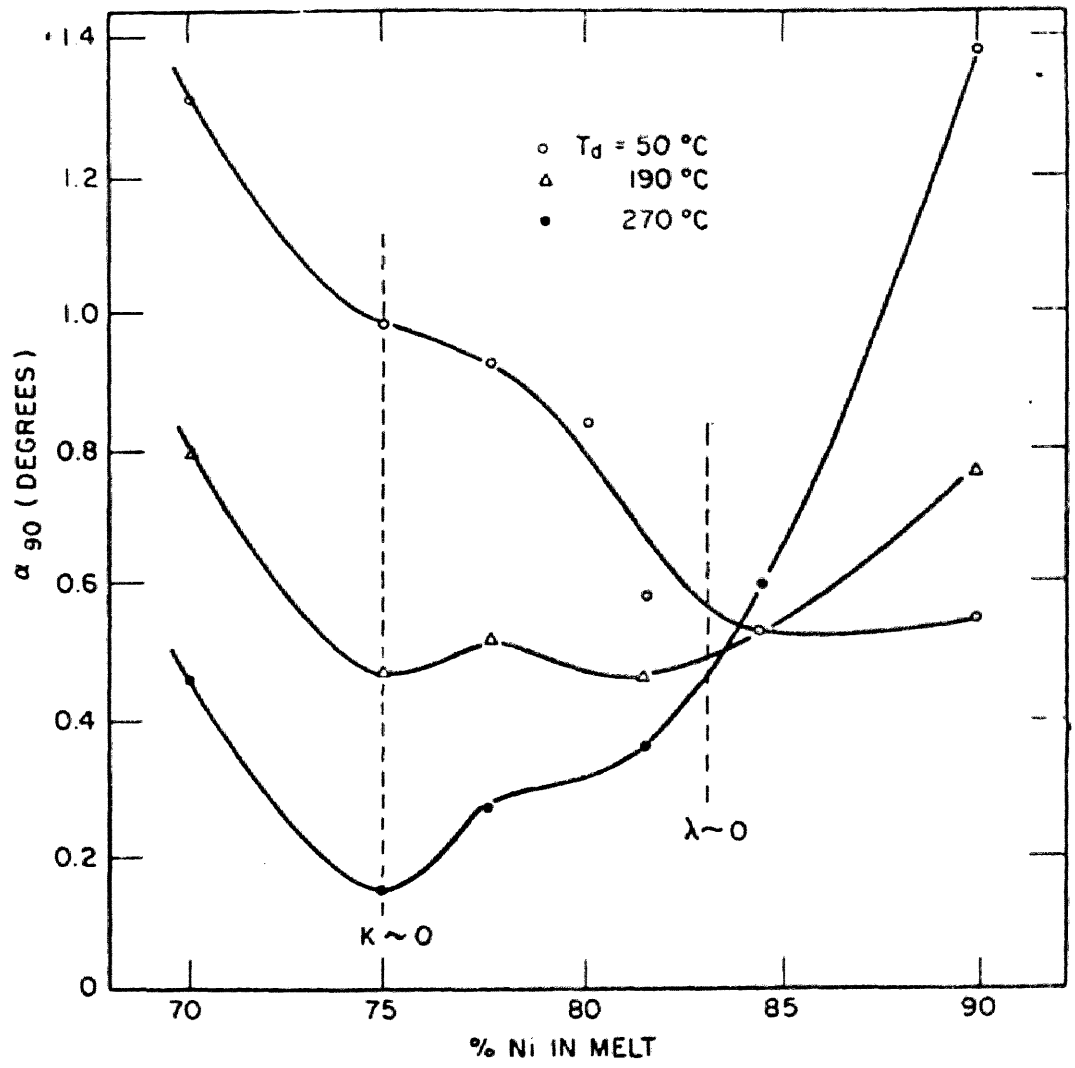

Fig. 1.9 Composition dependence of local fall back angle α_{90} in Ni-Fe films[32].

α_{90} is at 75%Ni (the composition for vanishing magnetocrystalline anisotropy) only when T_d is high enough to minimize the internal stress; otherwise the minimum is at 81%Ni (the composition for vanishing magnetostriction). Nevertheless, at that time quantitative agreement of their experimental results with Hoffmann's ripple theory was not obtained. In chapter 6, we will reexamine the α_{90} date more carefully and obtain satisfactory interpratations based on the micromagnetic model.

References

1) M. S. Cohen : Thin Film Phnomena (McGrow-Hill, New York, 1969) p.608.

2) J. I. Raffel, T.S. Crowther, A.H. Anderson and T. O. Herndon: Proc.IEEE 49 (1965) 155.

3) I. Danylchuk, J. T. Perneski and M. N. Sagel : 1964 Proc. New York, P.5-4-1.

4) M. Prutton : Thin Ferromagnetic Films (Butterworth, Washington, 1964)

5) M. S. Blois : J. appl. Phys. 26 (1955) 975.

6) S. Chikazumi : J. Phys. Soc. Japan, 11 (1965) 551.

7) A. Ferro, G. Gritta and G. Montalenti : IEEE Trans. Mag. MAG-2 (1966) 764.

8) L. Néel : J. Phys. Radium, 15 (1954) 225.

9) S. Taniguchi : Sci. Rep. Tohoku Univ. A7 (1955) 269.

10) S. Chikazumi and T. Omura : J. Phys. Soc. Japan, 10 (1955) 842.

11) G. Robinson : J. Phys. Soc. Japan, 17 (Suppl. B-I) (1962) 588.

12) F. G. West : J. appl. Phys. 33 (1964) 1827.

13) M. Takahashi, D. Watanabe, T. Kōno and S. Ogawa : J. Phys. Soc. Japan, 15 (1960) 1351.

14) N. T. Siegle and W. R. Beam : J. appl. Phys. 36 (1965) 1721.

15) C. H. Wilts : Basic Problems in Thin Film Physics (Vanderhoech und Ruprecht, Götingen, 1966) p422.

16) G. Kneer and W. Zinn : Proc. Internat. Symp. for Basic Problems in Thin Film Physics Clausthal-Göttingen (Vanderhoeck und Reprecht, Göttingen, 1965) p.437.

17) D. O. Smith, G. P. Weiss and K. J. Harte : J. appl. Phys. 37 (1966) 1464.

18) T. Fujii, S. Uchiyama, M. Masuda and Y. Sakaki : IEEE Trans. Mag. MAG-4 (1968) 515.

19) H. W. Wiedenmann and H. Hoffmann : IEEE Trans. Mag. MAG-5 (1969) 506.

20) E. T. Ferguson : J. appl. Phys. 29 (1958) 252.

21) E. Walsöe and G. Panpillo : Acta metallurgica 15 (1967) 1263.

22) K. J. Harte : J. appl. Phys. 39 (1968) 1803.

23) M. S. Cohen : IEEE. Trans. Mag. MAG-1 (1965) 156.

24) H. Oredson and E. Torok : J. appl. Phys. 36 (1965) 950.

25) H. Hoffmann : Phys. Kondens. Materie 2 (1964) 32.

26) H. Hoffmann : J. appl. Phys. 35 (1964) 1790.

28) H. Hoffmann : IEEE Trans. Mag. MAG-2 (1966) 560.

29) H. Hoffmann : IEEE Trans. Mag. MAG-4 (1968) 32.

30) T.Suzuki and C. H. Wilts : J. appl. Phys. 39 (1968) 1151.

31) H. Hoffmann and M. Okon : Z. Angew. Phys. 21 (1966) 406

32) S. Uchiyama, T. Fujii, M. Masuda and Y. Sakaki : Japan J. appl. Phys. 6 (1967) 512.

33) T. Fujii, S. Uchiyama, M. Masuda and Y. sakaki : Japan J. appl. Phys. 6 (1967) 1.

Chapter 2

Theory of Relaxation Process for Pair—Order Anisotropy

2.1 Introduction

For the purpose of elucidating the origin of the M-induced anisotropy in Permalloy films, the anisotropy relaxation has been widely studied from the experimental side [1-5]. However, none of theories except by Iwata and Hagedorn [1] have been formulated on the kinetics of the directional pair-order.

In most of magnetic annealing studies [1-8], the relaxation process of the M-induced anisotropy K_u was assumed to be the first order chemical reaction as given by

$$\frac{dK_u}{dt} = -\nu_k (K_u - K_u^e) \qquad (2.1)$$

where ν_k is the relaxation frequency and K_u^e the equilibrium value of K_u.

Iwata et al. [1] calculated the relaxation frequency for the directional pair-order anisotropy in the following manner. Atom pairs composed of two Fe atoms can take six different nearest neighbour directions, but never be decomposed or created during the relaxation process. Then, the orientation of the pairs takes place only when the Fe atom exchanges its position with a vacancy on one of four common nearest neighbour sites (Fig. 2.1).
By counting up such reorientation processes, one obtains the relaxation time τ_k (or the relaxation frequency $\nu_k = \tau_k^{-1}$).
In the case of polycrystalline films, ν_k is given by

$$\nu_k = 8 C_v \nu_o \exp(-E_m / K_B T_a) \qquad (2.2)$$

where C_v is the vacancy concentration, ν_0 the average frequency of

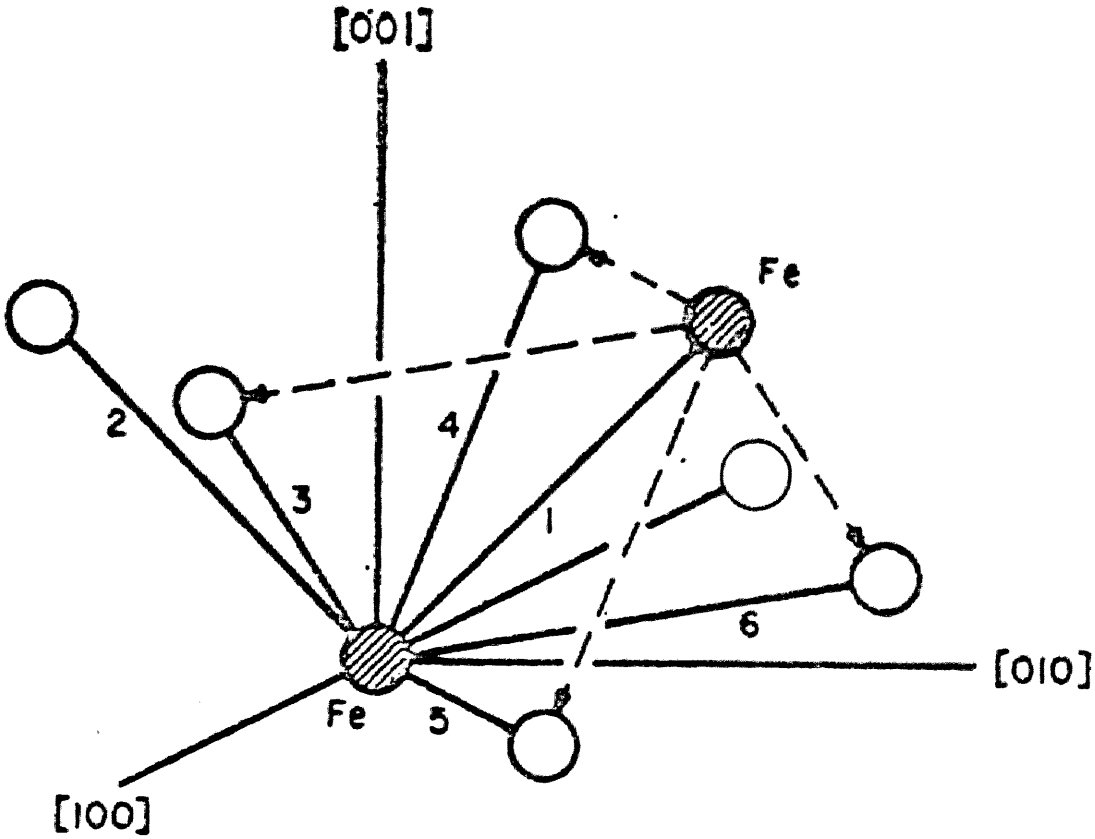

Fig. 2.1 Six nearest neighbor directions and elementaly processes for the atom pair reorientation in f.c.c. crystals. The Fe-Fe atom pair changes its direction from 1 to 2,3,5 or 6 by a jump (indicated by lines) of the Fe atom.

the lattice vibration, E_m the activation energy for the vacancy migration, and T_a the annealing temperature.

Equation (2.2), however, is based on such a simplification that the decomposition and creation of atom pairs are neglected. Actually, three kinds of elementary processes are conceivable for the f.c.c. lattice as shown in Fig. 2.2. On the other hand, the calculation of Iwata et al. involves only one of these three processes. Thus, in this chapter, we will derive more generalized expression for the relaxation frequency. This theory is based on the same model with Redelaar's [6] which deals with the isotropic short-range order.

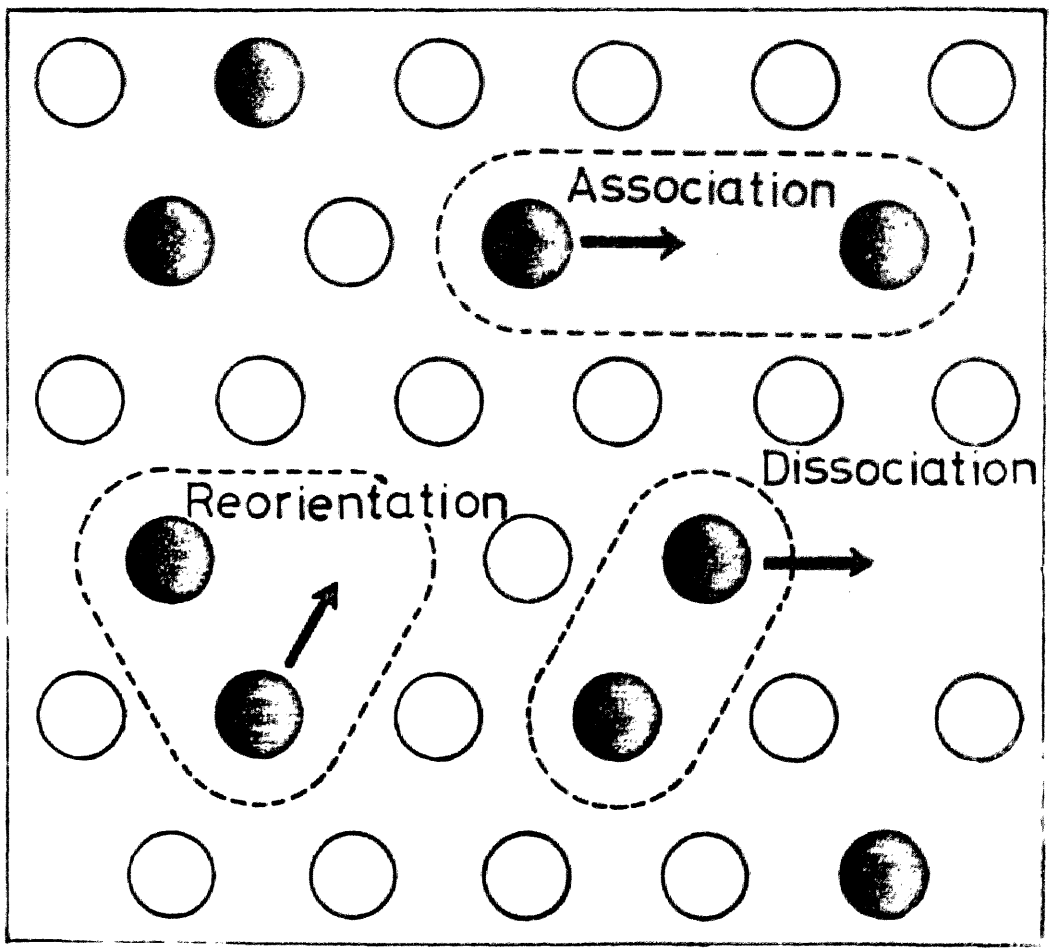

Fig. 2.2 Three types of elementary processes for the atom-pair reorientation conceivable in(111) plain of the f.c.c. lattice.

2.2 Ordering Process of Atom Pairs

2.2.1 Probabilities of finding the ordered arrangements of atoms

The cubic crystal of the binary AB-alloy containing no long-range ordered arrangement is considered. The lattice of the alloy consists of A-atoms, B-atoms, and vacancies, their concentrations being C_A, C_B, and C_V, respectively. Let the suffix i denote the direction of atom pairs and p_{XYi} (X=A, B, or V, Y=A, B, or V) be the directional pair probability that the nearest neighbour (NN)-sites of a X-atom in the ith direction are occupied by a Y-atom. Then following relations exist evidently among these probabilities.

$$p_{XAi}+p_{XBi}+p_{XVi}=1,\left(i=1,2,\cdots,\frac{z}{2}\right) \tag{2.3}$$

and

$$c_X p_{XYi}=c_Y p_{YXi},\left(i=1,2,\cdots,\frac{z}{2}\right) \tag{2.4}$$

where z is the coordination number, and X, as well as Y, is regarded as A, B, or V. Assuming that C_V, p_{AVi}, p_{BVi}, $p_{VVi} \ll 1$, any directional pair probability can be represented in terms of p_{AAi} and p_{VAi} from eqs. (2.3) and (2.4) as follows:

$$p_{ABi}\simeq 1-p_{AAi}\,, \tag{2.5a}$$

$$p_{AVi}\simeq \frac{C_V}{C_A}\,p_{VAi}\,, \tag{2.5b}$$

$$p_{BAi}\simeq \frac{C_A}{1-C_A}(1-p_{AAi})\,, \tag{2.5c}$$

$$p_{BBi}\simeq 1-\frac{C_A}{1-C_A}(1-p_{AAi})\,, \tag{2.5d}$$

$$p_{BVi} \simeq \frac{C_V}{1-C_A}(1-p_{VAi}) , \tag{2.5e}$$

and

$$p_{VBi} \simeq 1-p_{VAi} . \tag{2.5f}$$

Then, we express the probability of finding any ordered arrangement of atoms in terms of directional pair probabilities. Since the arrangement of atoms in cubic crystals is not one-dimensional, the probability of finding a three-dimensional arrangement can not be well represented by pair probabilities. The probability for the three-dimensional case, however, can be represented approximately by extending the method of the one dimensional case. When we pick up any n-linked group of sites in one-dimensional lattice, the probability of finding the group of atoms, X_1, X_2, ·····, X_n arranged in order of the subscript, is given by:

$$P(X_1, X_2, \cdots, X_n) = C_{X_1} \prod_{\xi=1}^{n-1} p_{X_\xi X_{\xi+1}} = \prod_{\xi=1}^{n} C_{X_\xi} \prod_{\xi=1}^{n-1} p'_{X_\xi X_{\xi+1}} , \tag{2.6}$$

where X_ξ represents either of A, B, or V, and $p_{X_\xi X_{\xi+1}}$ the probability of finding a $X_{\xi+1}$-atom at the NN-site of X_ξ-atom, and $p'_{X_\xi X_{\xi+1}}$ is defined by the following equation.

$$p'_{X_\xi X_{\xi+1}} = p'_{X_{\xi+1} X_\xi} = \frac{p_{X_\xi X_{\xi+1}}}{C_{X_{\xi+1}}} = \frac{p_{X_{\xi+1} X_\xi}}{C_{X_\xi}} = \left(\frac{p_{X_\xi X_{\xi+1}} p_{X_{\xi+1} X_\xi}}{C_{X_\xi} C_{X_{\xi+1}}} \right)^{1/2} . \tag{2.7}$$

In applying eq. (2.6) to the cubic lattice, the last expression of eq. (2.6) can be generalized as

$$P(X_1, X_2, \cdots, X_n) = \prod_{\xi=1}^{n} C_{X_\xi} \prod_{(X_\xi, X_\eta)} p'_{X_\xi X_\eta} = \prod_{\xi=1}^{n} C_{X_\xi} \prod_{(X_\xi, X_\eta)} \left(\frac{p_{X_\xi X_\eta} p_{X_\eta X_\xi}}{C_{X_\xi} \cdot C_{X_\eta}} \right)^{1/2} , \tag{2.8}$$

where $\prod_{(X_\xi, X_\eta)}$ is the product over the closest pairs. Replacing the

pair probability $p_{X_\xi X_\eta}$ in eq.(2.8) by the directional pair probability p_{XY_i} above defined, the probability of finding an ordered arrangement in the cubic lattice is given in terms of C_A, C_V, p_{AA1} p_{AA2}, $\cdots\cdots$, $p_{AA\frac{z}{2}}$, p_{VA1}, p_{VA2}, $\cdots\cdots$, $p_{VA\frac{z}{2}}$.

2.2.2 Migration Energies of Atoms

The interaction energy for a closest pair of atoms is determined by the kind of constituent atoms and the angle between the direction of the pair and that of the magnetization. The interaction energy is assumed to be given by

$$E_X(Y,i)=U_{XY}+L_{XY}\left(\cos^2\alpha_i-\frac{1}{3}\right), \tag{2.9}$$

where U_{XY} is the interaction energy for XY-pairs which does not depend on the direction of the magnetization, L_{XY} is the pseudo-dipolar interaction energy for XY-pairs, and α_i is the angle between the ith direction and that of the magnetization. Then, the activation energy for the X-atom to migrate toward a vacancy, which is surrounded by Y_1, Y_2, $\cdots\cdots$, Y_{z-1}-atoms, is given by:

$$E_X^M(Y_1,Y_2,\cdots,Y_{z-1})=V_X^S-\sum_{\xi=1}^{z-1}E_X(Y_\xi,i_\xi), \tag{2.10}$$

where V_X^S is the saddle point energy for the X-atom during the migration, and i_ξ is the direction of the XY_ξ-pair. If we assume that the saddle point energy is not influenced by the kind of the atoms surrounding the saddle point, in the case of the pure metal consisting of X-atoms alone, the migration energy averaged over the directions is given by:

$$E_X^M=V_X^S-(z-1)U_{XX}. \tag{2.11}$$

In AB-alloys the migration energy toward the vacancy in the jth direction is generally given by:

$$E_A^M(Y_1, Y_2, \cdots, Y_{s-1})$$
$$= E_A^M - \sum_{\xi} {}_B \left\{ U_A + L_A \left(\cos^2 \alpha_{i\xi} - \frac{1}{3} \right) \right\} + L_{AA} \left(\cos^2 \alpha_j - \frac{1}{3} \right), \qquad (2.12a)$$

for A-atoms and

$$E_B^M(Y_1, Y_2, \cdots, Y_{s-1})$$
$$= E_B^M - \sum_{\xi} {}_A \left\{ U_B + L_B \left(\cos^2 \alpha_{i\xi} - \frac{1}{3} \right) \right\} + L_{BB} \left(\cos^2 \alpha_j - \frac{1}{3} \right), \qquad (2.12b)$$

for B-atoms, where $\sum_{\xi} {}_A$, $\sum_{\xi} {}_B$ are the summations over the NN-sites of the migrating atom, only when they are occupied by the A-atom and the B-atom respectively, and notations are replaced as

$$U_A = U_{AB} - U_{AA}, \qquad (2.13a)$$

$$U_B = U_{AB} - U_{BB}, \qquad (2.13b)$$

$$L_A = L_{AB} - L_{AA}, \qquad (2.13c)$$

and

$$L_B = L_{AB} - L_{BB}. \qquad (2.13d)$$

Therefore the jump frequencies of A- and B-atoms at the temperature T are given respectively by

$$\nu_A^M(Y_1, Y_2, \cdots, Y_{s-1}) = \nu_A \exp(-E_A^M / k_B T) \cdot l_{AAj}^{-1} \prod_{\xi} {}_B u_A l_{Ai\xi}, \qquad (2.14a)$$

and

$$\nu_B^M(Y_1, Y_2, \cdots, Y_{s-1}) = \nu_B \exp(-E_B^M / k_B T) \cdot l_{BBj}^{-1} \prod_{\xi} {}_A u_B l_{Bi\xi}, \qquad (2.14b)$$

where ν_A and ν_B are frequency factors of the lattice vibration for A-atoms and B-atoms respectively, k_B is Boltzmann's constant, $\prod_{\xi} {}_A$, $\prod_{\xi} {}_B$ are the products over the NN-sites of the migrating atom in the same way as described for the case of $\sum_{\xi} {}_A$, $\sum_{\xi} {}_B$, and

$$u_X = \exp(U_X / k_B T), \ (X = A, B) \qquad (2.15)$$

$$l_{Xi}=\exp\left\{L_X\left(\cos^2\alpha_i-\frac{1}{3}\right)\Big/k_BT\right\}, \quad (X=A,\ B) \tag{2.16}$$

and

$$l_{XXi}=\exp\left\{L_{XX}\left(\cos^2\alpha_i-\frac{1}{3}\right)\Big/k_BT\right\}. \quad (X=A,\ B) \tag{2.17}$$

2.2.3 Thermal Equilibrium of Atom Pair Probabilities

In order to obtain rate equations for the numbers of directional atom pairs, we consider the arrangement of atoms which involves a vacancy, as shown in Fig. 2.3. In this figure, X(=A or B) is a migrating atom, V is a vacancy, and Y_1, Y_2, ·····, $Y_{z+z'-1}$(=A or B) are atoms occuping the NN-sites of X or V. Solid lines connect X(or V) with its NN-atoms. Notations beside the lines, i_1, i_2, ····, $i_{z+z'-1}$, indicate the directions of atom pairs connected with the lines. We call briefly such arrangement as shown in Fig.2.3 as the MVNN-arrangement hereafter.

The migration frequency of X, and the change of numbers of any directional pairs resulting from the migration of X, depend on what kind of atoms occupy the NN-site of X and V, namely Y_1, Y_2, ····, $Y_{z+z'-1}$. If a different ensemble of the atom occupation in the MVNN-arrangement is written in character I to distinguish it from the others, then the time rates of change of the total numbers of AA- and VA-pairs in any direction are given respectively by

$$\frac{d}{dt}N_{AAi}=NC_A\frac{d}{dt}p_{AAi}=N\sum_I D_{AAi}(I)\nu(I)P(I) \tag{2.18}$$

for AA-pairs and

$$\frac{d}{dt}N_{VAi}=NC_A\frac{d}{dt}p_{VAi}=N\sum_I D_{VAi}(I)\nu(I)P(I) \tag{2.19}$$

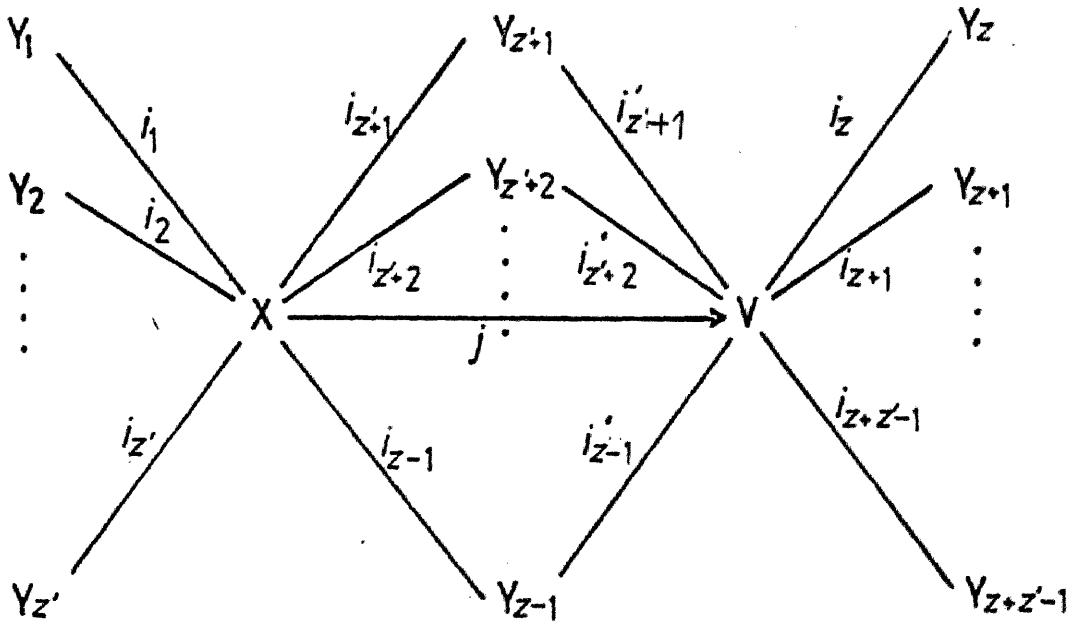

Fig. 2.3 General expression of the MVNN-arrangement in the cubic lattice. (See Sec.2.2.3)

for VA-pairs, where N is the total number of lattice sites in the unit volume of the alloy; $\nu(I)$ is the migration frequency of X in the MVNN-arrangement I; $D_{AAi}(I)$ and $D_{VAi}(I)$ are respectively the change of numbers of AA- and VA-pairs in the ith direction resulting from the migration; and $P(I)$ is the probability of finding the MVNN-arrangement I. The factor N in the last expression of eqs.(2.18) and (2.19) is introduced since there exist N groups of sites where the arrangement specified by I can be located. In eqs.(2.18) and (2.19), $\nu(I)$ and $P(I)$ can be calculated from eqs.(2.8) and (2.14) respectively but, since $P(I)$ contains higher degree terms of directional pair probabilities, eqs.(2.18) and (2.19) are simultaneous nonlinear differential equations.

Though the equilibrium values of directional pair probabilities can be calculated from algebraic eqs.(2.18) and (2.19) by putting $\frac{d}{dt}N_{AAi}=\frac{d}{dt}N_{VAi}=0$, they are obtained more easily by considering the detailed balance as follows. Let us consider the equilibrium between one MVNN-arrangement I and the other arrangement I'. The arrangement I' is created by exchanging X and V in the arrangement I. Since the transition probability from the state I to I' is $\nu(I)$, the conditions of the detailed balance are obtained from eqs.(2.8) and (2.14).

$$P(I)\nu(I)-P(I')\nu(I')$$

$$\propto\Big(\prod_{\xi=1}^{z'}{}_A\, p_{AAi\xi}\prod_{\xi=z'+1}^{z-1}{}_A\, p_{AAi\xi}p_{VAi'\xi}\prod_{\xi=z}^{z+z'-1}{}_A\, p_{VAi\xi}\prod_{\xi=1}^{z'}{}_B\, p_{ABi\xi}u_A{}^{l}{}_{Ai\xi}\prod_{\xi=z'+1}^{z-1}{}_B\, p_{ABi\xi}u_A{}^{l}{}_{Ai\xi}p_{VBi'\xi}\prod_{\xi=z}^{z+z'-1}{}_B\, p_{VBi\xi}\Big)$$

$$-\Big(\prod_{\xi=1}^{z'}{}_A\, p_{VAi\xi}\prod_{\xi=z'+1}^{z-1}{}_A\, p_{VAi\xi}p_{AAi'\xi}\prod_{\xi=z}^{z+z'-1}{}_A\, p_{AAi\xi}\prod_{\xi=1}^{z'}{}_B\, p_{VBi\xi}\prod_{\xi=z'+1}^{z-1}{}_B\, p_{VBi\xi}p_{ABi'\xi}u_A{}^{l}{}_{Ai'\xi}\prod_{\xi=z}^{z+z'-1}{}_B\, p_{ABi\xi}u_A{}^{l}{}_{Ai\xi}\Big)$$

$$=\prod_{i=1}^{z/2}\{P_{AA_i}^{a_i}\cdot(p_{AB_i}u_{A_i}l_{A_i})^{b_i}P_{AA_i}^{a'_i}\cdot(p_{AB_i}u_{A_i}l_{A_i})^{b'_i}\cdot P_{VA_{i'}}^{a'_i}\cdot P_{VB_{i'}}^{b'_i}\cdot P_{VA_i}^{a''_i}\cdot P_{VB_i}^{b''_i}\}$$

$$-\prod_{i=1}^{z/2}\{P_{VA_i}^{a_i}\cdot P_{VB_i}^{b_i}\cdot P_{VA_i}^{a'_i}\cdot P_{VB_i}^{b'_i}\cdot P_{AA_{i'}}^{a'_i}(p_{AB_{i'}}u_Al_{A_{i'}})^{b'_i}\cdot P_{AA_i}^{a''_i}\cdot(p_{AB_i}u_{A_i}l_{A_i})^{b''_i}\}=0 \quad (2.20a)$$

for X=A, and

$$P(I)v(I)-P(I')v(I')$$

$$\propto\prod_{i=1}^{z/2}\{P_{B}^{b_i}{}_{B_i}\cdot(p_{BA_i}u_{B_i}l_{B_i})^{a_i}\cdot P_{B}^{b'_i}{}_{B_i}\cdot(p_{BA_i}u_{B_i}l_{B_i})^{a_{i'}}\cdot P_{V}^{b_{i'}}{}_{B_{i'}}\cdot P_{V}^{a_i}{}_{A_{i'}}\cdot P_{V}^{b''_i}{}_{B_i}\cdot P_{V}^{a''_i}{}_{A_i}\}$$

$$-\prod_{i=1}^{z/2}\{P_{V}^{b_i}{}_{B_i}\cdot P_{V}^{a_i}{}_{A_i}\cdot P_{V}^{b'_i}{}_{B_i}\cdot P_{V}^{a'_i}{}_{A_i}\cdot P_{B}^{b'_i}{}_{B_{i'}}\cdot(p_{BA_{i'}}u_Bl_{B_{i'}})^{a_{i'}}\cdot P_{B}^{b''_i}{}_{B_i}\cdot(p_{BA_i}u_{B_i}l_{B_i})^{a''_i}\}=0 \quad (2.20b)$$

for X=B. In eqs. (2.20a) and (2.20b) a_i is the number of XA(or VA)-pairs of the ith direction among the pairs of XY_1, XY_2,$\cdots\cdot$, $XY_{z'}$(VY_1, VY_2,$\cdots\cdot$,VY_z) in the arrangement I (I'), and b_i is that of XB(VB)= pairs. In the same way, a'_i and b'_i are for $Y_{z'+1}$, $Y_{z'+2}$,$\cdots\cdot$, Y_{z-1}; and a''_i and b''_i are respectively the number of VA(XA)- and VB(XB)-pairs for Y_z, Y_{z+1},$\cdots\cdot$, $Y_{z+z'-1}$. If directional pair probabilities satisfy the following eqs.(2.21a) and (2.21b), then eq.(2.20a) holds.

$$p_{ABi}p_{VAi}u_A l_{Ai}=p_{AAi}p_{VBi}\ , \tag{2.21a}$$

and

$$p_{ABi}p_{AAi'}p_{VAi}p_{VBi'}l_{Ai}=p_{AAi}p_{ABi'}p_{VBi}p_{VAi'}l_{Ai'}\ . \tag{2.21b}$$

In the same way following eqs. (2.22a) and (2.22b) are derived from eq.(2.20b);

$$p_{BAi}p_{VBi}u_B l_{Bi}=p_{BBi}p_{VAi}\ , \tag{2.22a}$$

and

$$p_{BAi}p_{BBi'}p_{VBi}p_{VAi'}l_{Bi}=p_{BBi}p_{BAi'}p_{VAi}p_{VBi'}l_{Bi'}\ . \tag{2.22b}$$

Solving eqs. (2.21a) and (2.22a) for p_{AAi} by using eq(2.5), we obtain the equilibrium value of p_{AAi}.

$$p^{\circ}_{AAi}=\frac{1+r(2w_i-1)-\{1+r^2+2r(2w_i-1)\}^{1/2}}{2r(w_i-1)}\ , \tag{2.23}$$

where

$$r=\frac{C_A}{C_B}\ , \tag{2.24}$$

and

$$w_i=u_A u_B l_{Ai}l_{Bi}\ . \tag{2.25}$$

This expression also satisfies eqs. (2.21b) and (2.22b) and is equivalent to what was used in Néel's theory.

2.2.4 Directional Ordering Process of Atom Pairs in Dilute Alloy

When the concentration of the A-atom is very low, eqs.(2.18) and (2.19) can be linearized and solved easily. In the case where the migration frequency of the A-atom and that of the B-atom are nearly of the same order, namely,

$$\nu_A \exp(-E_A^M/k_B T) \simeq \nu_B \exp(-E_B^M/k_B T) , \tag{2.26}$$

the MVNN-arrangement that contains the smaller number of A-atoms, contributes to the whole ordering process. Thus we consider MVNN-arrangements which contain only one or two A-atoms, and make further assumptions that AA-pairs vary in the arrangement containing two A-atoms and that VA-pairs vary only in the arrangement containing one A-atom. Then the MVNN-arrangements which contribute to the process in the dilute alloy, are grouped as shown in Fig. 2.4 In the figure all sites, where the occupation of atoms are not specified, are filled with B-atoms. In the arrangement J=1~4, the numbers of directional AA-pairs vary, while in the arrangement J= 5~8, those of VA-pairs vary. Since we deal with the dilute alloy, we put

$$p_{ABi} = p_{BBi} = p_{VBi} = C_B = 1, \ (i = 1, 2, \cdots, z/2) , \tag{2.27}$$

Then, eq.(2.19) becomes

$$\frac{d}{dt} p_{VAi} = \nu_B \exp(-E_B^M/k_B T) \{ \sum_{J=5,8} \{ (C_A u_B l_{Bi} l_{BBJ} - p_{VAi} l_{BBJ}) + \sum_{J=7,8} (p_{VAi'} u_B l_{Bi} l_{BBJ} - p_{VAi} u_B l_{Bi'} l_{BBJ}) \} , \tag{2.28}$$

where $\sum_{J=5,6}$ etc. are the summation over the all possible arrangements

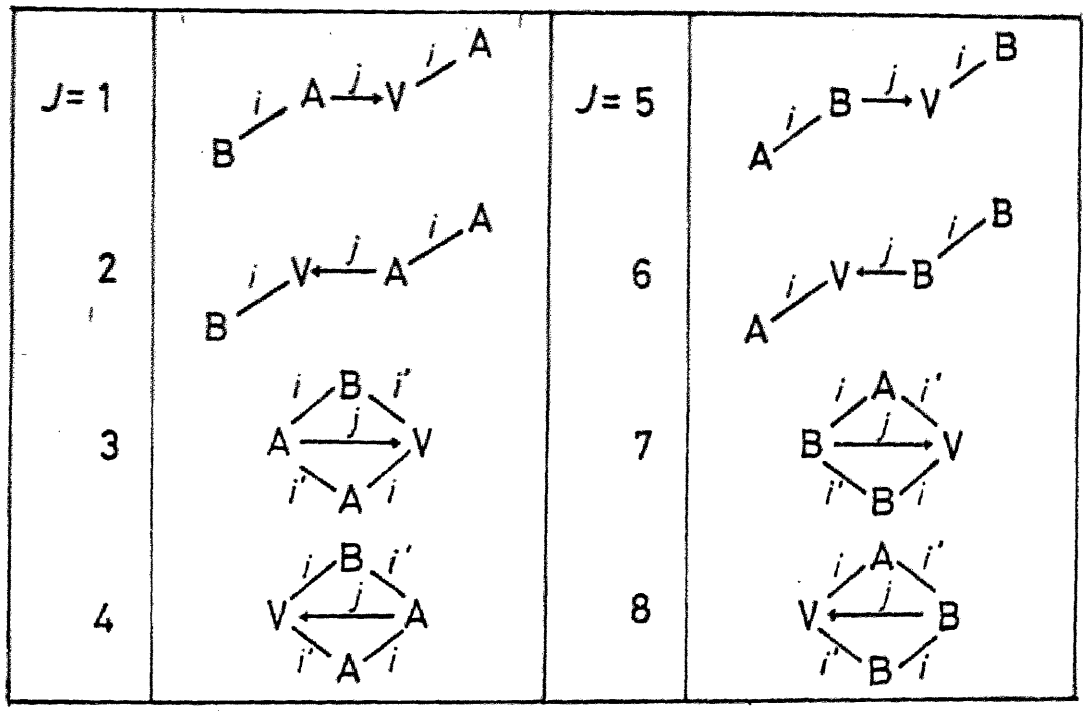

Fig. 2.4 Possible MVNN-arrangements which give rise to the relaxation of the directional pair-order anisotropy in dilute alloys.

with J=5,6 etc. The relaxation frequency of the ordering process of VA-pairs is approximately $\nu_B \exp(-E_B^M/k_BT)$, and on the other hand, the relaxation frequency for AA-pairs, as will be described later, is approximately $C_V \nu_A \exp(-E_A^M/k_BT)$. Therefore, if eq.(2.26) holds, the ordering process of VA-pairs finishes sooner than that of AA-pairs by a factor, C_V. Consequently, in calculating the ordering process of AA-pairs, we can replace p_{VAi} with its equilibrium value. When $L_{XY}/k_BT \ll 1$, the equilibrium value of p_{VAi} is given from eq.(2.28) as

$$p^e_{VAi} = C_A u_B (1+\delta_{Bi}) , \tag{2.29}$$

where

$$\delta_{Bi} = \frac{L_B}{k_B T}\left(\cos^2\alpha_i - \frac{1}{3}\right) . \tag{2.30}$$

Then we divide p_{AAi} into two components as follows:

$$p_{AAi} = p_{AA} + \Delta p_{AAi} , \tag{2.31}$$

where p_{AA} is the average value of p_{AAi} with respect to the direction of the pairs and Δp_{AAi} is the deviation of p_{AAi} from p_{AA}. If p_{VAi} is equal to its equilibrium value given by eq.(2.29) and $\Delta p_{AAi} \ll p_{AA}$, then rate equations for AA-pairs are given from eqs.(2.8), (2.14), and (2.18) as follows:

$$\frac{d}{dt} p_{AA} = 2z' C_V \nu_{AA} (C_A u_A u_B - p_{AA}) , \tag{2.32}$$

$$\frac{d}{dt} \Delta p_{AAi} = 2C_V \nu_{AA} \{ z' (p_{AA}\delta_{Ai} + C_A u_A u_B \delta_{Bi} - \Delta p_{AAi}) - (C_A u_A u_B - p_{AA})(\delta_{ABi} - \delta_{Bi}) \} \tag{2.33a}$$

for s.c. and b.c.c, and

$$\frac{\mathrm{d}}{\mathrm{d}t}\Delta p_{AA}=2C_V\nu_{AA}\{(z'+u_B\mathbf{R})(p_{AA}\delta_A-\Delta p_{AA})$$
$$+(z'C_Au_Au_B+u_B\mathbf{R}p_{AA})\delta_B+(C_Au_Au_B-p_{AA})\mathbf{S}(\delta_{AB}+\delta_B) \quad (2.33b)$$

for f.c.c, where $\Delta\mathbf{p}_{AA}$ etc. are vector representations of (p_{AA1}, p_{AA2}, ……, p_{AA6}) etc, and z'=5, 7, for s.c, and b.c.c. or f.c.c, respectively. In these expressions, following notations are used:

$$\delta_{Ai}=\frac{L_A}{k_BT}\left(\cos^2\alpha_i-\frac{1}{3}\right),\ \left(i=1,2,\cdots\cdots,\frac{z}{2}\right), \quad (2.34)$$

$$\delta_{ABi}=\frac{L_{AB}}{k_BT}\left(\cos^2\alpha_i-\frac{1}{3}\right),\ \left(i=1,2,\cdots\cdots,\frac{z}{2}\right), \quad (2.35)$$

$$\nu_{AA}=\nu_A\exp(-E_A^M/k_BT)u_A^{z'-1}u_B, \quad (2.36)$$

$$\mathbf{R}=\begin{pmatrix} 0 & 4 & -1 & -1 & -1 & -1 \\ 4 & 0 & -1 & -1 & -1 & -1 \\ -1 & -1 & 0 & 4 & -1 & -1 \\ -1 & -1 & 4 & 0 & -1 & -1 \\ -1 & -1 & -1 & -1 & 0 & 4 \\ -1 & -1 & -1 & -1 & 4 & 0 \end{pmatrix}, \quad (2.37)$$

and

$$\mathbf{S}=\begin{pmatrix} 0 & 1 & 0 & 0 & 0 & 0 \\ 1 & 0 & 0 & 0 & 0 & 0 \\ 0 & 0 & 0 & 1 & 0 & 0 \\ 0 & 0 & 1 & 0 & 0 & 0 \\ 0 & 0 & 0 & 0 & 0 & 1 \\ 0 & 0 & 0 & 0 & 1 & 0 \end{pmatrix}, \quad (2.38)$$

and the directions of the atom pairs in f.c.c. crystals are numbered as shown in Fig. 2.1

The solutions of eqs. (2.32) and (2.33) are given by

$$p_{AA}=C_A u_A u_B+(p^0_{AA}-C_A u_A u_B)\exp(-2C_V z' \nu_{AA} t); \tag{2.39}$$

$$\Delta p_{AAi}=C_A u_A u_B(\delta_{Ai}+\delta_{Bi})+\{\Delta p^0_{AAi}-C_A u_A u_B(\delta_{Ai}+\delta_{Bi})$$

$$+(p^0_{AA}-C_A u_A u_B)(z'\delta_{Ai}-\delta_{ABi}-\delta_{Bi})\cdot 2C_V \nu_{AA} t\}\exp(-2C_V z' \nu_{AA} t) \tag{2.40a}$$

for s.c. and b.c.c, and

$$\Delta p_{AA}=C_A u_A u_B(\partial_A+\partial_B)$$

$$+\frac{1-S}{2}\left[\Delta p^0_{AA}-\left\{p^0_{AA}-\frac{21}{12u_B}(p^0_{AA}-C_A u_A u_B)\right\}1-p^0_{AA}\partial_B-\frac{p^0_{AA}-C_A u_A u_B}{4u_B}(\partial_{AB}+\partial_B)\right]$$

$$\times\exp\{-2C_V(z'+8u_B)\nu_{AA}t\}$$

$$+\frac{1+S}{2}\left[\Delta p^0_{AA}-\left\{p^0_{AA}-\frac{14}{12u_B}(p^0_{AA}-C_A u_A u_B)\right\}1-p^0_{AA}\partial_B-\frac{p^0_{AA}-C_A u_A u_B}{6u_B}(\partial_{AB}+\partial_B)\right]$$

$$\times\exp(-2C_V(z'+12u_B)\nu_{AA}t\}$$

$$+(p^0_{AA}-C_A u_A u_B)\left\{\left(1-\frac{35-7S}{24u_B}\right)\partial_A+\partial_B+\frac{1-5S}{24u_B}(\partial_{AB}+\partial_B)\right)\right\}$$

$$\times\exp(-2C_V z' \nu_{AA} t)\,, \tag{2.40b}$$

for f.c.c, where p^0_{AA} and Δp^0_{AAi} show the initial value of p_{AA} and Δp_{AAi} respectively.

2.3 Anisotropy Energy

2.3.1 Thermal Equilibrium Value of Anisotropy Energy

The equilibrium of p_{AAi} in eq.(2.23) gives quite the same anisotrpy energy as Néel's expression:

$$E_a^* = \left\langle \sum_i (N_{AAi}L'_{AA} + N_{BBi}L'_{BB} + N_{ABi}L'_{AB}) \cdot \left(\cos^2\alpha_i - \frac{1}{3} \right) \right\rangle$$
$$= \frac{zNC_A}{2}(L'_{AA} + L'_{BB} - 2L'_{AB}) \left\langle p^*_{AAi} \left(\cos^2\alpha_i - \frac{1}{3} \right) \right\rangle$$
$$= -\frac{zNLL'}{15k_BT} \cdot \bar{S} \cdot \exp(-U/k_BT) \cos^2\theta \,, \qquad (2.41)$$

where $\langle\ \rangle$ denotes the average value with respect to the crystallographic orientation in the polycrystalline alloy. In eq.(2.41) L'_{AA} L'_{BB} , L'_{AB} are the values of L_{AA}, L_{BB}, L_{AB} at the measuring temperature, θ the angle between the magnetization and the saturating field during the magnetic annealing, U the ordering energy given by

$$U = U_{AA} + U_{BB} - 2U_{AB} \qquad (2.42)$$

and L the directional ordering energy

$$L = L_{AA} + L_{BB} - 2L_{AB} \,. \qquad (2.43)$$

The factor $\bar{S}$ is given by

$$\bar{S} = \frac{4}{\sqrt{1+x}(1+\sqrt{1+x})^2} \,, \qquad (2.44)$$

where

$$x = 4C_AC_B\{\exp(-U/k_BT) - 1\} \,. \qquad (2.45)$$

2.3.2 Relaxation Process of Anisotropy Energy

A polycrystalline dilute alloy has been initially annealed and attains the equilibrium. After that the annealing temperature and/or the annealing field are changed, and then the anisotropy energy begins to change toward new equilibrium value. The magnetic field during the annealing process to be considered here will be one of the following three types: (1) static field in the X-direction (2) static field in the Y-direction, (3) rotating field in the xy-plane. Regardless of the type of annealing field, initial values of p_{AA}, and Δp_{AAi} are given from eqs.(2.39) and (2.40) by

$$p^0_{AA}=C_A u_A{}^0 u_B{}^0 , \tag{2.46}$$

and

$$\Delta p^0_{AAi}=C_A u_A u_B(\delta^0_{Ai}+\delta^0_{Bi})=-p^0_{AA}\frac{L^0}{k_B T_0}\left(\cos^2\alpha_i{}^0-\frac{1}{3}\right), \tag{2.47}$$

where the suffix 0 denotes the value during the initial annealing . Substituting these equations into eqs.(2.39) and (2.40), and caluculating the relaxation process of the anisotropy energy, we obtain the following expression:

$$E_a=\frac{zNC_A L'}{2}\left\langle p_{AAi}\left(\cos^2\alpha_i-\frac{1}{3}\right)\right\rangle$$

$$=\frac{zNC_A L'}{15}\left\{\epsilon\frac{uL}{k_B T}-\left(\epsilon_0 u^0\frac{L^0}{k_B T_0}-\varepsilon u\frac{L}{k_B T}\right)\exp(-2z'C_V\nu_{AA}t)\right.$$

$$\left.-\varepsilon(u^0-u)\frac{2z'(L_{AB}-L_{AA})+2L_{AB}-L_{BB}}{k_B T}\cdot C_V\nu_{AA}t\cdot\exp(-2z'C_V\nu_{AA}t)\right\}\cos^2\phi$$

(2.48a)

for s.c. and b.c.c, and

$$E_{\alpha}=\frac{zNC_{A}L'}{60}\Bigg[4\varepsilon\frac{uL}{k_{B}T}+3\Bigg\{\varepsilon_{0}u^{0}\frac{L^{0}}{k_{B}T_{0}}+\varepsilon\Bigg(-u_{0}\frac{L}{k_{B}T}+\frac{7}{4}\cdot\frac{u^{0}-u}{u_{B}}\cdot\frac{L_{AB}-L_{AA}}{k_{B}T}$$

$$-\frac{u^{0}-u}{8u_{B}}\cdot\frac{2L_{AB}-L_{BB}}{k_{B}T}\Bigg)\Bigg\}\exp\{-2(z'+4u_{B})C_{V}\nu_{AA}t\}$$

$$+\Bigg\{\varepsilon_{0}u^{0}\frac{L^{0}}{k_{B}T}+\varepsilon\Bigg(-u^{0}\frac{L}{k_{B}T}+\frac{7}{6}\cdot\frac{u^{0}-u}{u_{B}}\cdot\frac{L_{AB}-L_{AA}}{k_{B}T}$$

$$-\frac{u^{0}-u}{12u_{B}}\cdot\frac{2L_{AB}-L_{BB}}{k_{B}T}\Bigg)\Bigg\}\exp\{-2(z'+6u_{B})C_{V}\nu_{AA}t\}$$

$$+\varepsilon(u^{0}-u)\Bigg(\frac{4L}{k_{B}T}-\frac{77}{12u_{B}}\cdot\frac{L_{AB}-L_{AA}}{k_{B}T}-\frac{7}{12u_{B}}\cdot\frac{2L_{AB}-L_{BB}}{k_{B}T}\Bigg)\exp(-2z'C_{V}\nu_{AA}t)\Bigg]\cos^{2}\phi$$

(2.48b)

for f.c.c, where

$$u=u_{A}u_{B}=\exp(-U/k_{B}T)\,; \tag{2.49}$$

$$\varepsilon=+1,-1,0 \tag{2.50}$$

for the annealing field in the x-direction, and that in the y-direction, and the annealing field rotating in the xy-plane respectively; and ϕ is the angle between the x-direction and that of the magnetization lying in the xy-plane.

Although eq.(2.48) is rather complicated, in the case of

annealing which is done at the same temperature with the initial annealing, the total number of AA-pairs dose not change($u=u^0$), and eqs. (2.48a) and (2.48b) are simplified as

$$K_u(t)=K_u^e+(K_u^0-K_u^e)\exp(-2z'C_V\nu_{AA}t)\ , \tag{2.51a}$$

for s.c. and b.c.c, and

$$K_u(t)=K_u^e+\frac{K_u^0-K_u^e}{4}[3\exp\{-2(z'+4u_B)C_V\nu_{AA}t\} +\exp\{-2(z'+6u_B)C_V\nu_{AA}t\}] \tag{2.51b}$$

for f.c.c, where the anisotropy constants $K_u(t)$, K_u^e, K_u^0 are defined as

$$E_a=-K_u(t)\cos^2\phi\ , \tag{2.52}$$

$$K_u^e=\varepsilon\frac{zNC_ALL'}{15k_BT}\cdot u\ , \tag{2.53}$$

and

$$K_u^0=\varepsilon_0\frac{zNC_AL^0L'}{15k_BT_0}\cdot u^0\ . \tag{2.54}$$

In this case, $K_u(t)$ is described by the simple relaxation process. But when the annealing temperature is different from that of the initial annealing ($u\neq u^0$) the relaxation process becomes complicated. In s.c. and b.c.c. crystals, however, eq. (2.48a) may be approximated by eq. (2.51a) regardless of the change of the annealing temperature, since the 3rd term with the form of $\tau\exp(-\tau)$ is less than 1/e. In f.c.c. crystals, on the other hand, the situation is somewhat different, because there exists the rotation of atom pairs without the change of the total number of AA-pairs. When $u_B\gg1$, equation (2.48b) becomes as follows:

$$K_u(t) \simeq K_u^e + \frac{K_u^0 - K_u'}{4}\left[3\exp\{-2(z'+4u_B)C_V\nu_{AA}t\}\right.$$

$$\left.+\exp\{-2(z'+6u_B)C_V\nu_{AA}t\}\right] + (K_u' - K_u^e)\exp(-2z'C_V\nu_{AA}t)\ , \quad (2.55)$$

where

$$K_u' = \varepsilon\frac{zNC_ALL'}{15k_BT}\cdot u^0\ . \quad (2.56)$$

In this case, it is not toward K_u^e, but toward K_u' that $K_u(t)$ changes at first. When $u_B \ll 1$, the rotation of AA-pairs is suppressed, and the relaxation process of eq.(2.48b) is thought to become similar to that of eq.(2.51a).

2.4 Disscusion and Conclusion

The relaxation of the M-induced anisotropy in the dilute alloy can be written by a simple process toward the new equilibrium state as is given by eq. (2.51), so long as the annealing temperature is constant. However, when the annealing temperature is changed, the total number of pairs becomes different from that of the new equilibrium. The difference of the total number of pairs from the equilibrium value gives rise to a peculiar behavior in the process. This is more remarkable in f.c.c. crystals than in s.c. and b.c.c. crystals, because in the former a trigonal arrangement consisting of the vacancy and the AA-pair is likely to appear. Since this peculiar relaxation term consists of the difference between K_u' and K_u^e in eq.(2.55), this behavior does not appear in the case of eliminating the anisotropy by rotating field annealing, namely, $K_u'=K_u^e=0$.

The relaxation curves of eq.(2.55) are shown in Fig.2.5 where K_u'/K_u^e is chosen as a parameter.

In magnetic annealing at the constant temperature, and/or in rotating field annealing, the relaxation frequency is approximately derived from eq.(2.51) as

$$\nu_K \equiv -\frac{\frac{d}{dt}K_u}{K_u-K_u^e} \simeq 2z'C_V\nu_{AA} \tag{2.57}$$

for s.c. and b.c.c, and

$$\nu_K = 2(z'+4u_B)C_V\nu_{AA} \tag{2.58}$$

for f.c.c. By putting $z'=0$, eq.(2.58) becomes identical with that obtained by Iwata et al.[1] Thus their expression is thought to hold for the special case where $u_B \gg 1$.

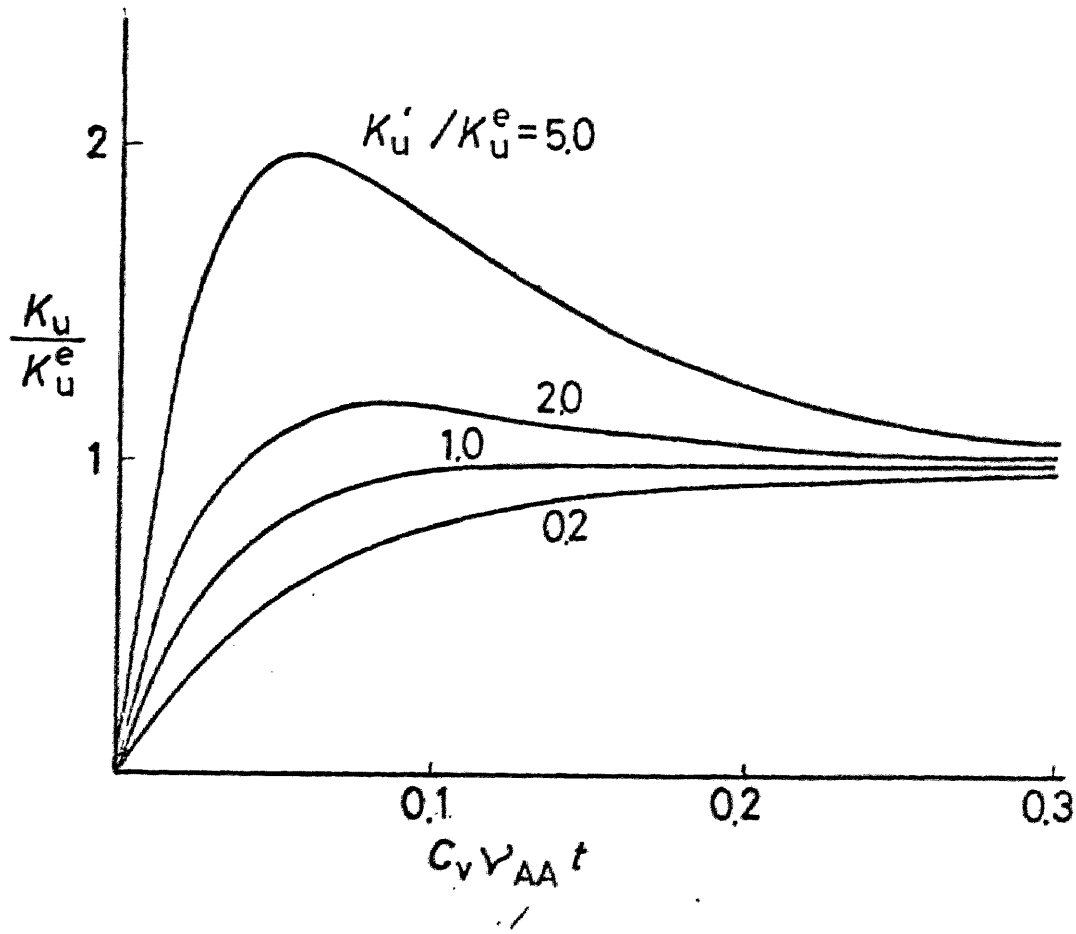

Fig. 2.5 Relaxation curves of the anisotropy constant in f.c.c. crystals calculated from eq.(2.54) by putting $K_u^0=0$, $z'=7$ and $u_B=2$, where K_u'/K_u^e is chosen as a parameter.

Since the quasi-chemical theory mentioned above is based on the pair probabilities alone, the phenomena arising from the long-range order or the inhomogeneity are beyond the limit of this theory. Therefore, the following two points still remain unsolved. The first is the influence of the long-range order on the pair-order anisotropy. This is experimentally recognized in the fact that K_u increases by magnetic annealing at first but it decreases with an approach to perfect order [10]. The second is about the relaxation frequency ν_k ; the factor $2z'$ or $2(z'+4u_B)$ in eq. (2.57) or (2.58) is thought to become practically smaller. This is because the development of the directional order seems to be more appreciable near the vacancy than in the other part.

References

1) T. Iwata and F. B. Hagedorn : J. appl. Phys. 40 (1969) 2258.

2) G. Kneer and W. Zinn : Proc. Internat. Symp. for Basic problems in Thin Film Physics Clausthal/Göttingen(Vanderhoeck und Ruprecht,Göttingen, 1965) p.437.

3) D. O. Smith, G. P. Weiss and K. J. Harte : J. appl. Phys. 37 (1966) 1466.

4) T. Fujii, S.Uchiyama, M. Masuda and Y. Sakaki : IEEE Trans. Mag. MAG-4 (1968) 515.

5) H. W. Wiedenmann and H. Hoffmann : IEEE Trans.Mag. MAG-5 (1969) 506.

6) S. Radelaar : J. Phys. Chem. Solids 31 (1970) 219.

7) L. Néel : J. Phys. Radium 15 (1954) 225.

8) L. Néel : Comp. Rend. 237 (1953) 1613.

9) F. B. Hagedorn : Rev. sci. Instrum. 38 (1967) 591.

10) S. Chikazumi : J. Phys. Soc. Japan 11 (1965) 551.

Chapter 3
Anisotropy Relaxation and Electrical Resistivity Recovery

3.1 Introduction

The anisotropy relaxation of Permalloy films due to magnetic annealing has been interpreted in intuitive way as the sum of several 1-st order processes, most of which have unusually small activation energies [1-4] as compared with the case of bulk Permalloy. The mechanisms proposed to explain such a small activation energy are grouped into two categories ; one is the reorientation of additional anisotropy sources such as anisotropic alignments of vacancy clusters [3,5,6] , the other is the reorientation of usual atom pairs aided by high diffusive lattice defects [1,7] . The latter mechanism seems to be more reasonable, because no experimental evidences for the additional anisotropy sources have yet been found in Permalloy films, and, moreover, the composition dependence of the anisotropy in Ni-Fe films can be explained fairly well by the sum of the pair-order and magnetostriction anisotropy[6]. Thus we may consider that the anisotropy of nonmagnetostrictive Permalloy films originates only from the directional pair-order of the constituent atoms and that the low activation energy of the relaxation process is attributed to the presence of many kinds of high diffusive lattice defects.

From this point of view, Iwata-Hagedorn [7] explained the anisotropy relaxation of 81% Ni Permalloy films in terms of vacancy-aided reorientation of Fe-Fe pairs, where the concentration of the vacancy was assumed to be much higher than thermal equilibrium one. (Hereafter we call this "excess-vacancy model"). According to their explanation, the annealing out of excess vacancies causes an increase of the relaxation time τ_k

[see eq. (2.2)], and consequently the relaxation process becomes substantially more complicated than the simple 1-st order reaction. Hence considerable parts of annealing stages shown in Table 1.1 may be understandable by the pair-order anisotropy alone.

The purpose of this chapter is to investigate the influence of lattice defects on the anisotropy relaxation. To investigate how the defects actually contribute to the anisotropy relaxation, it may be useful to make a simultaneous measurement of a certain independent annealing processes, such as the crystallographical or morphological change, electrical resistivity change, etc. In this study, the recovery process of the electrical resistivity is measured during isochronal magnetic annealing; and correlation of processes between the anisotropy and resistivity will be examined on the basis of the excess-vacancy model.

3.2 Experimental Procedure

Permalloy films were prepared by the vapor-deposition in the presence of a magnetic field. Most of films were deposited at relatively low temperature (10°C) and some of them were deposited at -50°C and -100°C to obtain films with the high defect concentration. Annealing and measurement were carried out in a vacuum deposition system as shown in Fig.3.1. The vapor source was Permalloy sheets of 81.5%Ni-18.5%Fe which were suspended on a tungusten wire heated resistively. A quartz glass substrate was attached to the bottom surface of the cryostat. The substrate temperature was controlled by the use of moribdenum heater and Liq. N_2 as shown in the figure. The deposition rate was usually about 5Å/sec, and the vacuum during the deposition and annealing was better than 1×10^{-5}Torr. The shape of deposited films was a stripe of 10mm×1mm and about 400Å thick(Fig.3.2). Immediately after the deposition, SiO≈ SiO_2 layer was deposited onto the Permalloy film to protect it from the oxidation. Resistance R was measured by the ordinal 4-proves method, and H_k was determined by improved Kovelev's[9] method using the magnetoresistance effect as shown in Fig.3.3 The temperature during the measurement (T_m) was kept either at -100°C or -150°C to suppress the proceeding of the relaxation of H_k. Films were subsequently subjected to a sequence of isochronal annealings in a magnetic field applied parallel to the hard axis (HA) or the easy axis (EA). The annealing was started at the temperature lower than the deposition temperature (T_d) and repeated up to about 430°C to obtain the entire annealing curve. Annealing temperatures were taken at the intervals of 10°C and the durations were 10 minutes. The cooling rate from T_a to T_m was 10~100°C/min.

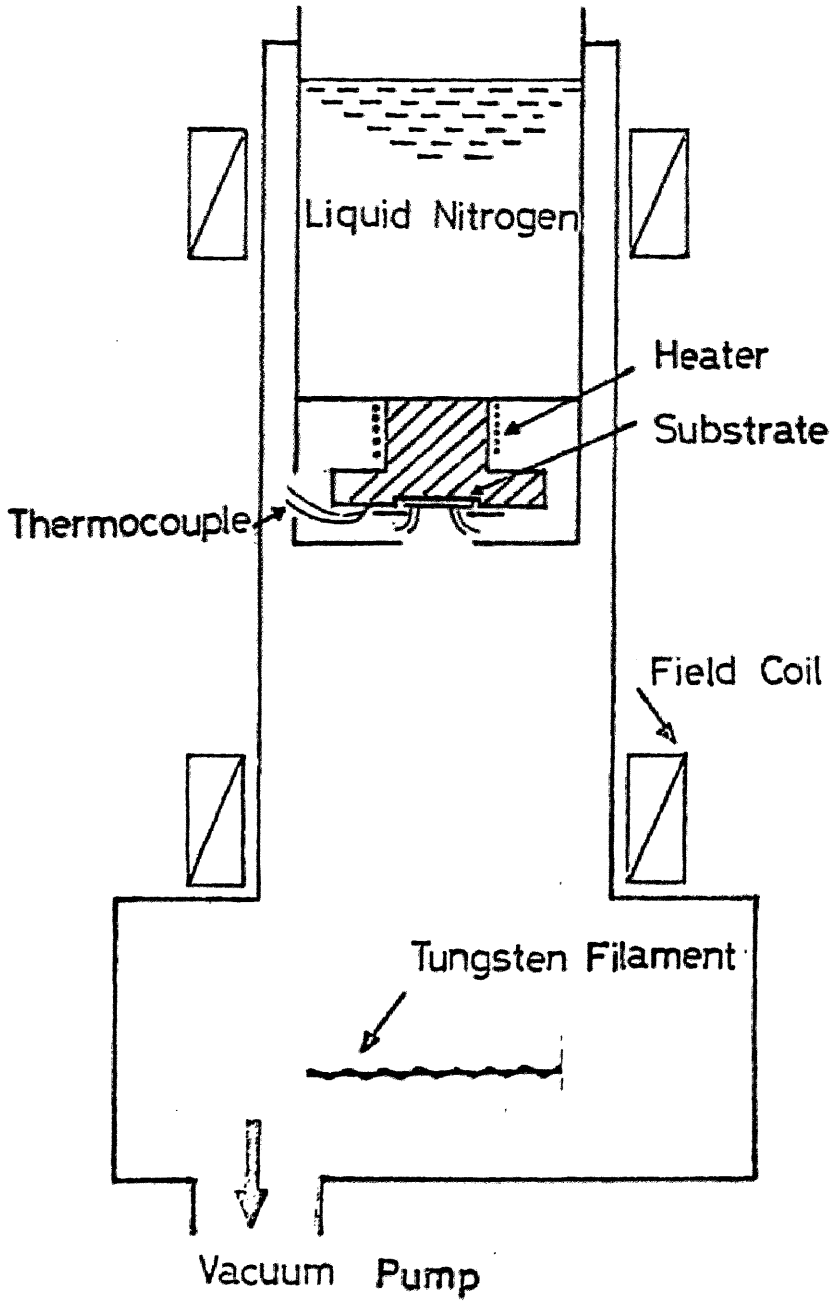

Fig.3.1 Schematic diagram of the vacuum apparatus for the deposition, annealing, and measurements.

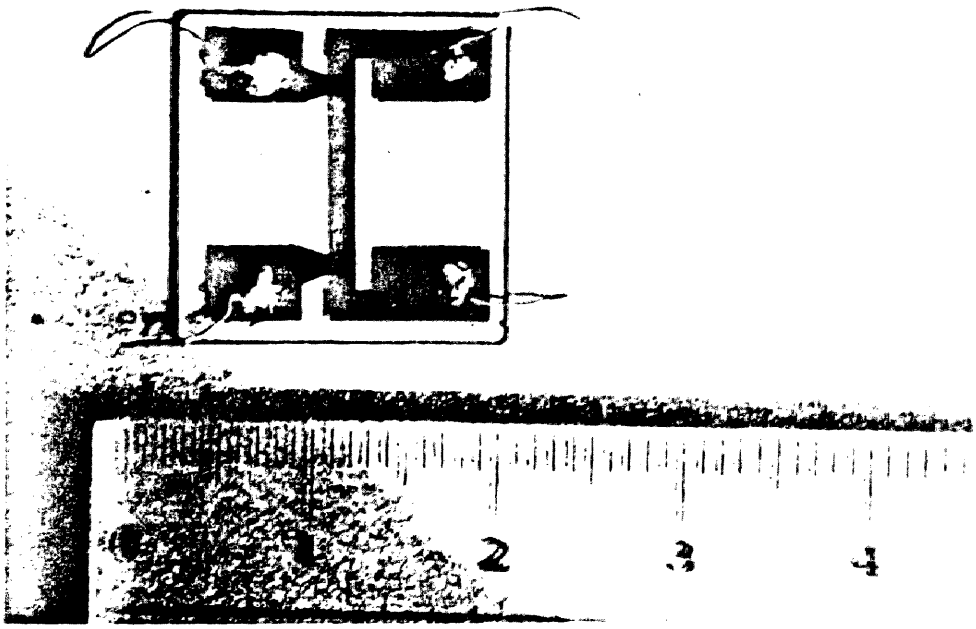

Fig.3.2 Permalloy film used for the measurement of the annealing behavior of H_k and R.

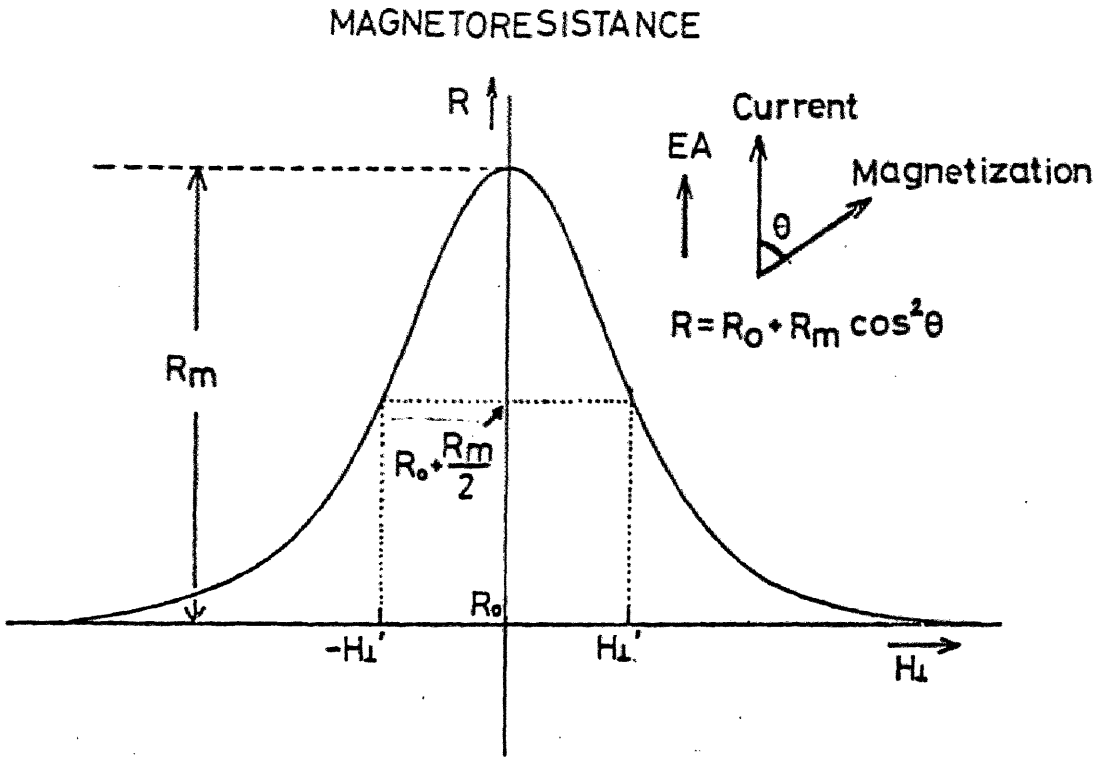

Fig.3.3 Magnetoresistance vs. HA applied field $H_{\perp}$ curve in the presence of EA bias field $H_{\parallel}$. The anisotropy field H_k is obtained from the formula as $H_k=\sqrt{2}(H_{\perp}'-H_{\parallel})$, where $H_{\perp}'$ is the magnitude of $H_{\perp}$ for $\theta=45°$.

For HA annealing, some of the films were subjected to the heat treatment at 280°C for 30 minutes in an EA field prior to HA= annealing, to examine the stabilization effect of the film structure.

3.3 Experimental Results

The anisotropy field H_k and the resistance R after each ten minutes' magnetic annealing are plotted in Fig.3.4 for films deposited at 10°C. The measurement was carried out at -100°C. When the film is annealed in the HA field, H_k decreases monotonously and becomes negative values, which means the interchange of the EA and the HA. The anisotropy field decreases successively up to 360°C and then increases slightly. When the film is annealed in the EA field, no remarkable changes of H_k appear up to about 300°C, and a slight decrease is found above 300°C. The HA annealing curve in Fig.3.4 is roughly the same as the isothermal HA annealing data of as-deposited films reported before.[3] Clearly distinguishable annealing stages, however, are not observed in this isochronal annealing experiment. The resistance annealing curve has a discrete stage at 20~140°C, and this is similar to the result obtained by Dietz et al. in the same temperature range.[10] Between 140°C and 170°C, the resistance does not decrease. Above 180°C, R decreases monotonously, and the slope of the curve becomes steeper at 300°C corresponding to the growth of the crystallites.[11,12]

The incremental change of H_k, namely, $-\Delta H_k$ and that of R, namely, $-\Delta R$ during ten minutes' annealing are plotted for films deposited at 10°C, -50°C, and -100°C in Figs.3.5 and3.6 respectively. By comparing the curves of $-\Delta H_k$

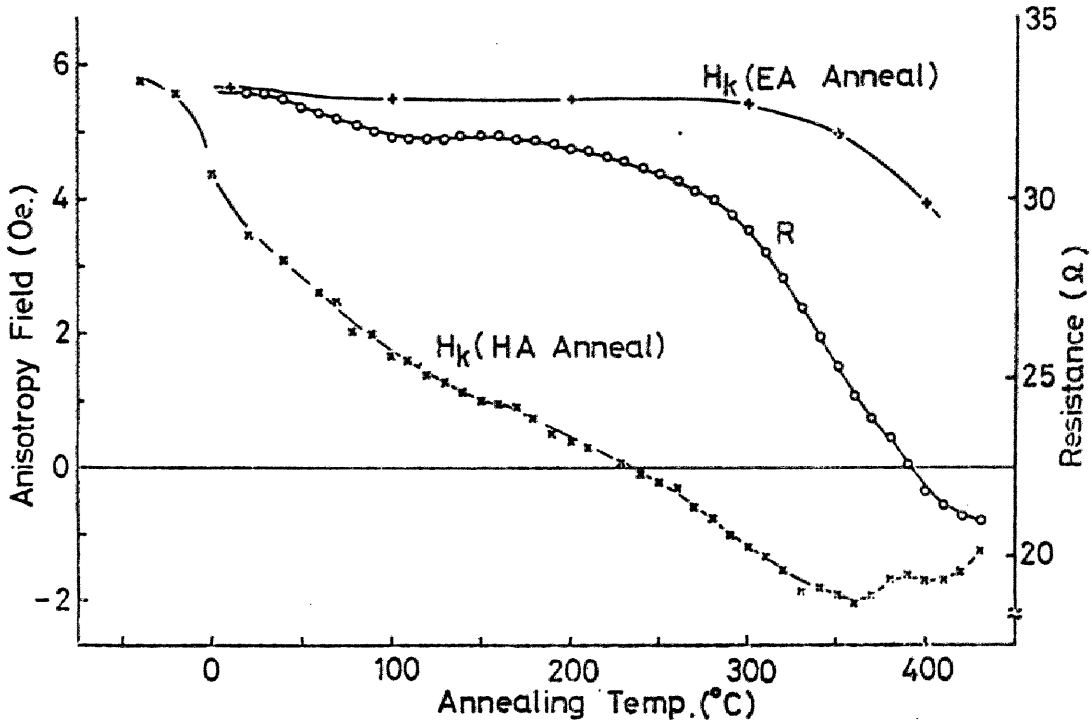

Fig.3.4 Annealing curves of the anisotropy field and the resistance for the film deposited at 10°C.

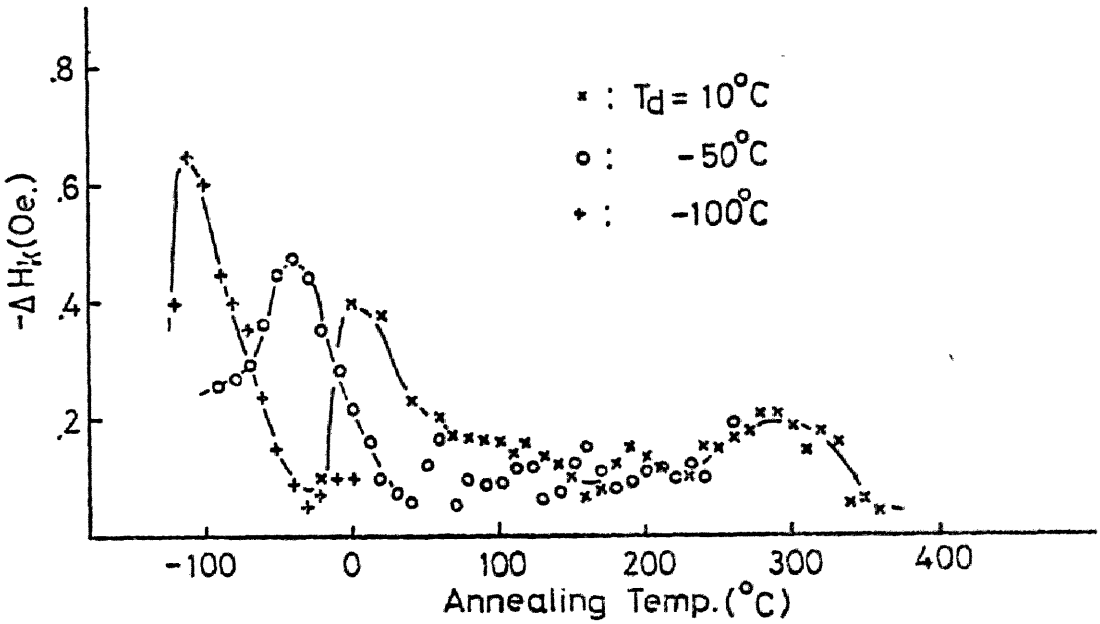

Fig.3.5 Changes of the anisotropy field as a function of the annealing temperature during ten minutes' isochronal annealing in the films deposited at various temperatures.

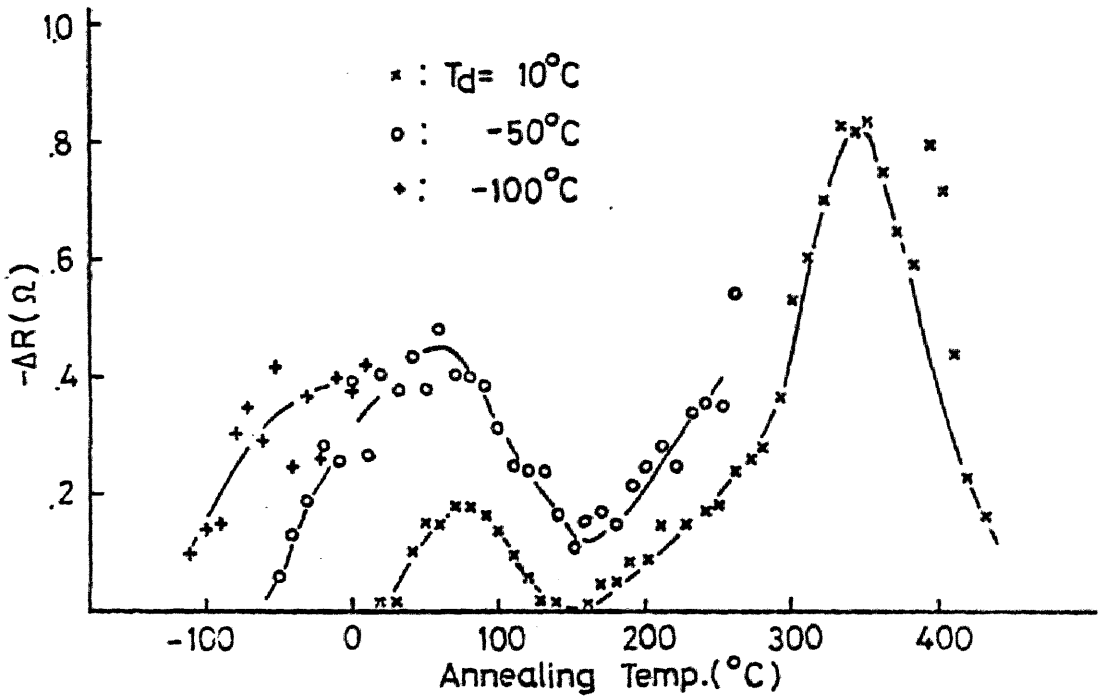

Fig.3.6 Changes of the electrical resistance vs. annealing temperature curve during ten minutes' isochronal in the same films.

with those of $-\Delta R$ in the film deposited at 10°C, the minimum of $-\Delta H_k$ is found at the temperature where ΔR is zero. This result suggests that both quantities are related with each other. The peak of $-\Delta H_k$, however , is found at the deposition temperature and shifts to lower temperatures with decreasing T_d, while R does not decrease below T_d.

The activation energies for annealing processes of H_k and R were measured by the slope change method [9] at several temperatures. Activation energies observed are listed in Table 3.1. for the films deposited at -50°C. The corresponding activation energies for H_k and R seem to be comparable, but the former are a little smaller than the latter . This fact also suggests that the relaxation of the induced anisotropy takes place relating to the reduction of the structual defects which give rise to scattering of electrons.

The annealing curves for the film stabilized at 280°C are shown in Fig.3.7. The amount of H_k decrease in the stabilized film is much smaller than that in as-deposited films. No changes in R take place below the stabilization temperature 280°C, while H_k begins to decrease at about 100°C.

The annealing behaviors are also influenced by the deposition rate. Fig.3.8 shows the influence of the deposition rate on annealing curves of H_k and R. The resistance of the film with the high depositon rate (10Å/ sec) decreases more smoothly with T_a than that of the film with the low deposition rate (5Å/sec), and this property agrees with the result of the very high deposition rate film (60Å/sec). [14] In the similar way to the R annealing curve, the small undulation of the H_k annealing curve disappears in the high deposition rate film.

Table 3.1 Activation energies of annealing processes measured by the slope-change method in the Permalloy film deposited at -50°C.

Temp. (°C)	Activation energy (eV)	
	Anisotropy	Resistivity
-50	0.2	0.3
60	0.5	0.7
240	1.1	1.2

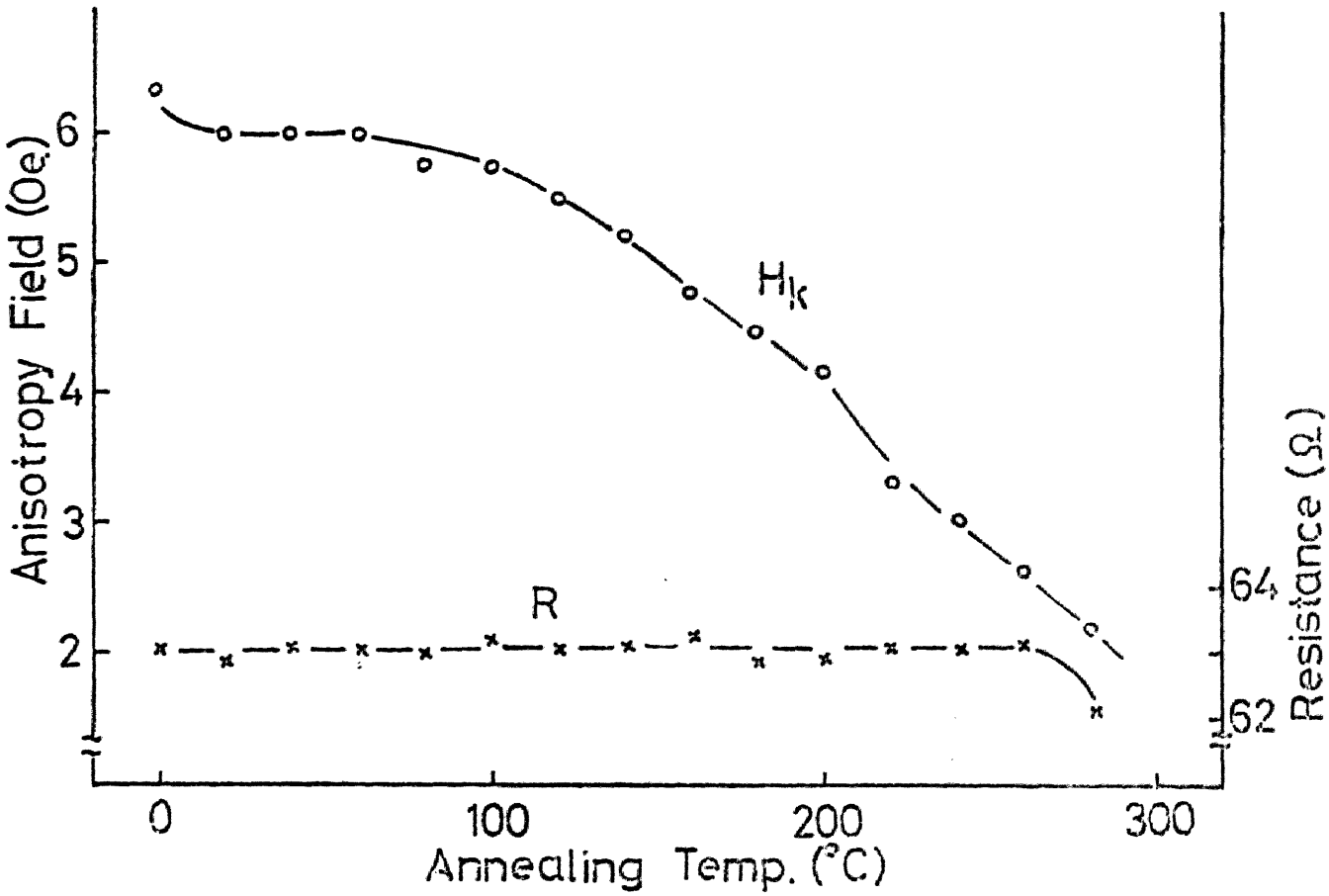

Fig.3.7 Annealing curves of H_k and R for the film stabilized at 280°C.

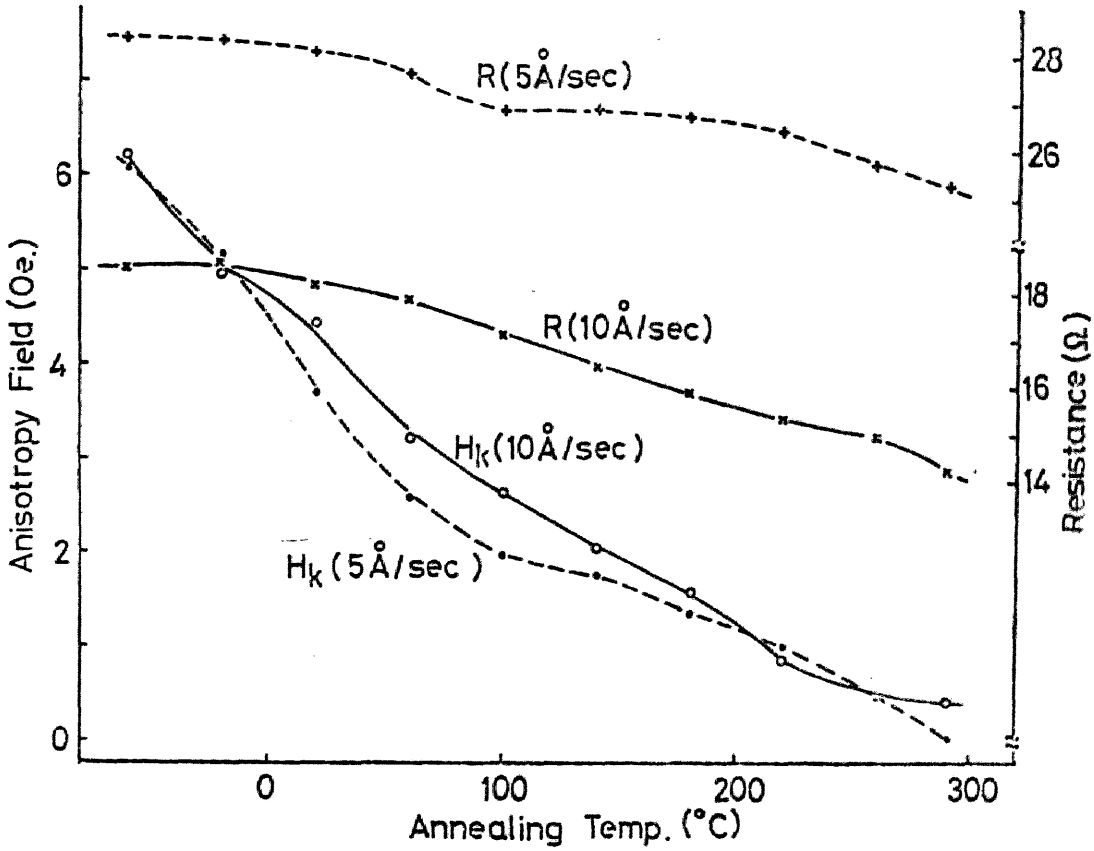

Fig.3.8 Influence of the deposition rate on the annealing curves of H_k and R.

3.4 Discussions

3.4.1 Comparison of experimental results with a simple relaxation model

In the simple anisotropy relaxation model, the reorientation of atom pairs is performed by the migration of vacancies. If both the concentration of the vacancy and the anisotropy energy density are uniform throughout the film, the relaxation process of H_k is written as shown in the preceeding chapter [eq.(2.58)];

$$\frac{dH_k}{dt} = -\left\{ 14+8\exp\left(\frac{U_{NiFe}-U_{NiNi}}{k_B T_a}\right)\right\} C_v \nu_{FeFe}(H_k - H_k^e) \qquad (3.1)$$

where H_k^e is the equilibrium value of H_k at T_a°K; U_{NiFe} and U_{NiNi} are respectively the interaction energies of Ni-Fe and Ni-Ni atom pairs, C_V is the concentration of the vacancy, and ν_{FeFe} the migration frequency for Fe-Fe pairs. Since in bulk Permalloy thermal equilibrium vacancies do not play a significant role below 300°C,[8] we shall consider only excess vacancies hereafter. During the anisotropy relaxation, excess vacancies migrate by the random walk and finally vanish at their sinks. Since film surfaces and grain boundaries are thought to be main sinks for excess vacancies, the concentration of the vacancy seems to decrease with the annealing time as eq.(3.2).[16]

$$\frac{dC_V}{dt} = -K_V C_V , \qquad (3.2)$$

where K_v is given by eq.(3.3) if vacancies disappear at grain boundaries.[17]

$$K_v = \frac{\pi^2 a^2}{3 r^2} \nu_V , \qquad (3.3)$$

where r is the radius of the grain, a the lattice constant, and

ν_V the migration frequency of the vacancy. In a recrystallization process, atoms are thought to migrate in a diffrent way from such a simple mechanism. This model, however, may be available to Permalloy films, since the growth of crystallites takes place remarkably only above 300°C.

By combining eq.(3.1) with eq.(3.2), we get readily

$$\frac{dH_k}{dt} / (H_k - H_k^e) = \frac{dC_V}{dt} \frac{\nu_{FeFe}}{\nu_V} \frac{3r^2}{\pi^2 a^2} \left\{ 14 + 8\exp\left(\frac{U_{NiFe} - U_{NiNi}}{k_B T_a} \right) \right\} . \qquad (3.4)$$

From eqs.(3.2) and (3.4), the initial concentration of vacancies which vanish below 300°C can be estimated by,

$$C_V^0 = \frac{\pi^2 a^2}{3r^2} \int_0^t C_V \nu_V dt = -\frac{\pi^2 a^2}{3r^2} \int_{H_k^0}^{H_k(t)} \frac{\nu_V}{\nu_{FeFe}} \left\{ 14 + 8\exp\left(\frac{U_{NiFe} - U_{NiNi}}{k_B T_a} \right) \right\} \frac{dH_k}{H_k - H_k^e} , \qquad (3.5)$$

where the integration is carried out over the time interval long enough to annihilate such excess vacancies. Even below 300°C, a drastic change of H_k was observed as seen from the reversal of its sign in Fig.3.5. This fact suggests that most part of the reorientation of atom-pairs is achieved in this temperature range. The integration in eq.(6) is therefore roughly estimated to be unity, if the factor $\frac{\nu_V}{\nu_{FeFe}} \left\{ 14 + 8\exp\left(\frac{U_{NiFe} - U_{NiNi}}{k_B T_a} \right) \right\}$ can be replaced by unity. In this way, C_V^0 is of the order of $\frac{\pi^2 a^2}{3r^2}$. This gives the initial vacancy concentration of 10^{-3} for r=100Å. On the other hand, the decrease of the resistivity observed below 300°C corresponds to the initial excess vacancy concentration of 10^{-3}, provided that the residual resistivity due to the vacancy is 4.0μΩ cm/ atom % .[18]

Although this agreement suggests that the anisotropy relaxation results from the migration of excess vacancies, there still remain some difficult problems:

i) Annealing curves of $-\Delta H_k$ and $-\Delta R$ are too broad to be ascribed to single 1st-order reaction. This might be explained to some extent by the distribution of the migration energy of vacancies[19] due to the stress field, the effect of vacancy clustering, etc.

ii) To obtain the relationship between the variations of $-\Delta H_k$ and $-\Delta R$ for HA annealing below 300°C, the equilibrium value of the anisotropy field H_k^e may be replaced by the initial value with opposite sign ($-H_k^0$), regardless of T_a below 300° C.[20,21] On the other hand, if $-\Delta R$ results only from the annihilation of excess vacancies, $-\Delta R$ should be proportional to the decrease of C_v. When all quantities in eq.(3.4) except H_k and C_v are assumed to be constant, independent of the annealing temperature, the relation between $-\Delta H_k$ and $-\Delta R$ becomes as

$$\frac{\Delta H_k}{H_k - H_k^e} \simeq \frac{\Delta H_k}{H_k + H_k^0} \propto \Delta R. \qquad (3.6)$$

The annealing curves of Figs.3.6 and 3.7 , however, do not agree well with eq(3.6), since the maximum of $-\Delta H_k$ is found at T_d, whereas $-\Delta R$ still remains nearly zero ; and, furthermore, $-\Delta H_k$ does not vanish at the temperature where $-\Delta R=0$ (130~160° C) in the film deposited at 10° C.

iii) For stabilized films, vacancies which are able to migrate far below the stabilization temperature should have already vanished in the preceeding heat treatment. Therefore, as to stabilized films it is difficult to explain the relaxiation process at the low temperature by the mechanism of the vacancy annihilation mentioned above.

3.4.2 Annealing mechanism of as-deposited films

To describe more precisely the annealing process of as-deposited films, the change of the film structure during the heat treatment should be taken into consideration. Annealing behaviors of vapor-quenched metal films have been extensively studied from the structual point of view. Structual changes of metal films have been studied by various methods, such as the direct observation of the electron microscopy,[11,12.22.23] the analysis of the X-ray diffraction, etc.[22,24-30] The structural changes observed, concerning the magnetic annealing of as-deposited Permalloy films, are (i) crystallites grow drastically above 300°C, the gradual growth, however, occurring even when the annealing temperature is lower than 300°C,[11,12] (ii) the rms value of the random strain in as-deposited films decreases with the increasing annealing temperature and becomes very small about 300°C,[25] and (iii) in aggregated Au films, the diffusion of atoms on the grain surface gives rise to the morphological change of grains just after the deposition.[26,27] This property, however, is not observed directly but is deduced from the change of the electrical and optical properties.
From these facts, especially (i) and (iii), the migration of atoms below 300°C may be caused not only by excess vacancies as is in quenched bulk metals, but also by the other mechanisms, such as the grain boundary diffusion, the surface diffusion, and the diffusion during the coalesence of the grains.

3.5 Concluding Remarks

The anisotropy field H_k and resistance R were simultaneously measured during isochronal HA magnetic annealing of nonmagnetostrictive Permalloy films. In the annealing curves of $-\Delta H_k$ vs. T_a, a prominent peak appears near the deposition temperature T_d, while in those of $-\Delta R$ vs. T_a the peaks appear above T_d. Although such a difference exists between the curves of $-\Delta H_k$ and $-\Delta R$, considerable correlations are found between both annealing behaviors; in particular, both annealing processes have nearly the same activation energies.

The abrupt decrease of R above about 300°C may be attributed to the grain growth, because the conduction electron in thin films is considerably scattered at the grain boundary [22, 31]. On the other hand, the gradual decrease of R below 300°C is not so clear up to date in spite of many studies, but may be ascribed to the atom (or defect) transport producing the reorientation of atom pairs. The excess vacancy model, however, by no means gives us a complete description for the annealing behaviors of H_k and R at the temperature below 300°C. This may be mainly due to the following two reasons ; (i) as for the anisotropy relaxation, the high diffusive region such as grainboundaries play a significant role, (ii) meanwhile the resistivity change arises partly from the grain growth or morphlogical change of grains.

References

1) G. Kneer and W. Zinn : Proc. Internat. Symp. for Basic Problems in Thin Film Physics Clausthal/Göttingen (Vanderhoeck und Ruprecht,Göttingen, 1966) p.437.

2) D. O. Smith, G. P. Weiss and K. J. Harte : J. appl. Phys. 37 (1966) 1464.

3) T. Fujii, S. Uchiyama, M. Masuda and Y. Sakaki : IEEE Trans. Mag. MAG-4 (1968) 515.

4) H. W. Wiedenmann and H. Hoffmann : IEEE Trans. Mag. MAG-5 (1969) 506.

5) K. J. Harte, D. O. Smith and M. Gross : private communication.

6) A. G. Lesnik : Phys. Stat. Sol. 35 (1969) 959.

7) T. Iwata and F. B. Hagedorn : J. appl. Phys. 40 (1969) 2258.

8) W. T. Siegle and W. R. Bean : J. appl. Phys. 36 (1965) 1721.

9) G. Kneer : IEEE Trans. Mag-2 (1966) 747.

10) R. Dietz and W. Hellenthal : Phys. Stat. Sol. 16 (1966) 789.

11) T. Fujii, S. Tsunashima, S. Uchiyama and Y. Sakaki : IEEE Trans. Mag. MAG-6 (1970) 619.

12) M. Roth : J. appl. Phys. 41 (1970) 286.

13) A. C. Damask and G. J. Dienes : Point Defects in Metals (Gordon and Breach, New York, 1963) p.147.

14) R. W. Hoffman, F. J. Anders and E. C. Crittenden, Jr.: J. appl. Phys. 24 (1953) 231.

15) C. M. Williams and A. I. Silinder : J. appl. Phys. 42 (1971) 1435.

16) A. C. Damask and G. G. Dienes : Point Defects in Metals (Gorden and Breach, New York, 1963) p.79.

17) Paul. G. Shewmon : Diffusion in Solid (McGrow-Hill, New York, 1963) p.52.

18) A. Seeger : Z. Phys. 144 (1956) 637.

19) M. Takayasu, S. Uchiyama, K. Takahashi and T. Fujii : IEEE Trans. Mag. MAG-10 (1974) 5521.

20) C. H. Wiltz : Proc. Internat. Symp. for Basic Problems in Thin Film Physics Clausthal/Göttingen (Vanderhoeck und Ruprecht, 1965) p. 422.

21) A. Ferro, G. Griffa and G. Montalenti : IEEE Trans. Mag. MAG-2 (1966) 764.

22) K. L. Chopra : Thin Film Phenomena (McGrow-Hill, New York, 1966)

23) N. Yoshida, R. Oshima and F. E. Fujita : J. Phys. F, 2 (1972) 237.

24) A. Gangulee : J. appl. Phys. 43 (1972) 867.

25) S. Yoshida, T. Yamaguchi and A. Kinbara : J. Opt. Soc. Amer. 61 (1971) 463.

27) M. Nishiura and A. Kinbara : Thin Solid Films, 24 (1974) 79.

28. A. Ganglee : J. electronic Materials, 2 (1973) 161.

29) A. Ganglee : J. electronic Materials, 2 (1973) 171.

30) G. Honjo and K. Yagi : J. vac. Sci. and Tech 6 (1969) 576.

31) A. F. Mayadas : J. appl. Phys. 39 (1968) 4241.

Chapter 4
Influence of Grain Boundary Diffusion on Anisotropy Relaxation

4.1 Introduction

In the preceeding chapter, we have discussed the anisotropy relaxation of Permalloy films on the basis of the " excess vacancy model", in which the film is assumed to contain excess vacancies which migrate randomly in the grain until they disappear at the grain boundary. This model, however, could not give full understanding of the problem. The lack of the agreement with the model is possibly due to the pair-reorientation associated with the grain boundary diffusion.

As is well known, surfaces and grain boundaries act as a high diffusive path in metals. In general , the diffusion of atoms in such region proceeds with lower activation energies than usual lattice diffusion, so that high diffusive path tends to become particularly important at low temperatures[1)] . Since, in thin films, atoms are generally diffused at relatively low temperature and since thin films contain unusually high density of grain boundaries, there are many situations where the grain boundary diffusion should become the dominant atom transport mechanism[2)].

In the case of Permalloy films, the importance of the grain boundary in the anisotropy relaxation was firstly pointed out by Roth [3)]. He explained magnetic annealing properties of preannealed (stabilized) films by the reorientation of atom pairs through thermal vacancies localized in the vicinity of grain boundaries.

In this chapter, we examine the contribution of the grain boundary to the anisotropy relaxation processes, especially to those with unusually low activation energies. For this purpose, films with various densities of grain boundaries are used for the annealing experiment.

4.2 Experimental Procedure

Nonmagnetostrictive Permalloy films were vacuum-deposited at the substrate temperature T_d=10°C. The film thickness was monitored by a quartz-crystal thickness meter. The deposition rate was always kept about 5Å/sec. After that, the films were annealed in a field parallel to the hard axis (HA) just in the same way as is described in Sec.4.2. The time duration at each annealing temperature was set so as to satisfy the condition of the constant rate of heating (10°C/min). The measurement temperature for the anisotropy was -100°C.

In the previous chapter, the structural change (recovery) during magnetic annealing was estimated from the reduction of the electrical resistivity. In the present work, however, the direct observation by electron microscopy was used to estimate the structural change during annealing. This is because the electrical resistivity is seriously affected by the island-like structure in very thin films. For the electron microscopic observation, samples sandwiched between silicon oxide layers are deposited onto rock salt substrates at 10°C. Any oxide lines were not observed in the diffraction pattern of these samples.

Some films were preannealed at 500°C for 30 min to compare the relaxation process of as-deposited films with that of recrystallized films.

4.3 Experimental Results

4.3.1 Thickness dependence of nominal grain size

The nominal grain size D was determined from the {220} ring of the selected area diffraction pattern by using Scherrer's formula,

$$\beta_1 = \frac{0.9\ \lambda}{D\ \cos\theta_B} + b_i ,$$

where β_1 is the half intensity line width of the diffraction ring, λ the wave length of the electron, θ_B the Bragg angle, and b_i the instrumental breadth. The instrumental breadth was determined by comparing the line width with the average grain size obtained directly from the micrograph. The estimated grain size D of as-deposited films decreases with the decrease of the film thickness as shown in Fig.4.1. So the effective area, which acts as the high diffusive pass, increases remarkably with the decrease of the film thickness. Fig.4.2 shows the grain growth during annealing for three films with the different thickness. In the thicker film (500Å) the grain growth proceeds rapidly above the temperature of about 200°C as is usually observed , while in the thinner film (80Å) it tends rather to saturate in this temperature range. In contrast to this, below 150°C the grain growth hardly takes place in the thicker film, while it considerably proceeds in the thinner film. This characteristic thickness dependence of the grain growth reflects that of the anisotropy relaxation mentioned in the next section.

4.3.2 Thickness dependence of the anisotropy relaxation

Figure 4.3 shows the isochronal annealing curves for H_k, of as-deposited films under a field parallel to the HA, where

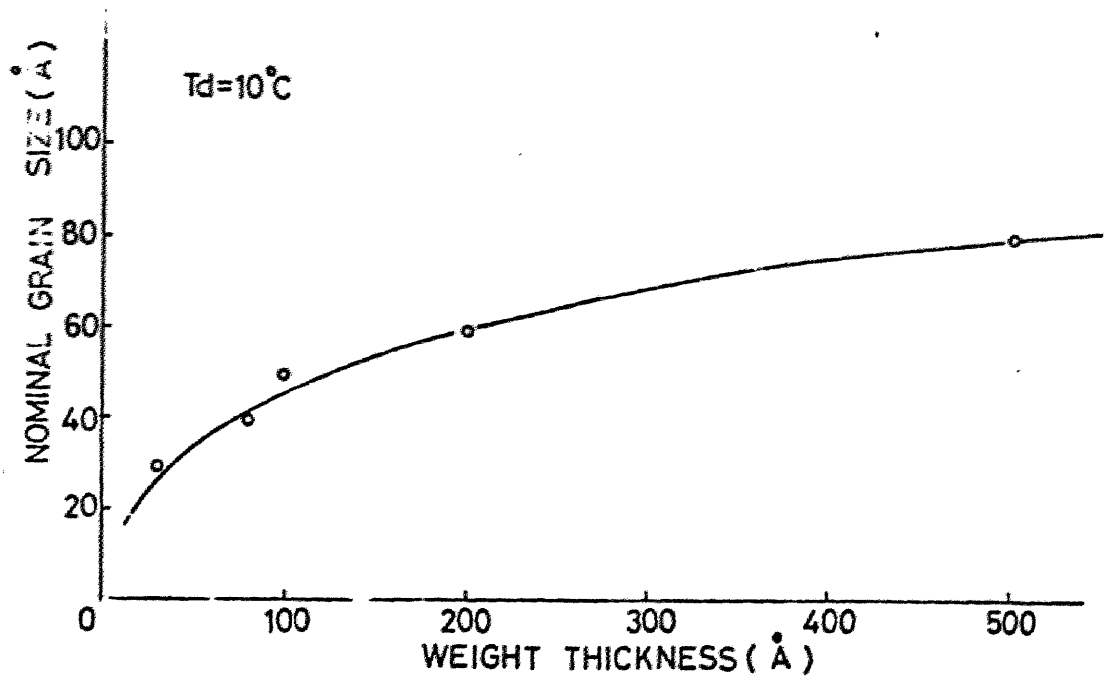

Fig. 4.1 Thickness dependence of the nominal grain size determind from {220} ring for films deposited at 10°C.

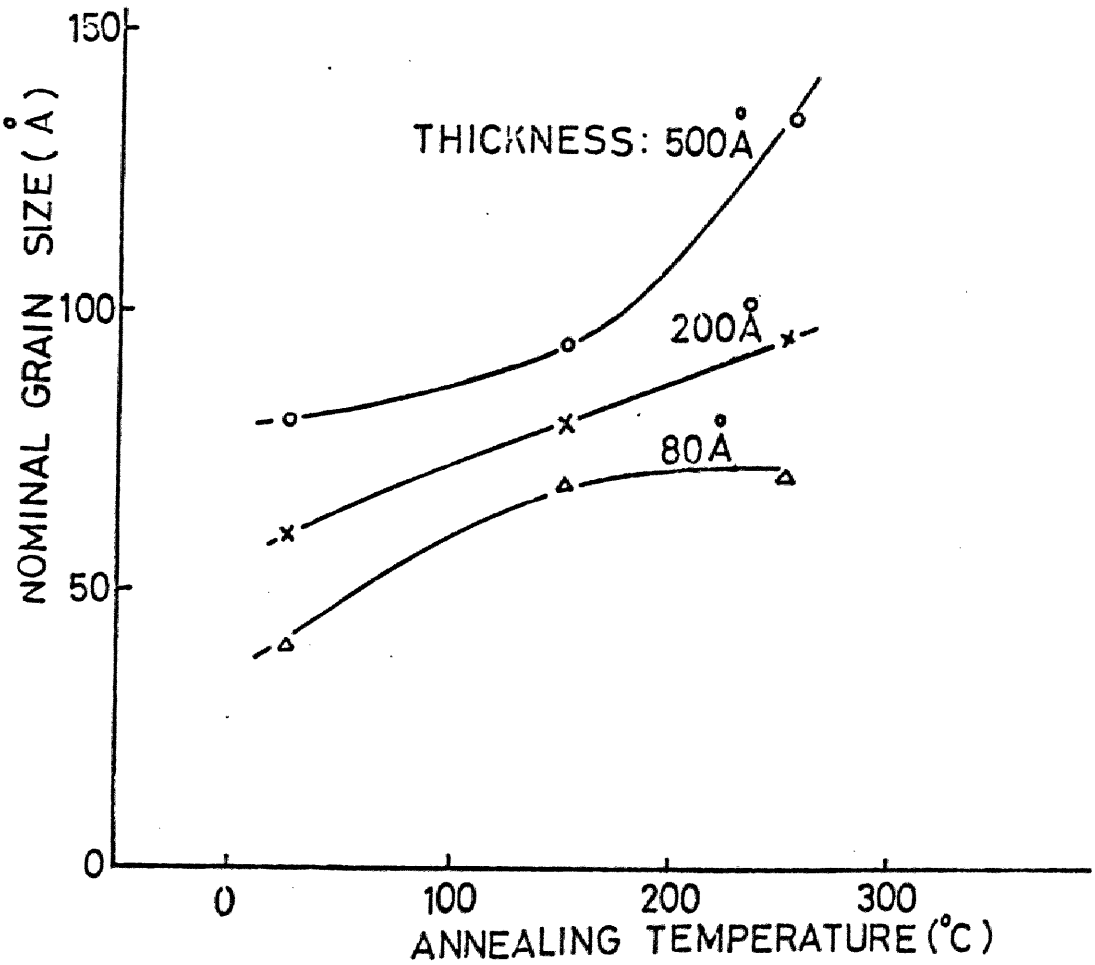

Fig. 4.2 Grain grwoth of three films with various thicknesses during annealing at 150°C and 250°C for 100 min.

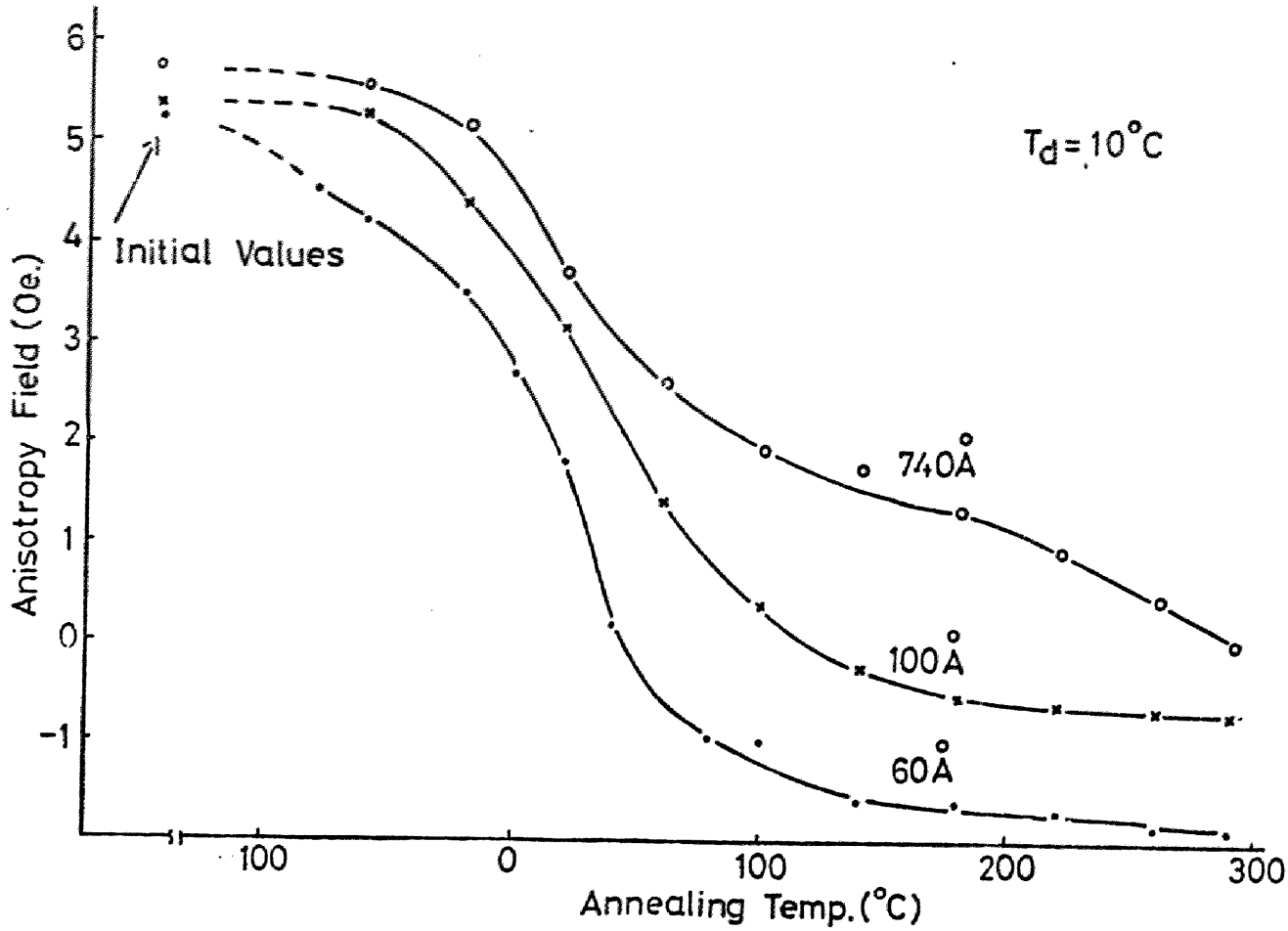

Fig.4.3 Isochronal annealing curves of the anisotropy field for as-deposited films in a field parallel to HA, where the film thickness is chosen as a parameter.

the film thickness is chosen as a parameter. As seen in the figure, though there are no substantial differences in the initial values of H_k, it changes more rapidly in thinner films at the temperature up to about 100°C. Hence the net variation of H_k increases with the decrease of film thickness in this temperature range. Above 120°C, H_k seems to saturate in very thin films as d=60Å, while it decreases monotonously in thicker films. It must be noted that the apparent saturation above 120°C in thinner films is by no means the accomplishment of the equilibrium state, because the magnitude of the equilibrium anisotropy field is considered to be 3∿4 Oe [4] and is actually attained in thinner films by HA isothermal annealing at 380°C for several days.

4.4 Discussion

In the anisotropy-relaxation model proposed by Roth[3], the concentration of thermal vacancies is assumed to fall off continuously with distance from the center of the grain boundary. However, little is known at present about the detailed aspect of such behavior [2], and therefore in analysing the atom transport along grain boundaries, it is customary to take the grain boundary as a homogeneous slab of width w which posseses a uniform diffusivity D_b [5].

This approximation may be also applicable to the reorientation of atom pairs in thin films (hereafter we call this "grain boundary model"). Since the activation energies for the grain boundary diffusion is generally considered to be about one half of those for the lattice diffusion [1], the anisotropy relaxation in films will progress in different two stages; the pair reorientation in the slab of the grain boundary (the 1-st stage) and within the grains (the 2-nd stage). The effective width of the grain boundary for the atom transport is considered to be a few atomic distances [1]. The reorientation of atom pairs at the first stage may also take place in the same grain boundary region. Thus the importance of the 1-st stage is more remarkable in the case of finer grains. By using typical values of the grain diameter D = 100 Å, and the grain boundary width w = 5 Å, the fractional contribution of the 1-st stage is estimated to be about 10%, provided that the anisotropy energy density in the grain boundary slab is the same as that within the grain. In this way, the grain boundary seems to form an important part of the anisotropy relaxation at the low temperature. Furthermore, the grain boundary model explains the lack of the 1-st stage in

the single crystal permalloy films. According to the experiments of Itō et al.[6], the inducing process of the anisotropy in single crystal films deposited epitaxially onto rock-salt, follows single 1-st order process with the activation energy corresponding to the lattice diffusion.

In the case of polycrystalline as-deposited films, the anisotropy relaxation at low temperatures is more prominent in thinner (finer grain) films. This fact seems to support the grain boundary model as well. This model, however, is insufficient to describe the anisotropy relaxation, especially, for as-deposited films; because in this model the grain boundary is idealized as an immutable slab with the definite width and diffusivity, but in actual films, the anisotropy relaxation is accompanied by the grain boundary movement, vanishment or its internal structural change.

As described in chapter 3, the anisotropy relaxation of as-deposited films never consists of discrete two stages, but rather consists of several stages. This may be explained from the stand point of the grain boundary model as follows; unusually small activation energies (0.2 ∿0.5 eV) appearing at the initial stage of isochronal annealing may be ascribed to the atom diffusion at the particularly unstable portions of the grain boundaries (or film surfaces), where the energy barrier for the atom transport is lowerd due to the spacial atomic arrangement. Since the activation energy is distributed among the various kinds of grain boundaries or surfaces (for example, the self diffusion energy on the (111) surface is as low as 0.165 eV in f.c.c. rhodium [7]), the anisotropy relaxation may consist of many stages corresponding to the different activation energies.

4.5 Concluding Remarks

By using grain boundary model, we can explain the grain size dependence of the anisotropy-relaxation process with low activation energies. Furthermore, this model may explain the anisotropy relaxation at the temperature lower than the deposition (or preannealing) temperature. On the other hand, the excess vacancy model is inexplicable for these annealing behaviors. Thus we should take into account the contribution of grain boundaries in the anisotropy relaxation.

Two anisotropy-relaxation models, namely, the excess vacancy model and grain boundary model, are thought to be two extrema for the real situation of lattice defects in polycrystalline films. The excess vacancy model is based on the assumption that vacancies exist uniformly and migrate at random within the grain and disappear completely at the grain boundary, whereas the grain boundary model on the assumption that defects are localized near the grain boundary and by no means disappear. Vacancies in the actual films might be in the various intermidiate states between these two extreme models. In other words, vacancies in thin films are thought to be not so free from stress field as postulated in the excess vacancy model; and not such a equilibrium state as in the grain boundary model. In any way, more precise knowledges on the atom transport in polycrystalline films are necessary to make clear this problem.

References

1) N. A. Gjostein : Diffusion (Am. Soc. Metals, Metal Park, Chio, 1973) p.241

2) R. W. Balluffi and J. M. Blakely : Thin Solid Films. 25 (1975) 363.

3) M. Roth : J. appl. Phys. 41 (1970) 1286.

4) S. J. Holowitz and M. L. Ruder : Phys. Stat. Sol. (a) 5 (1971) 427.

5) J. C. Fisher : J. appl. Phys. 22 (1951) 74.

6) S. Ito, S. Uchiyama, T, Fujii and S. Ishibashi : ICMTF Coll. Booklet 5 (1972) B3.

7) W. R. Graham and G. Ehrlich : Thin Solid Films, 25 (1975) 85.

Chapter 5
Verification of Micromagnetic Ripple Theory

5.1 Introduction

As described in sec. 1.4.3, it has been clarified experimentally that the magnetization ripple originates mainly from the local anisotropy of randomly oriented crystallites [1]. For the purpose of obtaining a detailed understanding about the magnetization ripple, it is indispensable to confirm the micromagnetic theory which relates the local anisotropy K with macroscopic quantities, such as the fall back angle, the susceptibility and so on.

According to the ripple (dispersion) theory developed by Hoffmann [2] on the basis of micromagnetic model, the dispersion (fall back angle) - anisotropy product $\alpha_{90} K_u$ depends on the local anisotropy K (or " structure constant" S) as

$$K_u \alpha_{90} = \frac{3}{16} \frac{D^2 \sigma_I^2}{\pi A d} K^2 \equiv \frac{3}{8\pi A} S^2 \quad . \tag{5.1}$$

In the previous work of Uchiyama et al. [3], however, this theory was criticized from the experimental point of view. Their results were well explained by the protodomain model rather than the micromagnetic model. In the protodomain model, $K_u \alpha_{90}$ is easily related with K as [3],

$$K_u \alpha_{90} = 0.82 N^2 K \propto S \quad , \tag{5.2}$$

Here N is the number of crystallites involved in each protodomain.

In this way, it is a very important problem to confirm experimentally which ripple (dispersion) model is valid. To begin with, we shall examine the validity of Hoffmann's dispersion

theory [eq. (5.1)] by measuring the bias susceptibility, which is the most useful and reliable method for testing the theory.

5.2 Transverse Bias Susceptibility [4)]

The transverse bias susceptibility means the initial susceptibility under the bias field applied pependicular to the mesurment direction. In the case of Ni-Fe film, the susceptibility is measured by applying a dc bias field and a small ac field perpendicular to each other, both being in the film plain; and detecting the magnetization change in the ac field direction. The initial susceptibility is determined, in general, by the effective field acting on the each magnetic moment in the sample. In the uniaxial film, the effective field is given by the sum of the single domain field h_1 [eq. (1.5)] and the local demagnetization field h_d resulting from the internal magnetic pole of the ripple (Fig. 1.4a).

According to the calculation of Hoffmann [5)], the average value of h_d is given by

$$\langle h_d \rangle = \frac{2M^2}{K_u} \frac{K_u h^{1/2}}{A} \cdot d \cdot \langle \phi_1^2 \rangle = \frac{1}{4\pi\sqrt{2}} \frac{M d^{1/2}}{(Ak_u)^{5/4}} \frac{S^2}{h_1^{1/4}}, \qquad (5.3)$$

where ϕ_1^2 is the mean square value of the ripple amplitude given by eq. (1.9). The transverse bias susceptibility χ_t is hence written as

$$\chi_t(h,\beta) = \frac{\chi_0}{h_1+\langle h_d \rangle} = \frac{\chi_0}{h_1+ch_1^{-1/4}} . \qquad (5.4)$$

Here $\chi_0 = M/H_k$ and

$$c = \frac{1}{4\pi\sqrt{2}} \frac{M d^{1/2}}{(AK_u)^{5/4}} S^2 . \qquad (5.5)$$

5.3 Experimental Procedure

Experiments of both χ_t and α_{90} were carried out by two techniques. The one using the magneto-optic Faraday effect, enabled us to measure them on small area of about 0.05 mm^2 in samples [1] . The other was the conventional inductive sensing to measure on whole sample area of about 100 mm^2. In the measurement of χ_t, an ac tickle field of 20 ∿ 50 m Oe and a dc bias field up to about 20 Oe were applied in the film plane parallel and perpendicular to the EA direction, respectively. For the magneto-optical detection, 25 Hz was chosen as the frequency of tickle field so as to avoid the high frequency noise from the photomultiplier tube, whereas for the inductive detection the frequency was 1KHz. In both cases, the signal was detected by a lock-in amplifier and the output signal was plotted on a X-Y recorder against the bias field. Figure 5.1 shows the block diagram of the arrangement for the measurement of χ_t using the magneto-optical detection.

As for the measurement of α_{90}, the fall back angle was observed in the small area of a film. The anisotropy field H_k was determined by the following methods, (i) from the field corresponding to the maximum of Im (χ_t), (ii) from the transverse hysteresis curve, (iii) from the field corresponding to the linear extrapolation of χ_t^{-1} vs. H plot to $\chi_t^{-1} \rightarrow 0$. For films with large α_{90}, however, the precise determination of H_k was difficult by the use of these three methods.

Samples examined here were Permalloy films (70 ∿ 80%Ni) vacuum-deposited onto quartz-glass substrates at room temperature. Some of them were subjected to the appropriate heat treatment at the temperature of 30 ∿ 300°C for obtaining various magnitude of S.

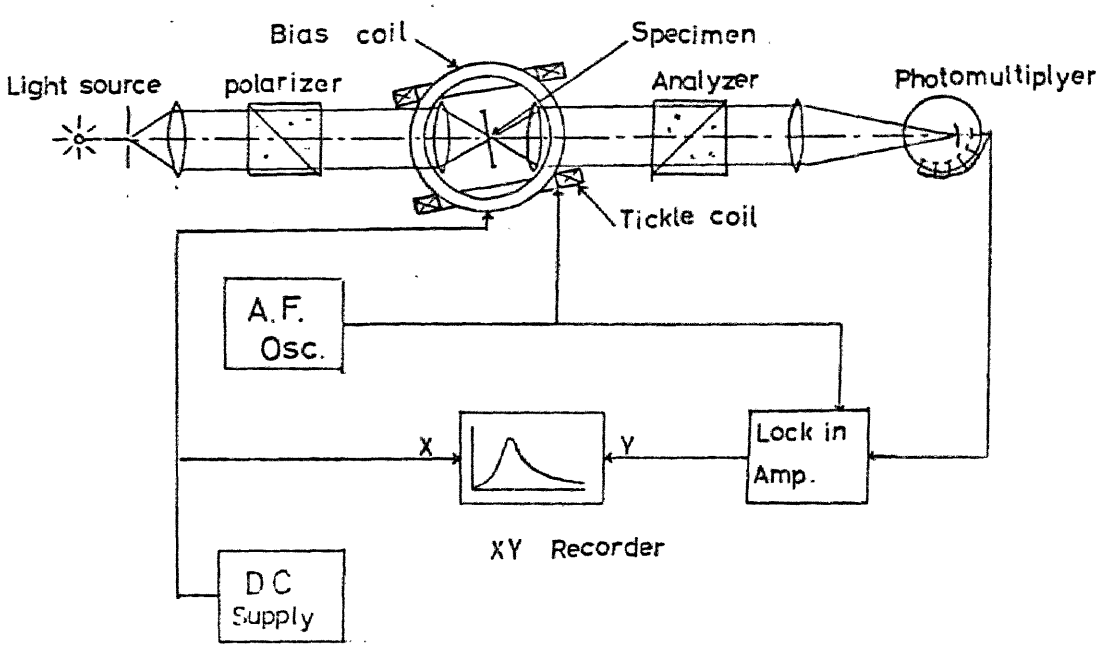

Fig. 5.1 Block diagram of the experimental arrangement for the measurement of transverse bias susceptibility using magneto-optical Faraday effect.

5.4 Results and Discussion

5.4.1 Determination of structure constant S

To begin with, let us consider how to determine the structure constant S precisely. This is the most important subject in examing the validity of the micromagnetic ripple (dispersion) theory.

When the bias field h greater than anisotropy field (h > 1) is applied along the HA, then eq. 15.4) reduces to eq. (5.6) by putting ,

$$\chi_t(h) = \frac{\chi_0}{(h-1)+c(h-1)^{-1/4}} \qquad (5.6)$$

From eq. (5.6), we can determine the value of c or the structure constant S through eq. (5.5). Following three methods were considered here in estimating S.

(i) Plotting χ_t^{-1} vs. h, making linear extrapolation of data at $h \gg 1$ to $h \simeq 1$, and determing c from the difference between the experimental curve and the extrapolated line.

(ii) From the difference between the anisotropy field H_k and the bias field magnitude H_p corresponding to the maximum susceptibility.

(iii) Plotting χ_t (h) normalized by $\chi_t(h)$ at a certain bias field magnitude (e.g. at h = 2) and comparing it with theoretical curves.

Method (i) was adopted by Leaver et al.[6] for the transverse bias susceptibility as well as by Comstock et al.[8] for the incremental susceptibility. As is evident from eq. (5.6), this is a very useful and simple method for films with small c. With larg c , however, χ_t^{-1} vs. H plot does not become linear even

when H is relatively large with respect to H_k. Furthermore, in the case of $H \gg H_k$, the value of χ_t becomes very small, so that the noise in the output signal plays serious role to the determination of c. In this way, method (i) was not found to be appropriate to the determination of c covering a very wide range in magnitude.

Method (ii) was used by Leaver et al[6] and Finnegan and Doyle[8]. Differentiating eq. (5.6) with respect to k, we can easily obtain eq. (5.7),

$$(H_p - H_k)/H_k = h_p - 1 = (c/4)^{4/5} . \qquad (5.7)$$

There is, however, a strong suspicion that this method is beyond the limit of the theory owing to the marked nonlinear effect near $h = h_p$[10].

Method (iii) may be the most reliable of the three because the experimental curve is fitted with the theoretical curve in the wide range of $h > h_p$.

For these reasons, method (iii) was adopted into the determination of c or S. Fig. 5.2 shows the experimental results of $\chi_t(h)$ for three typical samples measured on the small inspection area together with the theoretical curves (broken lines) of eq. (5.6), where the values of c are chosen to give the best fit to the experimental curves. As clearly seen in the figure, the experimental curves of $\chi_t(h)$ agree well with the theoretical ones in the wide range of h extending from H_p of several Oersteds to about 20 Oe. This suggests that the measurment of very small area is quite usefull in eliminating the effect of the long-range anisotropy dispersion.

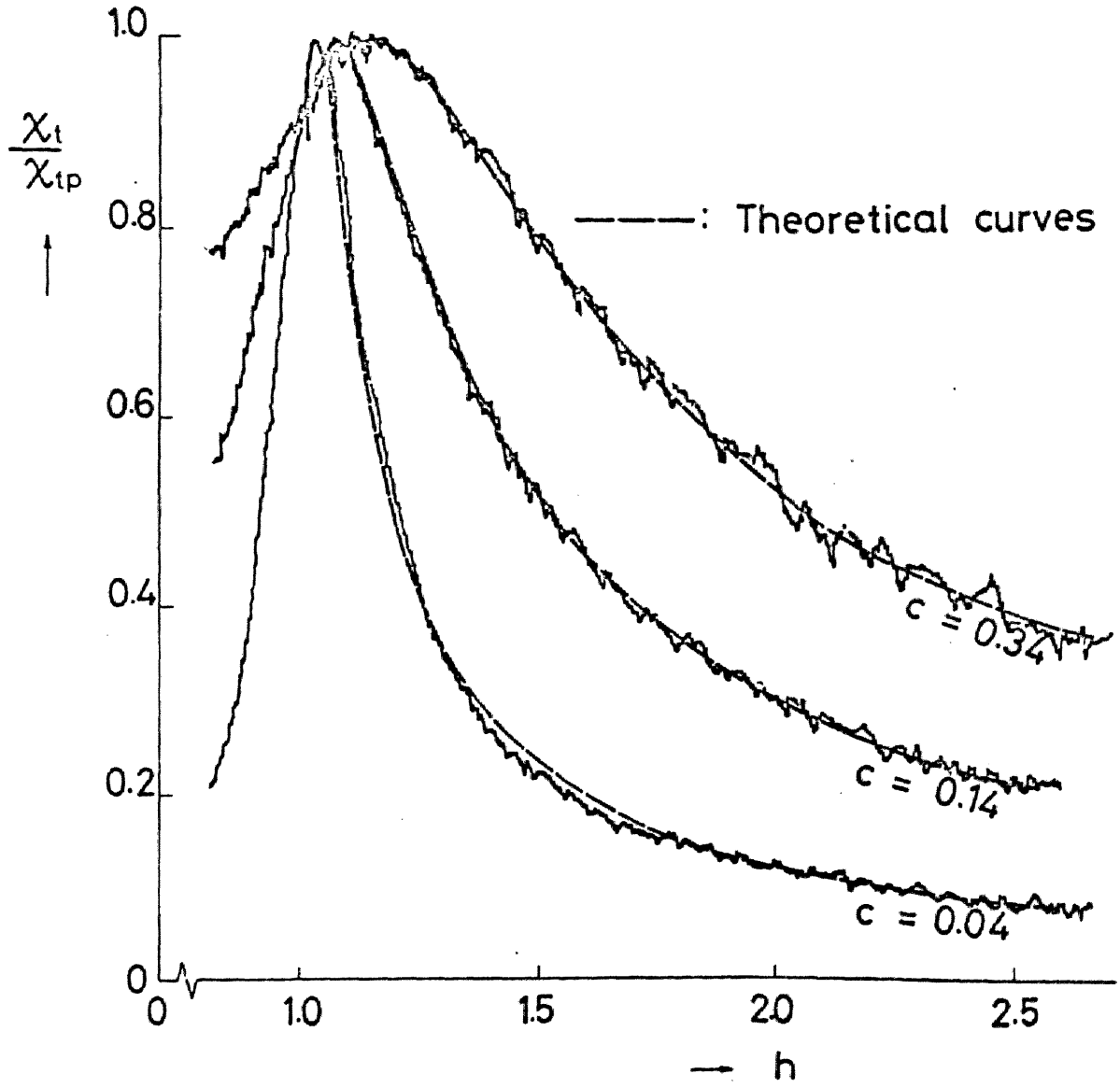

Fig. 5.2 Transverse bias susceptibility χ_t vs. HA bias field h measured on a very small area of about 0.05 mm^2 in typical three films. The bloken lines show theoretical curves of eq. (5.6) for appropriate values of c.

On the contrary, $\chi_t(h)$ curves measured on the whole film area, in general, do not agree well with the theoretical ones.

5.4.2 Comparison of the experimental results with micromagnetic dispersion theory.

Now, we should like to examine how the dispersion-anisotropy product $\alpha_{90} K_u$ depends on the structure constant S. Log-log plots of $\alpha_{90} K_u$ against S are shown in Fig. 5.3, where S is determined as described above. The solid line in the figure is the theoretical dependence of eq. (5.1), where the exchange stiffness A is taken as 10^{-6} erg /cm. As seen in the figure, experimental results agree fairly well with the prediction of the micromagnetic theory.

5.4.3 Influence of the long-range dispersion on the transverse bias susceptibility characteristics

In this section, let us discuss the results of the susceptibility measured for the whole film area. Figure 5.4 demonstrates the correlation between the fall back angles α_{90} and α_{90}^*. Hereafter, the asterisk denotes the value for whole film area. The deviation of α_{90}^* from α_{90} seems to be due to the contribution of the long-range dispersion which is sometimes called "skew". Figure 5.5 shows χ_t^* as a function of h for the same films as shown in Fig. 5.3, together with the theoretical curves shown in Fig. 5.2. Comparing Fig. 5.5 with Fig. 5.2, we find that $\chi_t^*(h)$ curve is broader than $\chi_t(h)$ curve. By fitting the $\chi_t^*(h)$ curves to the theoretical ones, the values of S^* was determined. The relation between S and S^* is plotted in Fig. 5.6, showing

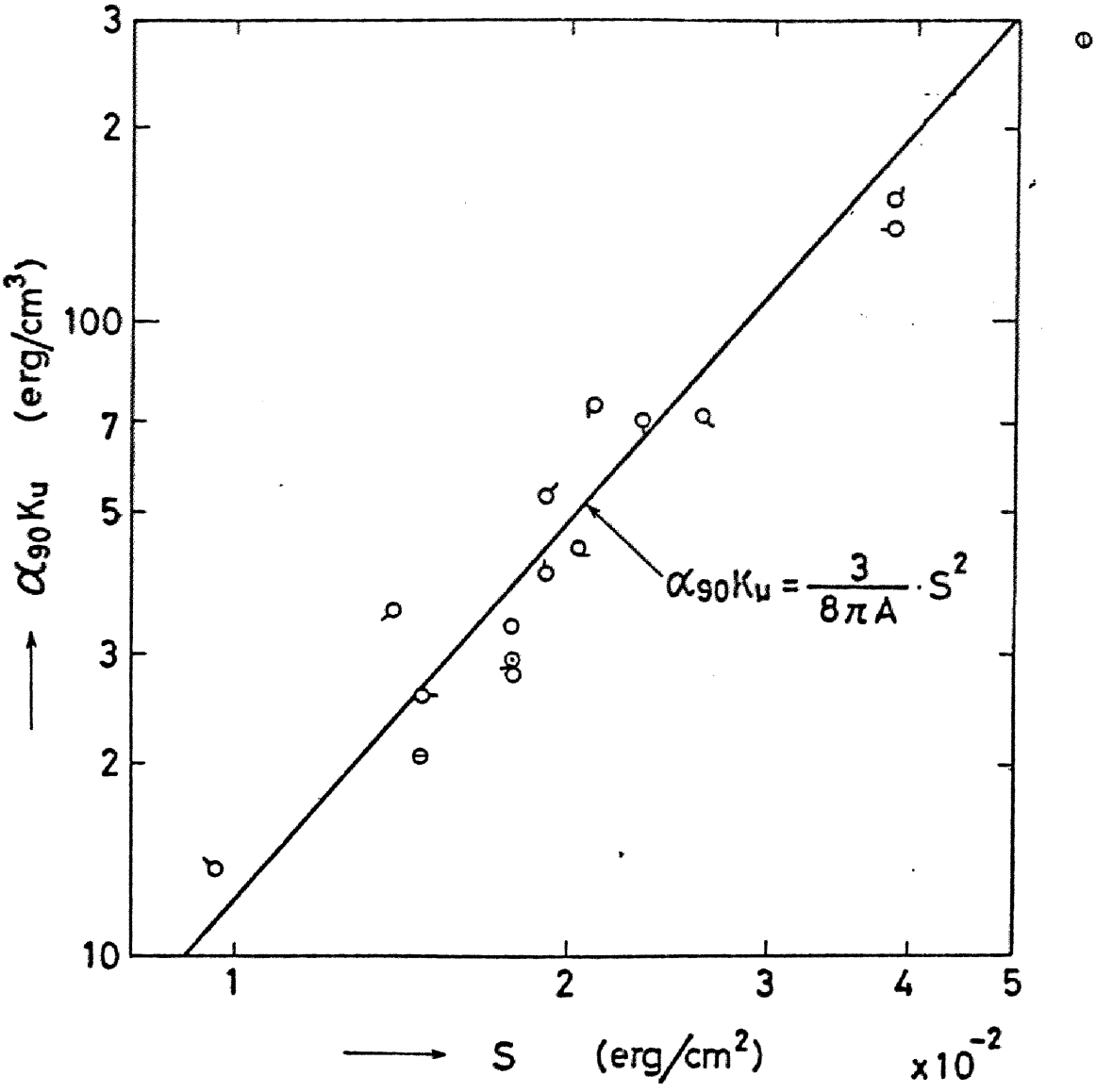

Fig. 5.3 Dispersion-anisotropy product $\alpha_{90}K_u$ vs. structure constant S determined from $\chi_t(h)$. The solid line is the theoretical relation of eq. (5.1), where A = 10^{-6}erg/cm.

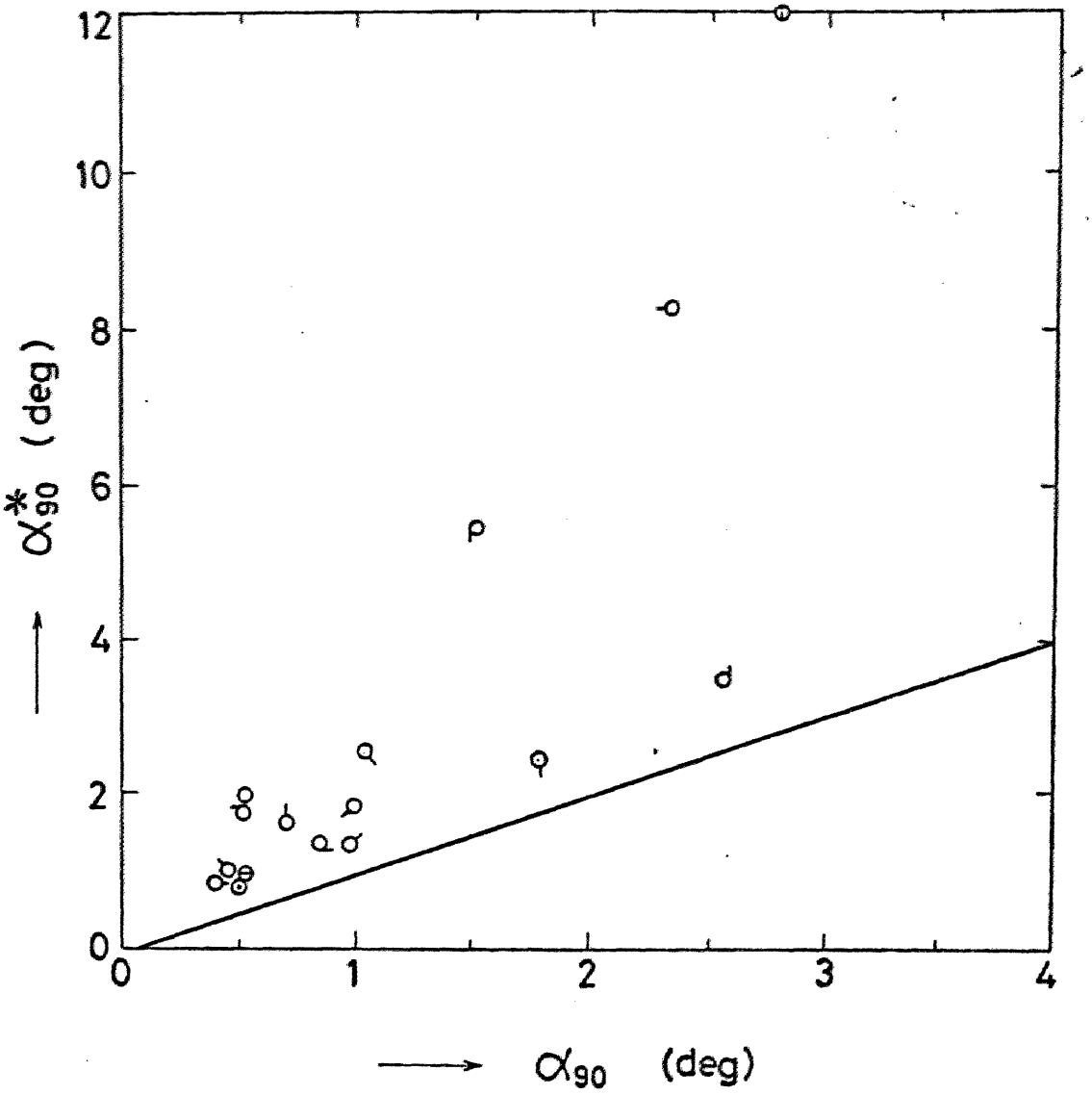

Fig. 5.4 Fall back angle α_{90} measured on the small area vs. α_{90}^* for whole film area.

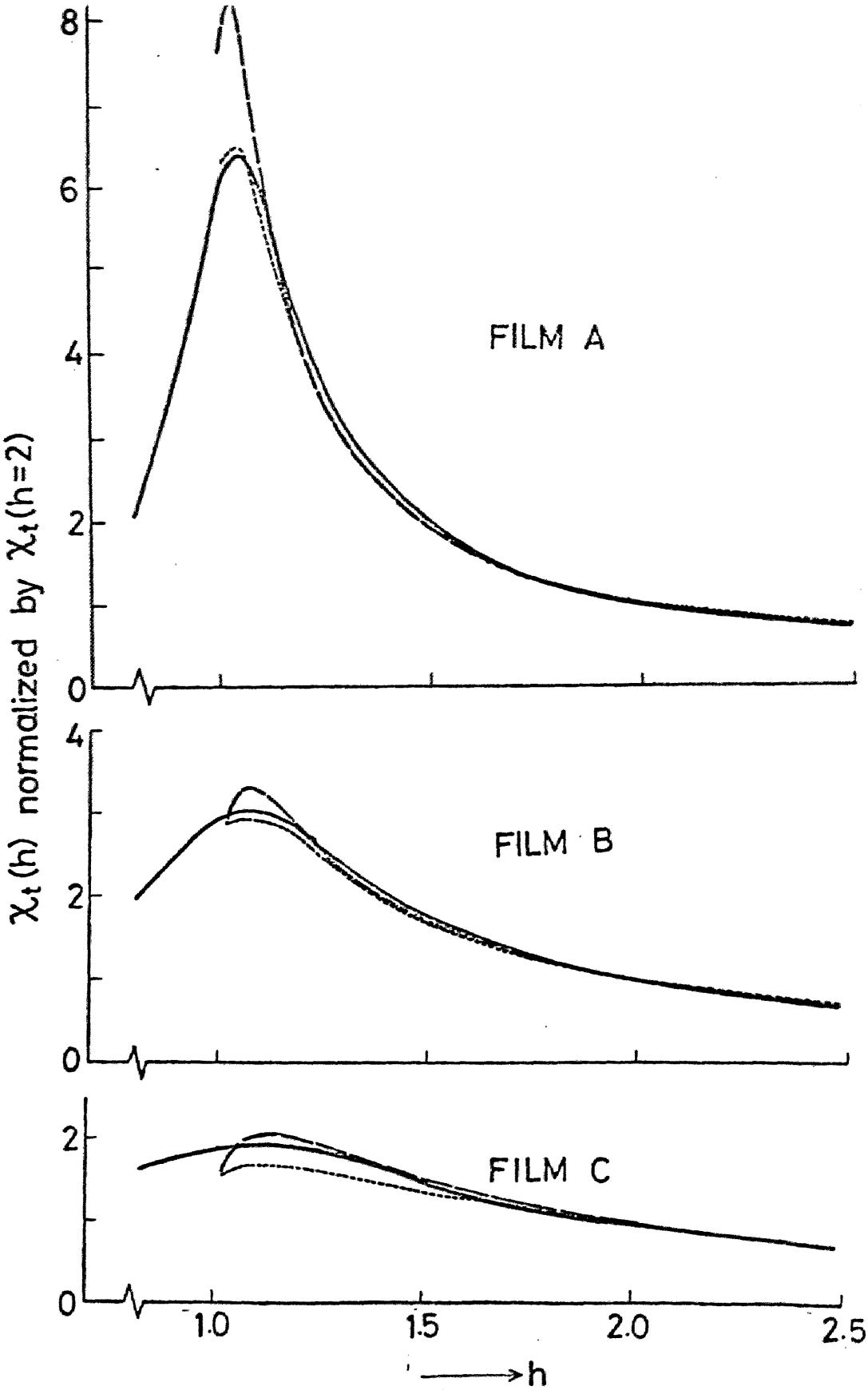

Fig. 5.5 Transverse bias susceptibility χ_t^* vs. HA bias field h, measured on the whole film area for the same films with Fig. 5.1. The solid, broken and doted lines are the experimental, theoretical [eq.(5.6)] and calculated [eq.(5.8)] curves respectively.

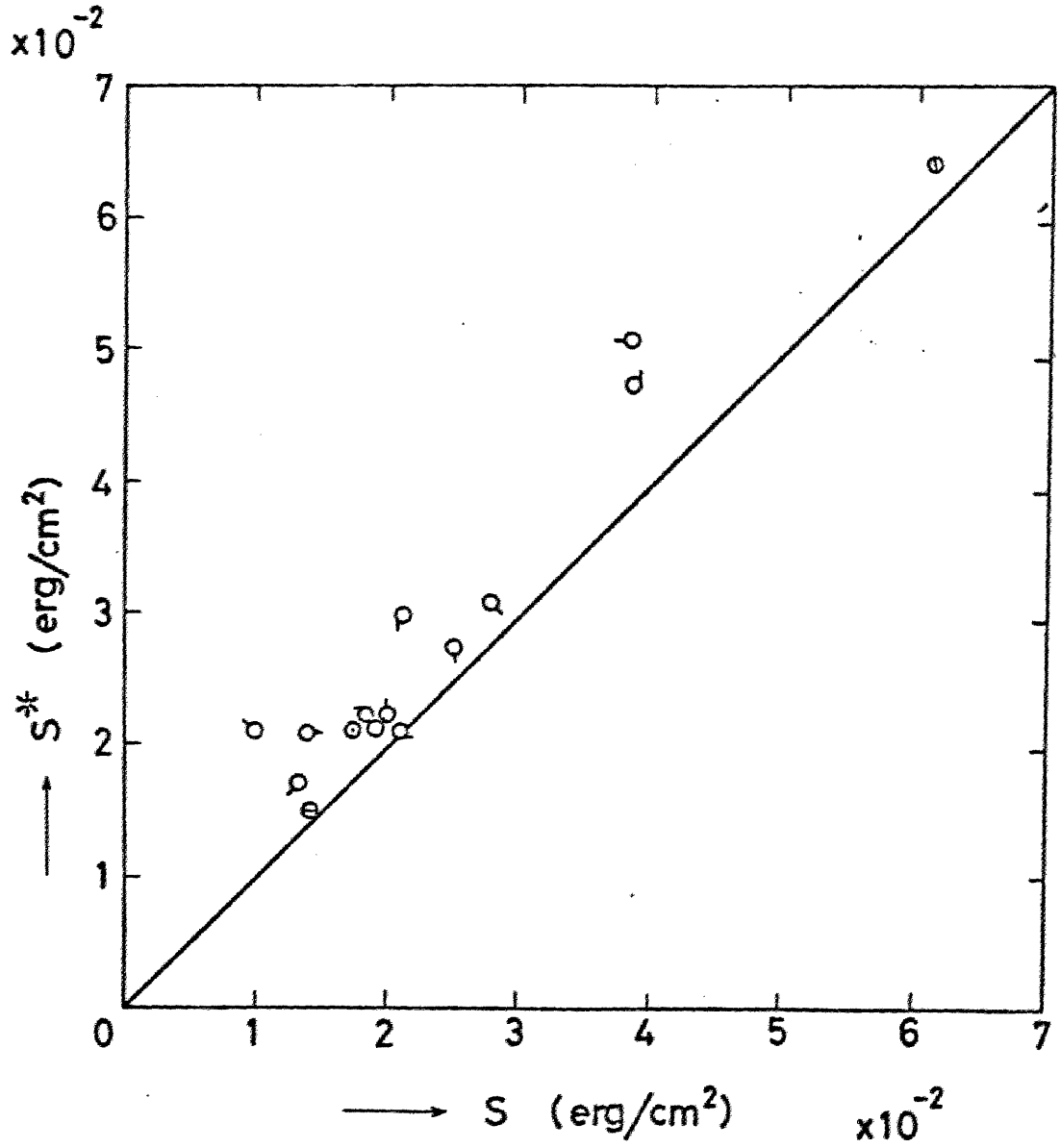

Fig. 5.6 Correlations between S and S^* for the films shown in Fig. 5.3. Asterisk denotes the value determined from $\chi_t(h)$ of whole film area.

that long-range dispersion raises the value of S.

As a simple interpration of this situation, a numerical calculation of $\chi_t^*(h)$ was carried out on the basis of the following assumptions:

(i) The film consists of independant regions not interacting with each other as is in the case of anisotropy-dispersion model.

(ii) The distribution for the EA direction of each region is of the Gaussian type around the average EA.

The resulting $\chi_t(h)$ may, therefore, be calculated by integrating the susceptibility of each region.

Thus,

$$\chi_t^*(h) = \int \rho(\delta) \chi_t(\tfrac{\pi}{2}-\delta, h)\, d\delta \ , \qquad (5.8)$$

where $\rho(\sigma)$ denotes the angular distribution function of the Gaussian type, being expressed as

$$\rho(\delta) = \frac{1}{\sqrt{2\pi}\sigma_0} \exp\left(-\frac{\delta^2}{2\sigma_0^2}\right) . \qquad (5.9)$$

Here σ_0 is the standard deviation of δ and related to α_{90}^* as $\sigma_0 = 0.61\alpha_{90}^*$. Substituting eq. (5.9) into eq. (5.8), we obtain

$$\chi_t^*(h) = \frac{0.654}{\alpha_{90}^*} \int_{-\frac{\pi}{2}}^{\frac{\pi}{2}} \chi_t(\tfrac{\pi}{2}-\delta,\ h) \exp\left\{-1.345\left(\frac{\delta}{\alpha_{90}^*}\right)^2\right\} d\delta \qquad (5.10)$$

Dotted lines in Fig. 5.5 are the results calculated from eq. (5.10) by using the data of c and α_{90}^*, listed in Table 5.1. The agreement between the calculation and the mesurment seems fairly satisfactory.

Table 5.1 Fall back angles, structure constants and uniaxial anisotropy constants for typical three films.

Film	Composition (% Ni in melt)	Fall back angle (deg)		Structure const. (erg/cm^2)		Anisotropy const. (erg/cm^3)
		α_{90}	α_{90}^*	$Sx10^2$	S^*x10^2	K_u
A	75.0	0.38	0.9	1.51	2.1	3.98×10^3
B	75.0	1.00	2.5	2.72	3.1	3.76×10^3
C	75.0	2.72	12.0	6.27	6.4	5.35×10^3

5.5 Conclusion

It is experimentally confirmed that the transverse susceptibility χ_t (h) measured on the restricted area agrees well with the micromagnetic ripple theory and the deviation from the theoretical curve can also be explained by the effect of the long-range dispersion. Furthermore, Hoffmann's dispersion theory based on the micromagnetic model proved to be reliable from the experimental point of view. It should be noted, therefore, that the previous conclusion of Uchiyama et al. on the origin of the magnetization ripple must be reexamined on the basis of Hoffmann's dispersion theory. This problem will be discussed in the next chapter.

References

1) T. Fujii, S. Uchiyama, E. Yamada and Y. Sakaki : Japan J. appl. Phys. 6 (1967) 1.

2) H. Hoffmann : Z. angew. Phys. 18 (1965) 479.

3) S. Uchiyama, T. Fujii, M. Masuda and Y. Sakaki : Japan. J. appl. Phys. 18 (1965) 499.

4) H. Hoffmann : Phys. Stat. Sol. 17 (1966) K105.

5) H. Hoffmann : IEEE Trans. Mag. MAG-2 (1966) 566.

6) K. D. Leaver, M. Prutton and F. G. West : Phys. Stat. Sol. 15 (1966) 267.

7) K. D. Leaver : J. appl. Phys. 39 (1968) 1157.

8) C. S. Comstock, A. C. Sharp, R. L. Samuels and A. V. Pohm: IEEE Trans. Mag. MAG-4 (1968) 39.

9) W. D. Doyle and T. F. Finnegan : J. appl. Phys. 39 (1968) 3355.

10) H. Hoffmann : private communication.

Chapter 6
Effective Crystalline Anisotropy

6.1 Introduction

A number of efforts have been made to investigate the nature of the anisotropy inhomogeneity in Permalloy films, which is believed to cause the local magnetization fluctuation such as the magnetization ripple and the skew in memory arrays. In the previous works of Fujii, Uchiyama et al.[1-3], this problem was dealt with for vacuum-deposited Permalloy films, and they succeeded, to some extent, in interpreting the physical properties of the ripple phenomena and the relationship between the ripple and the skew by the local measurment of the fall back angle. However, some essential points have yet remained unsolved : 1) The local anisotropy K was determined from the experimental values of α_{90} by the use of the simple protodomain model [eq. (5.2)] rather than the rigorous theory based on micromagnetics [eq. (5.1)]. 2) As for the origin of the local anisotropy a very intuitive expression seemed to fit with experimental results better than more precise expression derived by Doyle-Finnegan[4]. This intuitive expression is given by

$$K^2 = K_1^2 + \left(\frac{3}{2}\lambda\sigma_a\right)^{3/2}, \tag{6.1}$$

where K_1 is the first magnetocrystalline anisotropy constant, λ the saturation magnetostriction constant for the polycrystalline sample, σ_a the anisotropic stress acting on each crystallite. This equation is based on the assumption that the contributions from the magnetocrystalline anisotropy and the magnetoelastic anisotropy are independently superimposed on each other.

As for the first point, however, it has been verified in the preceeding chapter, that the micromagnetic dispersion theory is quite reliable. Thus, in this chapter, we shall reexamine the origin of magnetization ripple by using the micromagnetic disperion theory.

6.2 Modified Doyle-Finnegan's Model for Effective Crystalline Anisotropy

We shall begin with a brief explanation about the local anisotropy (effective crystalline anisotropy) constant K. In Doyle-Finnegan's model[4], the M-induced uniaxial anisotropy in polycrystalline film is assumed a priori parallel in each crystallite. However, it should fluctuate from crystallite to crystallite depending on its crystallographic orientation as was first pointed out by Roth[5]. This effect was previously recognized by Chikazumi[6] for bulk Ni_3Fe single crystal samples. Considering this effect, the total anisotropy energy of each crystallite E_c of a particular crystallite under the isotropic planar stress σ is given by,

$$E_c = E_k + E_\sigma + E_a \ , \tag{6.2a}$$

where the magnetocrystalline anisotropy E_k is given as

$$E_k = K_1 \sum_{i>j} \alpha_i'^2 \alpha_j'^2 \ , \tag{6.2b}$$

and the magnetostriction anisotropy E_σ as

$$E_\sigma = -\frac{3}{2} \lambda_{100} \sigma \sum_i (1-\gamma_{i3}^2) \alpha_i'^2 + 3\lambda_{111} \sigma \sum_{i>j} \gamma_{i3} \gamma_{j3} \alpha_i' \alpha_j' \ , \tag{6.2c}$$

where λ_{100} and λ_{111} are magnetostriction constants in [100]

and [111] directions, respectively, and as for the M-induced anisotropy E_a, we adopt Néel's expression

$$E_a = -Q \left(\sum_i \gamma_{i1} \alpha_i'^2 + k \sum_{i>j}' \gamma_{i1} \gamma_{j1} \alpha_i' \alpha_j' \right) , \qquad (6.2d)$$

where k is a constant depending on the mechanism of the anisotropy and Q is related to the uniaxial anisotropy constant K_u as $K_u = \frac{3k + 4}{10} Q$. In these equations, α_i' (i=1,2,3) denotes the direction cosine of the magnetization with respect to the crystallographic principal axes (x', y', z'), and γ_{ij} (i,j =1, 2, 3) the direction cosines between the axes (x', y', z') and the reference axes (x, y, z) which are so fixed that the film is in the xy-plane and the average EA in the x-direction. Since, during the measurement of the fall back angle α_{90} or the bias susceptibility, the HA applied field is grater than H_k, the magnetization of each crystallite is restricted to a small angle from the average magnetization parallel to the HA. Therefore, we can rewrite eq. (6.2) in the (x, y, x) co-ordinate system, expand the result in powers of ϕ_1, where ϕ_1 is angle between the magnetization direction of each crystallite and the average magnetization ($\cos \phi_1 = \alpha_1$), and retain only first order terms in ϕ_1. Then eq. (6.2) is reduced to

$$E_c = -2 [\left\{ K_1 + \frac{3}{2} (\lambda_{100} - \lambda_{111}) \sigma \right\} \eta' + \left\{ \frac{3}{2} (\lambda_{100} - \lambda_{111}) \sigma + \gamma K_u \right\} \zeta'] \phi_1 , \qquad (6.3)$$

where

$$\eta' = \sum_i \gamma_{i1} \gamma_{i2}^3 , \qquad (6.4a)$$

$$\zeta' = \sum_i \gamma_{i1}^3 \gamma_{i2} , \qquad (6.4b)$$

and

$$\gamma = \frac{5(2-k)}{3k+4} \quad . \tag{6.}$$

The quantities η' and ζ' are random variables with vanishing averages, but with definite dispersion. Then E_c has vanishing mean, but it has a definite mean square. In the absence of σ and γK_u, the mean square of E_c is given by

$$\langle E_c^2 \rangle = 4K_1 \langle \eta^2 \rangle \phi_1^2 = \frac{8}{105} K_1^2 \phi_1^2 , \tag{6.}$$

while in the presence of σ and γK_u, it is given by

$$\langle E_c^2 \rangle = \frac{8}{105} K^2 \phi_1^2 , \tag{6}$$

where the effective crystalline anisotropy K is given as

$$K^2 = \left\{K_1 + \frac{3}{2}(\lambda_{100} - \lambda_{111})\sigma\right\}^2 - \frac{3}{2}\left\{K_1 + \frac{3}{2}(\lambda_{100} - \lambda_{111})\sigma\right\}$$

$$\times \left\{\gamma K_u + \frac{3}{2}(\lambda_{100} - \lambda_{111})\sigma\right\} + \left\{\gamma K_u + \frac{3}{2}(\lambda_{100} - \lambda_{111})\sigma\right\}^2 . \tag{6.8}$$

It should be noted that γ in eq. (6.5) varies with the lattice type as well as with the mechanism of the induced anisotropy itself[5], because k depends on these quantities[7]. Some theoretical values of γ for Permalloy are, for the pair-order anisotropy, $\gamma = -0.63$ ($k = 4$) or $\gamma = 0$ ($k = 2$) in the case of the single crystal and polycrystal, respectively; and for the M-induced magnetostriction anisotropy[8], γ varies -0.7 to + 2.0 with composition, according to eq. (6.9).

$$k = \frac{3c_{44}\lambda_{111}\lambda_{111}'}{(c_{11} - c_{12})\lambda_{100}\lambda_{100}'} , \tag{6.9}$$

where c_{ij} is the ordinary elastic constant and the prime

denotes the value at the constraint (annealing) temperature.

Let σ be zero in eq. (6.8), and we readily obtain

$$K_{min}^{\ 2} = K_1^{\ 2} - \frac{3}{2}\gamma K_1 K_u + \gamma^2 K_u^{\ 2} \qquad (6.10)$$

This may be realized if the internal stress becomes small by an appropriate heat treatment.

6.3 Experimental Procedure

Both the measurments of fall back angle α_{90} and the uniaxial anisotropy constant K_u were made by means of magneto-optical technique as described in chapter 5. Films of 400 Å thick used in this experiment were deposited in a vacuum of $2 \sim 5 \times 10^{-5}$ Torr. onto substrates kept about 30°C with the rate of about 4 Å/sec.

For the purpose of changing the film parameters, samples were then sequentially subjected to isochronal EA annealing at 100 ~ 330°C. Magnetic properties were measured at room temperature after cooling from each annealing cycle.

6.4 Experimental Results

Figure 6.1 shows the composition dependence of α_{90} for 50% to 95% Ni with annealing temperature as a parameter. When T_a = 30°C, distinct minima of α_{90} are found in the vicinity not only of 84%Ni but also of 60% Ni. Around these two compositions, α_{90} remains almost constant regardless of the annealing temperature.

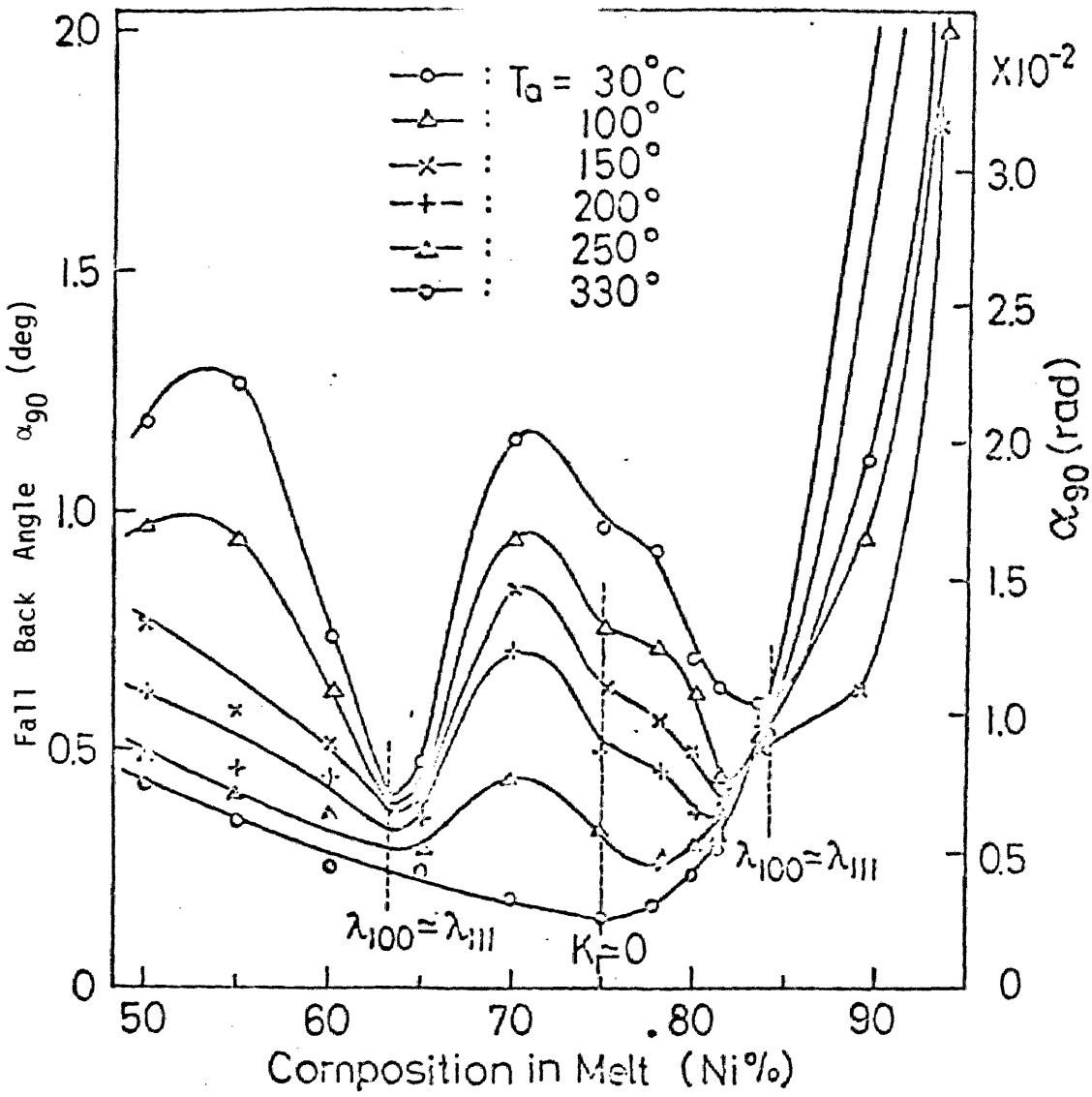

Fig. 6.1 Fall back angle α_{90} vs. composition for Ni-Fe films annealed at T_a.

In addition, it may be noted that these compositions lie very close to the point of $\lambda_{100} = \lambda_{111}$ as seen from Fig. 6.2[9]. For films with $\bar{\lambda} > 0$ ($\bar{\lambda} = \frac{3}{5}\lambda_{100} + \frac{2}{5}\lambda_{111}$), α_{90} always decreases with rising annealing temperature and takes minimum near 330°C. The least value of α_{90} located near the composition with vanishing crystalline anisotropy (about 75% Ni), may be reasonable if the decrease of α_{90} is mainly due to the reduction of the internal stress σ .

Another important quantity in estimating local anisotropy K from the micromagnetic ripple theory [eq. (5.1)], is the uniaxial anisotropy constant K_u. Figure 6.3 shows the composition dependence of K_u for the same films as shown in Fig. 6.1 . In this figure are also shown typical theoretical curves, one of which denotes the pair-order anisotropy proportional to $C^2(1-C)^2$ (C : the fractional concentration of Ni), the other two the M-induced magnetostriction anisotropy calculated from West's theory[8] for $T_m = T_a = 30°C$ and $T_m = 30°C$, $T_a = 330°C$ (T_m : the measurment temperature), respectively. As seen from the figure, the experimental K_u curves may be expressed as the superposition of these theoretical ones.

6.5 Estimation of Local Anisotropy

Let us now estimate the local anisotropy K from the experimental results by using eq. (5.1). To obtain K from eq. (5.1), some supplemental parameters of d (the film thickness), D (the mean crystallite diameter) and A (the exchange stiffness) are required. We assume $A = 10^{-6}$ erg/cm and use the measured value

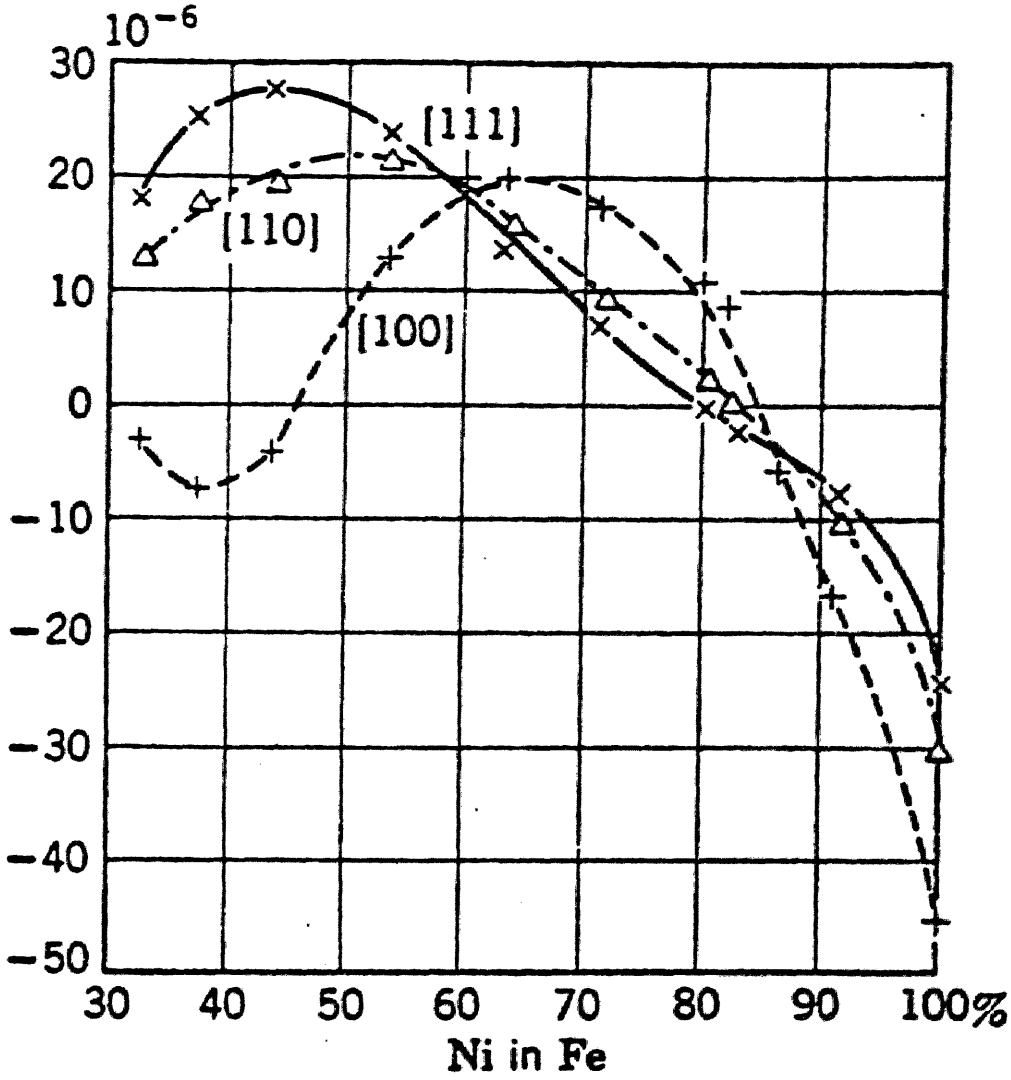

Fig. 6.2 Magnetostriction constants λ_{100}, λ_{111}, λ_{110} vs. composition for Ni-Fe alloy[9].

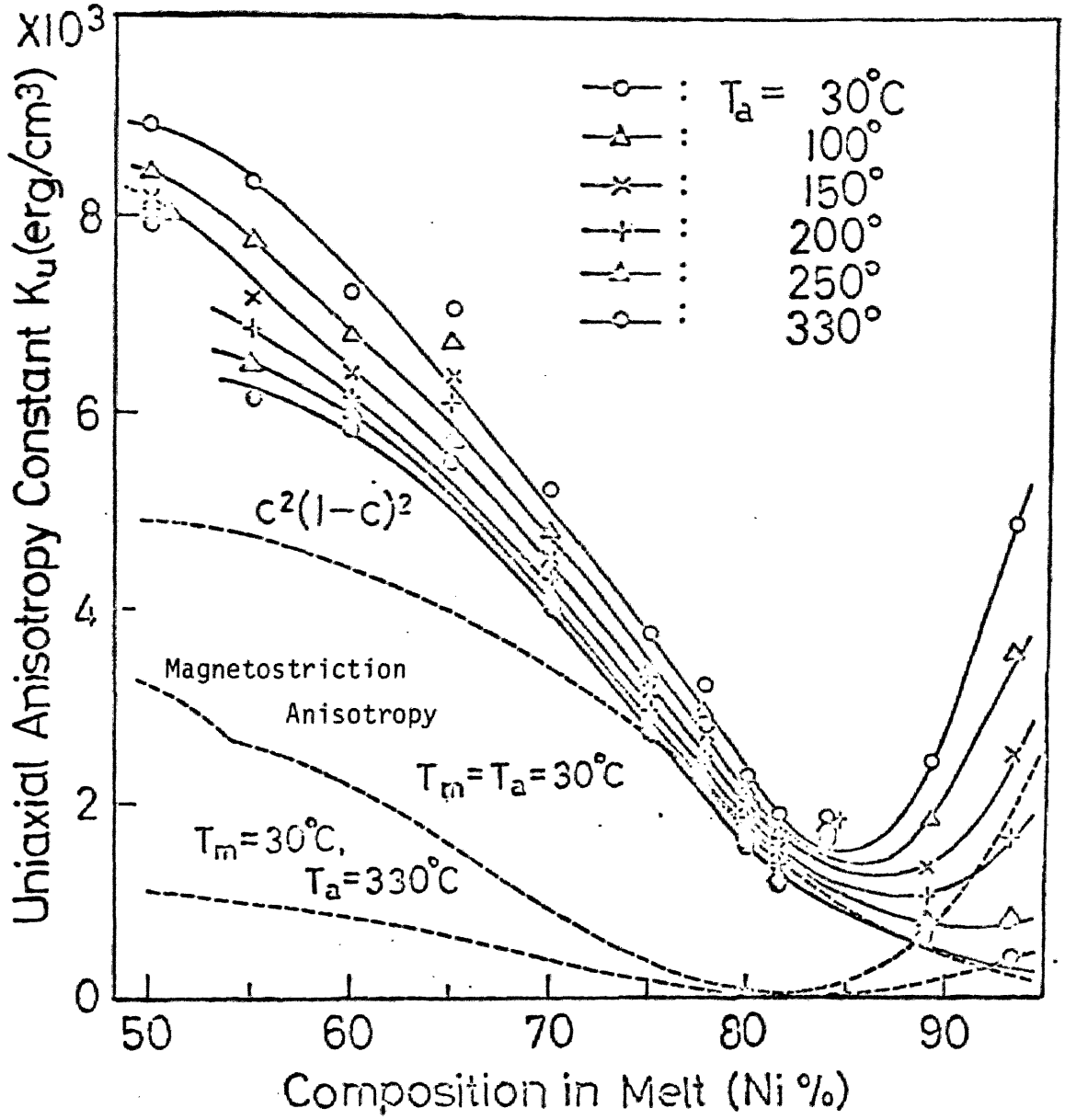

Fig. 6.3 Uniaxial anisotropy constant K_u vs. composition for the same films with Fig. 6.1 Dashed curves are theoretical ones; pair-order anisotropy $C^2(1-C)^2$ (C : fractional concentration of Ni) and magnetostriction anisotropy, where T_m, T_a are measurement and annealing temperature, respectively[10].

of d = 400 Å. The mean crystallite diameter D, on the other hand, was measured for films deposited onto rock-salt substrates and annealed, under similar condition, in the specimen chamber of an electron microscope. As shown in Fig.6.4, crystallite grows considerably with rising annealing temperature. By using these data, K was obtained from eq. (5.1) as is shown in Fig. 6.5. Theoretical curves of eq. (5.7) are also shown in the figure, where the internal isotropic stress σ is chosen as a parameter. For simplicity, the effect due to the uniaxial anisotropy is taken into account in the form of $\gamma K_u = \gamma_p K_{up} + \gamma_e K_{ue}$, where $\gamma_p K_{up}$ and $\gamma_e K_{ue}$ are contributions of the pair-order and magnetostriction anisotropy, respectively, as described in Secs. 6.2 and 6.4.

As shown in Fig.6.5, experimental results agree satisfactorily with theoretical curves so far as films with 70 to 95% Ni are concerned. We may therefore estimate the magnitude of the internal stress σ in a quantitative way for given annealing temperature T_a ; σ is approximately $8 \sim 9 \times 10^9$ dyne/cm^2 at 30°C in the composition range 70% Ni to 81.5% Ni, and decreases almost linearly with increasing T_a, and then almost vanishes near T_a = 330°C as shown in Fig.6.5. Therefore, the data of K for T = 330°C seem to be interesting to check the validity of eq. (6.10). So we rewrite the curve corresponding to T_a = 330°C in Fig.6.5, as shown in Fig.6.6, in a magnified scale together with the theoretical curves of eq. (6.10) by putting γ = -0.63 (k = 4) and γ = 0 (k = 2) : the former corresponds to the pair-order anisotropy for f.c.c. crystal, and the latter the ideal uniaxial anisotropy. In other word, the latter case corresponds to that the influence of the induced anisotropy on K is utterly neglected

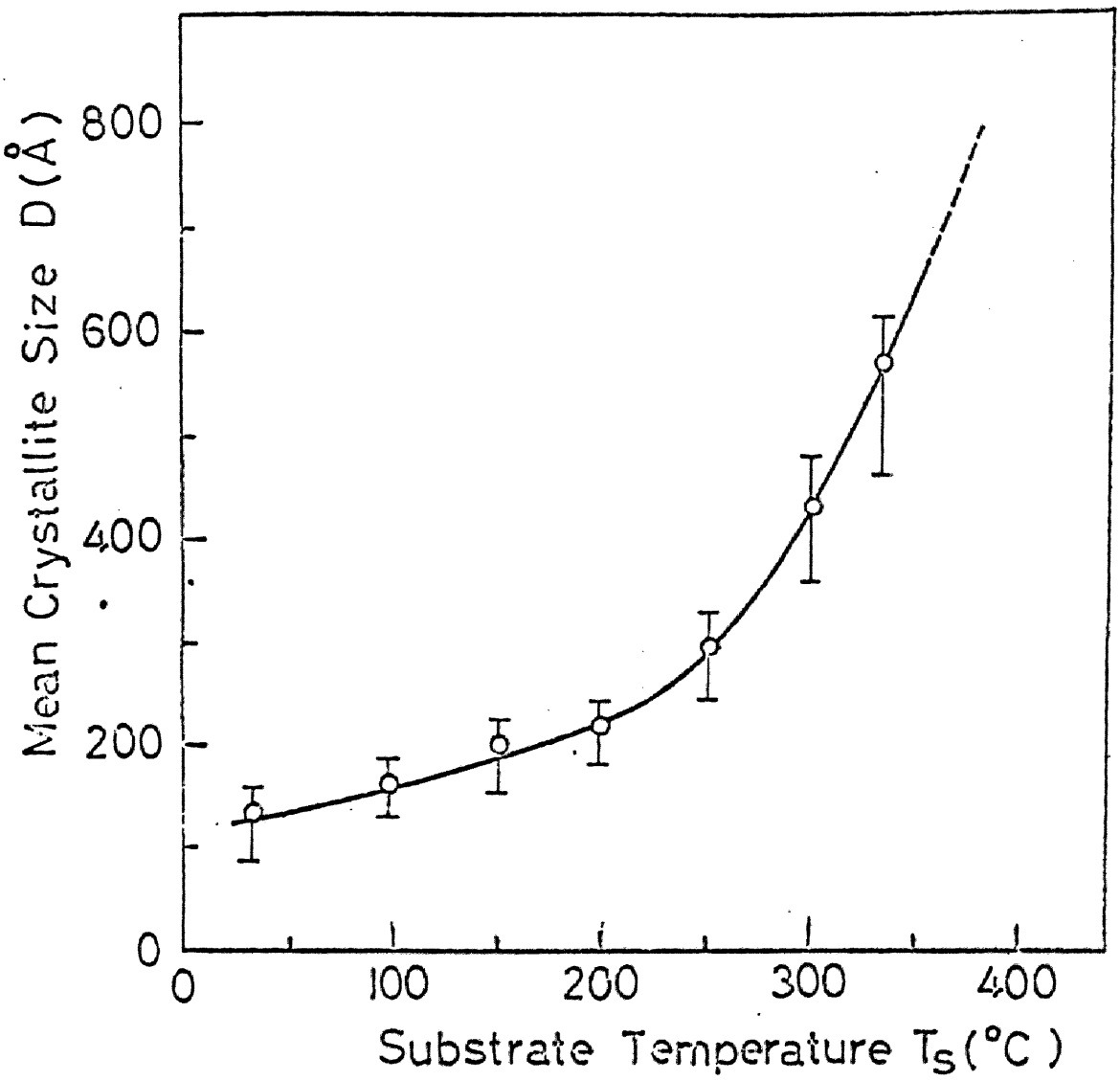

Fig. 6.4 Crystallite diameter vs. annealing temperature for Permalloy films during 15 min. heat treatment.

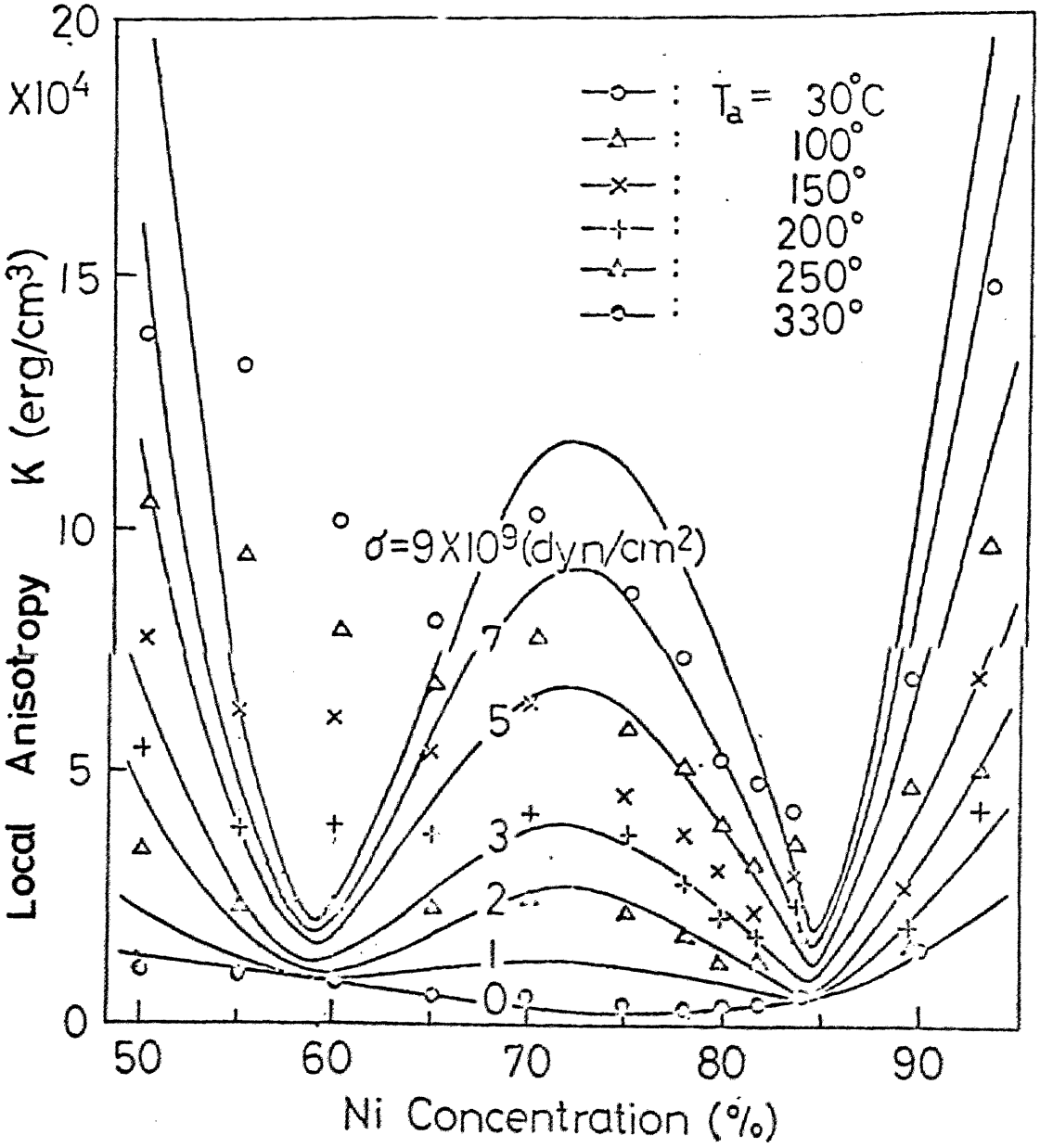

Fig. 6.5 Theoretical dependence of local anisotropy K on composition and on isotropic planar stress σ calculated from modified Doyle-Finnegan's expression [eq.(6.7)] . Local anisotropies estimated from $\alpha_{90}K_u$ by using eq. (5.1) are also plotted in the figure.

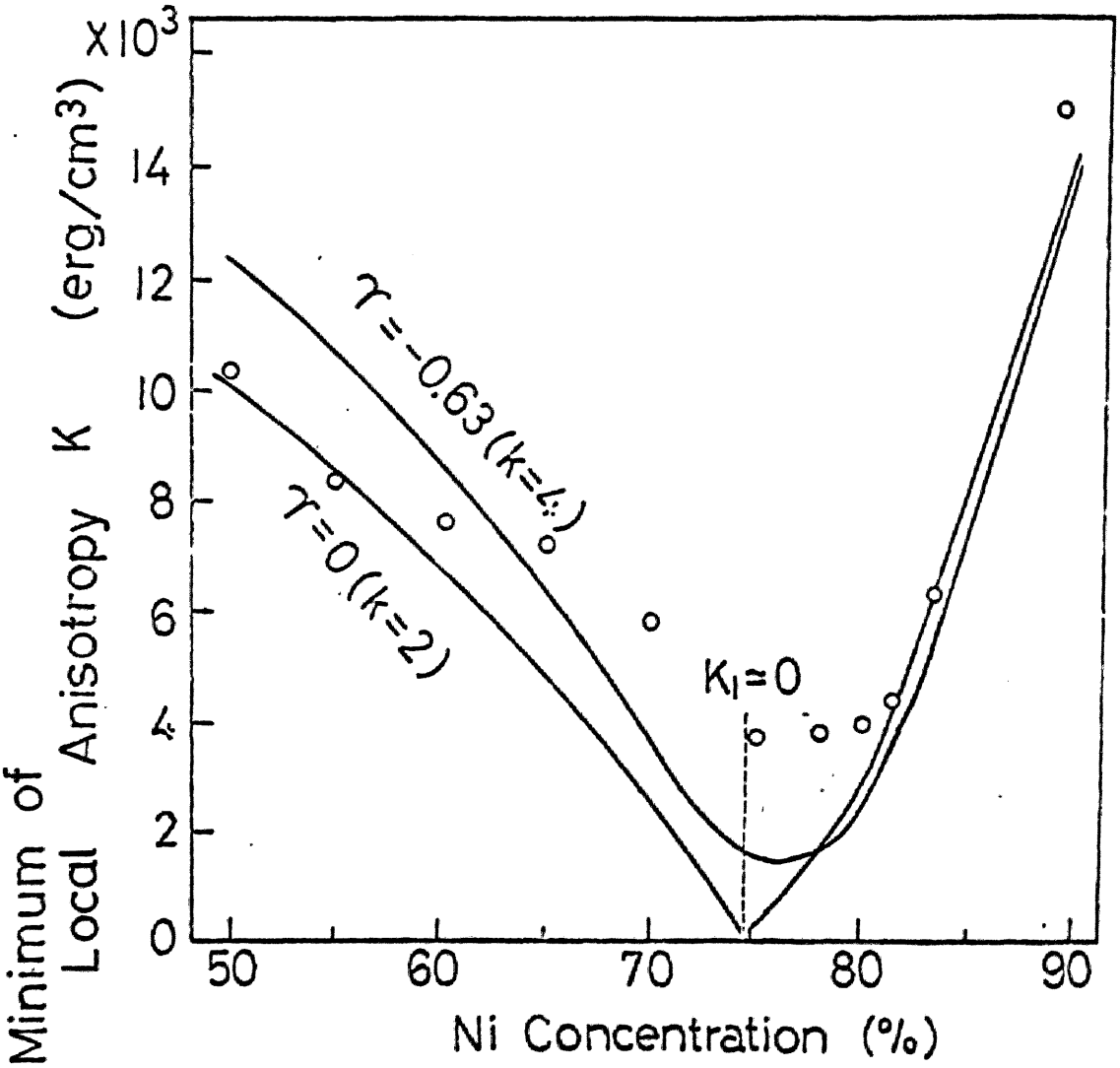

Fig. 6.6 Comparison of theoretical K_{min} of eq. (6.10) with estimated minimum K at T_a = 330°C.

and thus only the magnetocrystalline anisotropy K_1 is responsible for K. Although, the uniaxial anisotropy has a minor contribution, it may be seen from the figure that the curve of $\gamma = -0.63$ holds appreciably well for the experimental results, especially for the behavior near the composition of $K_1 = 0$.

6.6 Discussion and conclusion

The first point to be discussed is the component of the local anisotropy associated with internal stress. As seen from Fig. 6.5, the local anisotropy K estimated from the measurement of $\alpha_{90} K_u$ by using eq. (5.1) does not show such a prominent minimum near 60% Ni (the composition of $\lambda_{100} \simeq \lambda_{111}$) as is expected from eq. (6.7). This discrepancy may be due to the anisotropic stress acting on crystallites. Fujii et al.[10] has calculated the effect of the anisotropic stress by introducing the stress tensor with the form of

$$(\sigma_{ij}) = \begin{pmatrix} \sigma & \Delta\sigma & 0 \\ \Delta\sigma & \sigma & 0 \\ 0 & 0 & 0 \end{pmatrix} , \qquad (6.11)$$

where σ and $\Delta\sigma$ indicate the isotropic planar stress and anisotropic one, respectively. In this situation, eq. (6.7) can be rewritten as

$$K^2 = K_\sigma^2 + K_{\Delta\sigma}^2 , \qquad (6.12)$$

where K_σ is the local anisotropy constant for the ideal isotropic planar stress and $K_{\Delta\sigma}$ the additional term due to the anisotropic planar stress which is given by

$$K_{\Delta\sigma}^2 = 27\left\{\frac{35}{8}\lambda_{111}^2 + \frac{7}{2}\lambda_{111}(\lambda_{100}-\lambda_{111}) + (\lambda_{100}-\lambda_{111})^2\right\}\Delta\sigma^2 . \qquad (6.13)$$

As can be easily seen from eqs. (6.7) and (6.13), if $\Delta\sigma \ll \sigma$, the anisotropic stress term $K_{\Delta\sigma}$ plays a significant role only

near the composition with $\lambda_{100} \simeq \lambda_{111} \neq 0$. This is the case at the comosition of 60% Ni. Then, assuming the anisotropic stress $\Delta\sigma$ of only 0.05 σ in magnitude, the experimental results are fairly well explained as shown in Fig. 6.7.

The second point is concerned with the magnitude of the planar stress σ. The value of σ was estimated from the data of K in the composition of 70 ~ 81.5% Ni by using eq. (6.7). The result is shown in Fig. 6.8 as a function of the annealing temperature. In the same figure, are also shown previous results of Uchiyama et al.[3] which were obtained in the same manner with this experiment and those of Prutton which were measured directly from the mechanical strain[11]. Prutton's results agree well with the present result. This is owing to the consideration of the crystallite growth; in the previous work, the diameter of crystallite was assumed to be 150 Å regardless of the annealing temperature. Thus it should be noted that the quantitative estimation of σ, as well as of K, is seriously dependent on the determination of the crystallite size.

The third point to be mentioned is the composition dependence of K_{min}. As seen in Fig. 6.1, it is impossible to reduce α_{90} to zero even at the composition of $K_1 = 0$. Therefore, for the purpose of interpreting this fact, the effect of the local variation of M-induced anisotropy has been introduced into the local anisotropy, which is shown in Fig. 6.6 as solid lines. It is seen from the figure that this modification can explain, to some extent, the discrepancy between the original Doyle-Finnegan's expression and the experimental results. This modification, however, might be blamed for having little meaning, because there

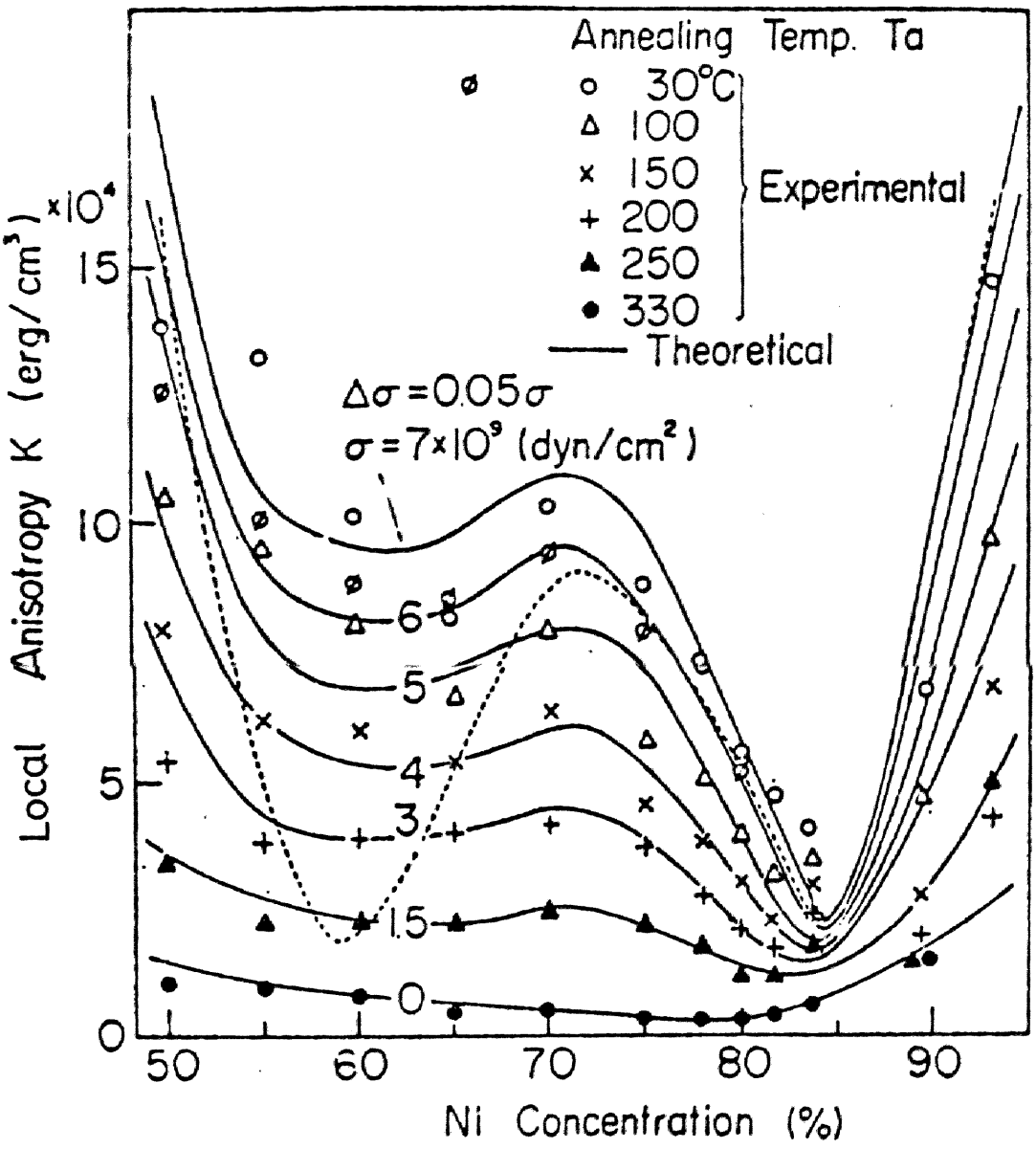

Fig. 6.7 Comparison of theoretical and experimental local anisotropies. In calculating theoretical curves, anisotropic stress $\Delta\sigma$ is taken as $0.05\,\sigma$. Dotted curve is calculated from original Doyle-Finnegan's expression for $\sigma = 7 \times 10^9$ dyn/cm.[10)]

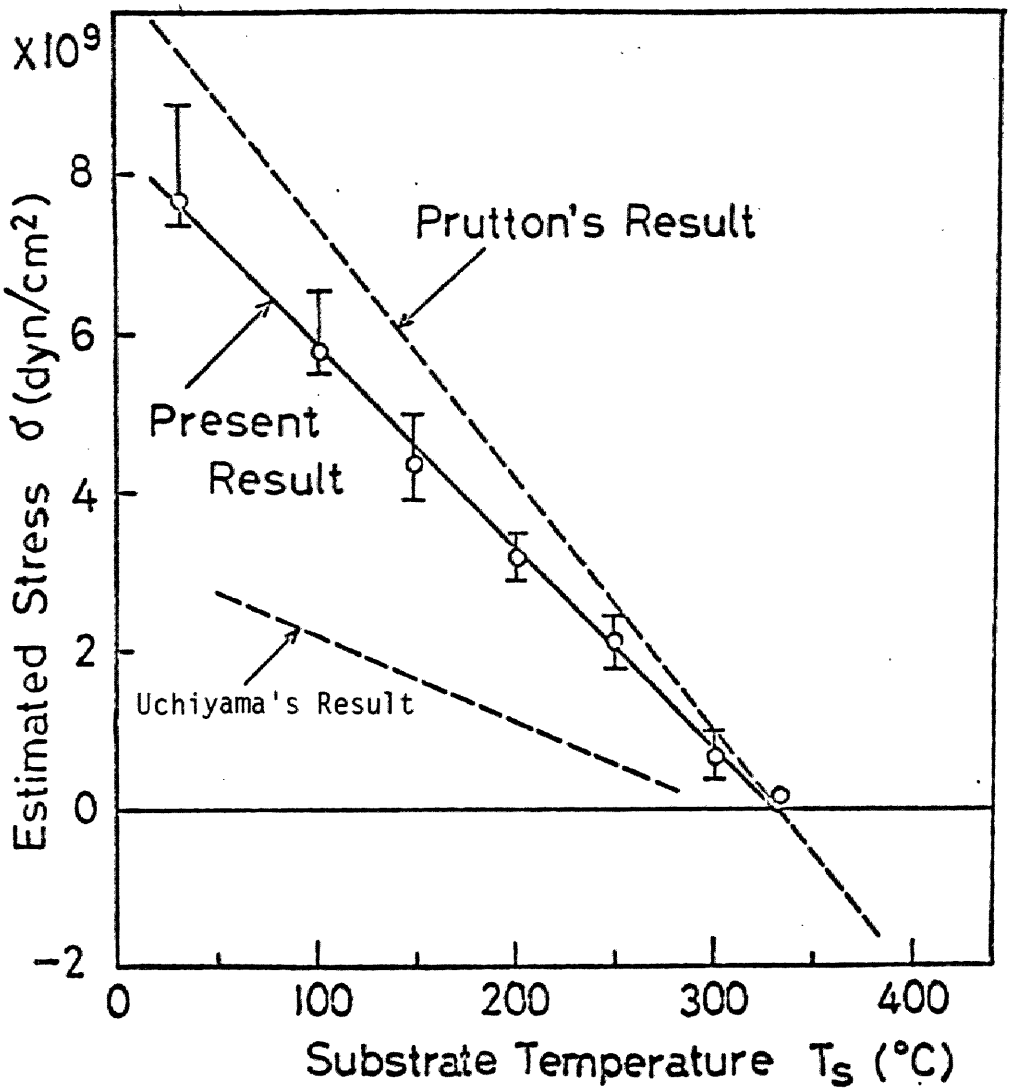

Fig. 6.8 Estimated isotropic planar stress σ from Fig.6.5 as a function of substrate temperature T_s. Vertical bars denote scattering limits of σ in the composition range of 70%Ni to 81.5%Ni. Dashed curves are results of Uchiyama et al.[3] and of Prutton[11].

exist some other possibilities of the minor contribution to K. Their examples are the magnetoelastic and/or magnetostatic anisotropies due to the variation of the composition from crystallite to crystallite or due to the anisotropic shape of crystallites.

In conclusion, the local anisotropy, estimated from $\alpha_{90}K_u$ by using micromagnetic dispersion theory is well interpreted by Doyle-Finnegan's expression. More satisfactory agreement over wide range of composition is obtained by introducing the local fluctuation of the M-induced anisotropy and the additional anisotropic planar stress.

References

1) F. Fujii, S.Uchiyama, E. Yamada and Y. Sakaki: Japan appl. Phys. 6 (1967) 1.

2) S. Uchiyama, T. Fujii, M. Masuda and Y. Sakaki: Japan J. appl. Phys. 6 (1967) 512.

3) S. Uchiyama, T. Fujii, M. Masuda and Y. Sakaki: IEEE Trans. Mag. MAG-4 (1968) 495.

4) W. D. Doyle and T. F. Finnegan : J. appl. Phys. 39 (1968) 3355.

5) M. Roth : Phys. Stat. Sol. 14 (1966) 115.

6) S. Chikazumi : J. Phys. Soc. Japan, 11 (1956) 551.

7) M. Roth : IEEE Trans. Mag. MAG-2 (1966) 566.

8) F. G. West : J. appl. Phys. 35 (1964) 1827.

9) R. M. Bozorth and J. G. Walker : Phys. Rev. 89 (1953) 624.

10) T. Fujii, T. Tanaka, S. Uchiyama and Y. Sakaki : Japan J. appl. Phys. 10 (1971) 1372.

11) M. Prutton : Nature, London (1962) 565.

Chapter 7
Summary

This research is concerned with two problems of the uniaxial anisotropy and the magnetization ripple in Permalloy films:
(1) As for the uniaxial anisotropy, the relaxation phenomena in nonmagnetostrictive films are investigated theoretically in chapter 2 and experimentally in chapters 3 and 4.
(2) As for the magnetization ripple, experimental verifications of the micromagnetic ripple theory and of the effective crystalline anisotropy model are dealt with in chapters 5 and 6, respectively. Conclusions are summerized as follows:

Chapter 2 describes the kinetics of the directional pair-order in the binary alloys with the cubic lattice. The rate equations for the probabilities of directional atom pairs are obtained. It is found that the relaxation behavior of the pair-order anisotropy varies depending on the lattice type. The relation between the relaxation frequency and the vacancy concentration was obtained for the case of dilute alloys.

In chapter 3, the anisotropy relaxation of nonmagnetostrictive Permalloy films is discussed on the basis of the pair reorientation through excess vacancies (excess vacancy model). In order to make clear the mechanism of the anisotropy relaxation, simultaneous measurements of the anisotropy relaxation and resistance recovery were made during isochronal HA annealing. Appreciable correlations were found between both annealing curves; especially the activation energies for both processes are nearly the same. The excess vacancy model, however, gives an insufficient explanation on the aniso-

tropy relaxation process, especially for the relaxation stage with low activation energies.

The anisotropy relaxation with low activation energies was reexamined from the view point of the grain boundary diffusion in chapter 4. The dependence of the anisotropy relaxation on grain size was investigated in nonmagnetostrictive films by changing the film thickness. The grain boundary model explains qualitatively the grain size dependence of the anisotropy relaxation process with low activation energies. This model explains the lack of such a process in single crystal films as well.

In chapter 5, Hoffmann's micromagnetic ripple theory was examined experimentally. The transverse bias susceptibility χ_t and fall back angle (dispersion) α_{90} in Permalloy films were measured on a restricted small region of the sample. The effective crystalline anisotropy K, which gave rise to the ripple, was determined from the field dependence of χ_t for a variety of films. The value of K obtained agreed well with the value evaluated from the dispersion-anisotropy product $\alpha_{90}K_u$ by using micromagnetic ripple theory. This fact shows that Hoffmann's micromagnetic ripple theory is reliable.

In chapter 6, the value of K evaluated from $\alpha_{90}K_u$ was compared with that predicted by the modified Doyle-Finnegan's expression, where the ordinal crystal anisotropy, the magnetoelastic anisotropy due to the isotropic planar stress, and the fluctuation of the M-induced anisotropuy are considered as the origin of K. Assuming the presence of the anisotropic planar stress, the compositional dependence of K was satisfactorily explained by the modified Doyle-Finnegan's model for wider range of composition.

Furthermore, by taking into account the grain growth due to annealing, the magnitude of the planar stress estimated from $\alpha_{90}K_u$ agreed well with the magnitude observed directly.

In this way, the grain size plays very significant role in the anisotropy relaxation as well as in the magnetization ripple, for polycrystalline films. The large grain size yields large magnitude of the magnetization ripple, so that magnetic properties are affected badly by manifesting the anisotropy dispersion. On the other hand, small grain size causes delicate ageing properties due to the grain boundary diffusion. Thus in applying Permalloy films to the practical use, the films have to be subjected to the stabilization heat treatment at relatively low temperature (below 300°C) so as to avoid the over growth of grains.

Acknowledgement

The Author would like to express his sincere thanks to Prof. S. Uchiyama and Dr. T. Fujii of Nagoya University for their valuable guidances and warmhearted encouragement throughout the resarch. He is also much indebted to Prof. M. Ieda for many suggestions made in the preparation of the manuscript.

The author is grateful to Prof. Emeritus Y. Sakaki of Nagoya University and Dr. M. Masuda of Mie University for their instructive advices and encouragement in performing the resarch.

The author takes pleasure in mentioning that a part of this resarch was carried out with Mr. T. Niwa (Shimadzu Seisakusho Co.,Ltd), Mr T. Nakashima (Nippon Denso Co.,Ltd) and Mr. M. Suzuki (Aishin Seiki Co.,Ltd).

The author also expresses his appreciation to Prof. S. Maruse, Dr. M. Hibino and Dr. M. Takayasu and other members of Uchiyama and Maruse Laboratories for their valuable discussions.

List of Published Parpers

(Title)		(Coauthors)
1. An Experimental Verification of Dispersion Theory in Soft Magnetic Films	IEEE Trans.on Magnetics, MAG-5 (1969) 223.	T.Fujii S.Uchiyama Y.Sakaki
2. Random Anisotropy of Crystallite in Thin Permalloy Films	IEEE Trans.on Magnetics, MAG-6 (1970) 619.	T.Fujii S.Uchiyama Y.Sakaki
3. Relaxation Process of M-Induced Uniaxial Magnetic Anisotropy	J.Phys.Soc.Japan, 39 (1975) 303.	T.Fujii S.Uchiyama
4. Annealing Behivior of As= Deposited Permalloy Films	Japan J.appl. Phys. 14 (1975) 1501.	T.Fujii S.Uchiyama
5. Thickness Dependence of Annealing Behavior in Permalloy Films	Japan J.appl. Phys. 15 (1976)	M.Suzuki T.Fujii S.Uchiyama